Synthesis and Characterization of Lead-based Core-shell-shell Quantum Dots and Studies on Excitation-dependent Quantum Yield Measurement

by

Jieming Cao
B. Eng., Zhejing University, 2008

A thesis Submitted in Partial Fulfillment
of the Requirements for the Degree of

MASTER OF SCIENCE

in the Department of Chemistry

Supervisory Committee

Synthesis and Characterization of Lead-based Core-shell-shell Quantum Dots and Studies on Excitation-dependent Quantum Yield Measurement

by

Jieming Cao
B. Eng., Zhejing University, 2008

Supervisory Committee

Dr. Frank C. J. M. van Veggel (Department of Chemistry)

Supervisor

Dr. Alexandre G. Brolo (Department of Chemistry)

Departmental Member

Abstract

Supervisory Committee

Dr. Frank C. J. M. van Veggel (Department of Chemistry)

Supervisor

Dr. Alexandre G. Brolo (Department of Chemistry)

Departmental Member

Nano-sized semiconductors, known as quantum dots (QDs), are one of the hottest research areas in recent years. The energy gaps of QDs change with their diameters, giving them size-dependent optical properties. By controlling reaction conditions, people are able to make QDs that can emit in certain wavelength ranges. So far, QDs have shown great potential in telecommunication, bio-imaging, single-photon laser source, etc.

This thesis starts with Chapter 1, which first introduces the finding of QDs and why they have such special properties. The quantum confinement and energy gap are discussed, followed by the absorption and emission of QDs. Moreover, the synthesis methods and mechanism involved are reviewed in brief.

Chapter 2 presents the synthesis of lead-based core, core-shell and core-shell-shell QDs and previous work by other people. A few techniques including transmission electron microscopy (TEM), UV-absorption, photoluminescence (PL) measurement, and X-ray photoelectron spectroscopy (XPS) were used and shown in this chapter. Core-shell and core-shell-shell QDs are shown to present excellent stability over 20 months. The ZnS shell was proved by energy-dependent XPS and TEM measurements.

A detailed discussion on quantum yield (QY) is given in Chapter 3. Absolute and relative QY measurements and some standard dyes are discussed. After that, Chapter 4 shows systematic QY measurements on lead-based core and core-shell QDs. For each type of QDs, at least two batches are selected with their emission spectra presented as well. It is revealed by collected data that they have excitation-dependent QYs. The QY drops as the excitation light increases in energy (higher wavelength), which is due to non-radiative decays from higher excited states or the Auger effects. QY of PbS and PbSe QDs can be as high as 50%.

Eventually, the conclusion and future work are included in Chapter 5. All experimental work is described in detail in the experimental section.

Table of Contents

List of Tables

List of Figures

List of Abbreviations

QD	quantum dot
PL	photoluminescence
$(CH_3)_2Cd$	dimethyl cadmium
TOPSe	tri-n-octylphosphine selenide
TOPO	tri-n-octylphosphine oxide
$Cd(OAc)_2$	cadmium acetate
MBE	molecular beam epitaxy
MOVPE	metallorganic vapor phase epitaxy
TBP-Se	tributyl-phosphineselenide
TEM	transmission electron microscopy
FWHM	full width at half maximum
E-MAA	ethylene-15% methacrylic acid copolymer
$(TMS)_2S$	bis(trimethylsilyl)sulfide
XRD	X-ray diffraction
HAADF	high-angle annular dark field imaging
XPS	X-ray photoelectron spectroscopy
UV	ultraviolet
TCE	tetrachloroethylene
CLS	Canadian Light Source
QY	quantum yield
IUPAC	International Union of Pure and Applied Chemistry
PTFE	polytetrafluoroethylene
PAS	photoacoustic spectroscopy
HPLC	high performance liquid chromatography
SAXS	small angle X-ray scattering
NIR	near infrared
MEG	multiple exciton generation

Acknowledgments

I would like to give my thanks to Dr. Frank Van Veggel, who has been my supervisor since autumn, 2012. Beyond a responsible and intelligent professor, he is also such an interesting and humorous person to get along with. Without his patient guidance, I could never have made it this far. His motivation for science and brilliant ideas benefited me tremendously. It's been a great time working with him, to which I sincerely send my gratitude. I wish him an even more successful career in the future as an outstanding researcher.

Also, the past three years being in the Van Veggel group is a memorable experience. It is my pleasure to be able to know all these great people who have been or still are in the group. You made my time here incredibly enjoyable. Thank you all for the discussion and fun time we had together. Hope that we can stay in touch and this journey never ends.

During our time at the Canadian Light Source, Dr. Tom Regier and Dr. Jay Dynes had helped us a lot. I must thank them for their generous support. All the faculty members and staff in the Chemistry department are amazing. They put huge amount of effort in making this department a lovely family.

To all my friends and relatives in China, I am so enthusiastic about going home. Research may be one part of life, but you are the rest of it and everything that matters. I will be seeing you soon.

Chapter 1 Introduction to core-shell-shell QDs

1.1 What is quantum dots?

Quantum dots (QDs) are nanocrystals made of semiconductors. Their sizes are usually in the range of 1 to 100 nm. Because of the fact that they are so small, they show some quantum mechanical properties that cannot be seen in bulk semiconductors. These nanocrystals were first named "quantum dots" by M. Reed in the year 1988.[1] However, the properties of them had been studied before. The discovery of QDs in the solid state was first reported by A. Ekimov et al.[2] They proved that there is a size effect on the optical properties of these crystals by growing CdSe, CdS, CuBr and CuCl nanocrystals in a multicomponent silicate glass by measuring their absorption. The absorption peaks of nanocrystals shifted towards lower wavelength (i.e. higher energy) when the size was decreased.[2] Thanks to L. E. Brus and co-workers, a new gate to colloidal synthesis of QDs was opened in 1985.[3] Colloidal solution refers to a solution in which particles with size ranging from 1 to 1000 nm evenly distributed and will not settle down.[4] Through their work, colloidal ZnS and CdS nanocrystals in the range of 1.5 to 5 nm were made. Size-dependent absorption property was also observed on the both CdS and ZnS nanocrystals. Their preliminary work built up the foundation of QDs research, which is greatly advanced since then.[5-8]

1.2 Semiconductor, QDs and insulators

As mentioned above, QDs can exhibit unique quantum mechanical properties, one of which is size-dependent absorption. To understand these properties, we must start from the band structure of QDs. Semiconductors are materials that have electrical conductivity in between insulators and conductors. What makes them so special is the Fermi level. The

Fermi level is an energy level originated from the Fermi-Dirac dispersion. It is defined as the energy level that has 50% chance of being occupied by an electron at thermodynamic equilibrium at any temperature.[9] For a conductor like gold, its Fermi level lies in the conduction band so that, given a very little amount of energy, electrons can become delocalized and move freely to convey current. In the case of insulator and semiconductor, the Fermi energy level is in the middle of the valence band and the conduction band. The gap between the bottom of the conduction band and top of the valence band is called the bandgap. Normally, we refer to materials with such a bandgap larger than 4 eV as insulators. Insulators have such large bandgaps that it's almost impossible to excite electrons into the conduction band unless a very high voltage is applied. This voltage is known as the breakdown voltage. Conductors don't have bandgaps, and materials with energy gap in between 0 and 4 eV are considered semiconductors. Here we use E_g to represent the energy of bandgap. The relative scale of E_g is shown below in Figure 1.1.

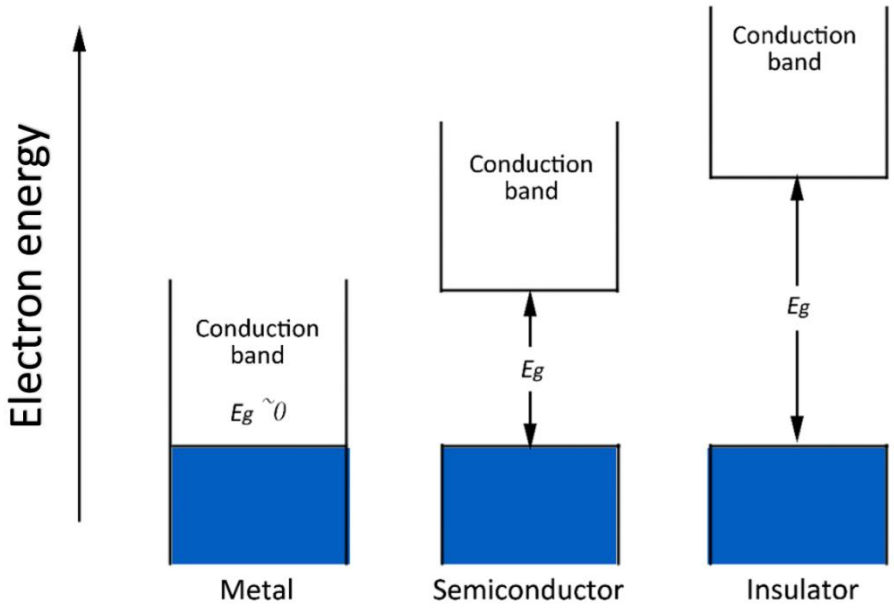

Figure 1.1. Bandgap of metal, insulator and semiconductor.

When a semiconductor absorbs energy from incident light or a heat source, the electron in the valence band can get excited into the conduction band, leaving a hole in the original valence band, this electron-hole pair (bounded through the Coulomb interaction) is known as the exciton.[10] Holes in the valence band and promoted electrons can convey current, thus the semiconductor becomes conductive. Due to this effect, semiconductors are sensitive to light and heat, which lead to various important applications like television and cellphone.

1.3 Quantum confinement

As QDs are nano-scale semiconductors, they exhibit very different electrical and optical properties from those of their bulk materials. That is due to the quantum confinement effect, which can be understood with the "particle in a box" model.[11]

Imagine a one-dimensional system, where a little particle can move freely forward and backward, but only in a straight line. At both ends of the line, there is a wall that is impenetrable, so that every time the particle hits the wall, it goes back at the same speed without any energy loss. This model is a 1-D "particle in a box" model. In classic physics, the particle travelling with any speed can appear at any point along the line. Moreover, the chance of it being at each point will be the same, independent of the speed.

In an ideal 1-D "particle in a box" model, the space between the two walls is defined as where the potential is 0, whereas outside, the potential is regarded as infinitely large. Assume the distance between the two walls is L, and x represents the position of the particle inside the box. The potential energy in this model is:

$$V_{(x)} = \begin{cases} 0 & (0 < x < L) \\ \infty & (x \leq 0 \; or \; x \geq L) \end{cases}$$

If the particle has a mass m and kinetic energy E, the time-independent Schrödinger equation for the particle will be:

$$-\frac{\hbar^2}{2\mathrm{m}}\frac{d^2\psi(x)}{dx^2}+V_{(x)}\psi(x)=E\psi(x)$$

where $\hbar$ is the reduced Plank's constant, and $\psi(x)$ is a time-independent wavefunction. The behavior of the particle can be described using this wavefunction, which is defined as:

$$\psi(x)=Asin(kx)+Bcos(kx)$$

where A and B are constants, and k is the wavenumber. The wavefunction gives the possibility of the particle showing up at each point. According to the boundary condition, the particle has no chance being at $x=0$, and we know that $\sin(0)=0$ and $\cos(0)=1$, then B can only be 0 to fulfil the requirements. As a result, the wavefunction becomes:

$$\psi(x)=Asin(kx)$$

Since the particle has no chance of being at $x=L$ either, kL must equal $n\pi$ (n is nonzero integar), which makes $k=\frac{n\pi}{L}$. The total chance of the particle inside the box is 1, so we have:

$$\int_0^L\psi^2dx=1$$

A can be calculated from this equation, which is $\sqrt{\frac{2}{L}}$. As a result, the wavefunction turns out to be:

$$\psi(x)=\sqrt{\frac{2}{L}}sin\left(\frac{n\pi}{L}x\right)$$

By taking this wavefunction back into the Schrödinger equation, the energy of the particle can be derived:

$$E=\frac{n^2\pi^2\hbar^2}{2mL^2}$$

People thus found that the particle can only take on certain discrete kinetic energy values which are higher than 0, meaning that the particle can never stay still. In addition, the chance of it showing up at each point is not the same, according the wavefunction. There are points called nodes where the particle can never be at. The energy of the particle is quantized in this case, and it affects the chance of finding the particle at each point.

So far, we have talked about 1-D "particle in a box" model. A QD, can be deemed as a 3-D "particle in a box" model where quantum mechanical properties can only occur when the size of the QDs is smaller than its Bohr radius (the most probable distance between the bound electron-hole pair). As mentioned already, a bound electron-hole pair is an exciton. Excitons in QDs are confined in all three dimensions.[12] This is also known as the quantum confinement. Excitons in quantum well and quantum wire are confined in 1 and 2 dimensions, respectively.[13] Figure 1.2 below shows the effect of different degrees of quantum confinement from bulk semiconductor to QDs.

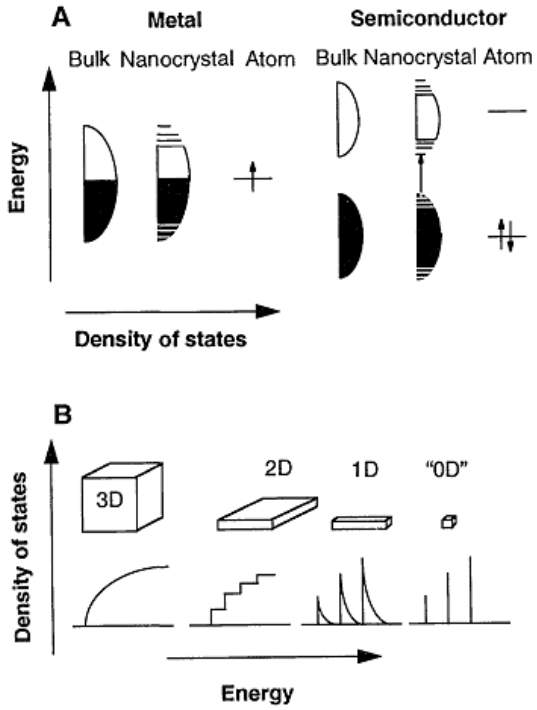

Figure 1.2. A. Illustration of density of states of metal and semiconductor. B. Density of states in one band of a semiconductor as a function of dimensions. (With permission from publisher)[14]

In Figure 1.2.A, the discrete lines represent energy levels. The continuous part in the conduction and valence bands is formed by a number of energy levels. The up and down arrows stand for electrons with different spins. The three-dimensional quantum confinement caused the edge of both bands from continuous to discrete.

The Bohr radius of an exciton can be approximated by the equation:[15]

$$a_b = \frac{\hbar^2 \varepsilon}{e^2}\left(\frac{1}{m_e} + \frac{1}{m_h}\right)$$

In the equation ε is the bulk optical dielectric coefficient, e is the elementary charge, m_e and m_h are the effective masses (the mass a particle seems to have when responding to forces) of the electron and hole, and $\hbar$ is the reduced Planck's constant.

Since they are quantized, the energy gap of QDs can approximately be calculated using the particle in a box model.[16] The equation indicates that bandgap of QDs is closely related to size of the particles.[6]

$$E_g = E_{g_0} + \frac{\hbar^2 \pi^2}{2 m_{eh} R^2}$$

Where E_{g_0} is the bandgap energy of the bulk semiconductor made of the same material, $m_{eh}$is the average effective mass of the electron and the electron hole and R is the radius of the QDs. It can be seen that for the same type of QDs, E_g is only affected by R. As R increases, E_g decreases, leading to a red shift in the emission spectra.

1.4 Optical property of QDs

As we have discussed already, QDs have discrete energy levels in both valence and conduction bands. Discrete energy levels of a typical NIR quantum dot is shown in Figure 1.3. These energy levels are labeled using atomic-like notations for orbitals (1S, 1P, 1D, etc.).[10] The letters e and h beside notations stand for electron and hole, respectively. The energy of 1S(h)1S(e) transition equals to the energy gap of QDs. Also, this transition leads to the first peak starting from the right in the absorption curve in Figure 1.3 (right), which fits both theoretical calculation and experiment results.[17] The next absorption peak had been debated over for years, but was confirmed to be the 1P(h)1P(e) transition.[18] So far, the origin of higher order absorption peaks has not been settled, but 1D(h)1D(e) is one possible explanation. Ideally, QDs synthesized in one reaction would have the same size, which would give them the same discrete energy levels. However, there exists a small size deviation due to imperfect synthesis conditions. This explains why the first absorption peak shows a Gaussian dispersion rather than a sharp peak. With better quality, QDs should have a smaller size dispersion, and the full width at half maximum (FWHM) of the absorption will thus be smaller as well.

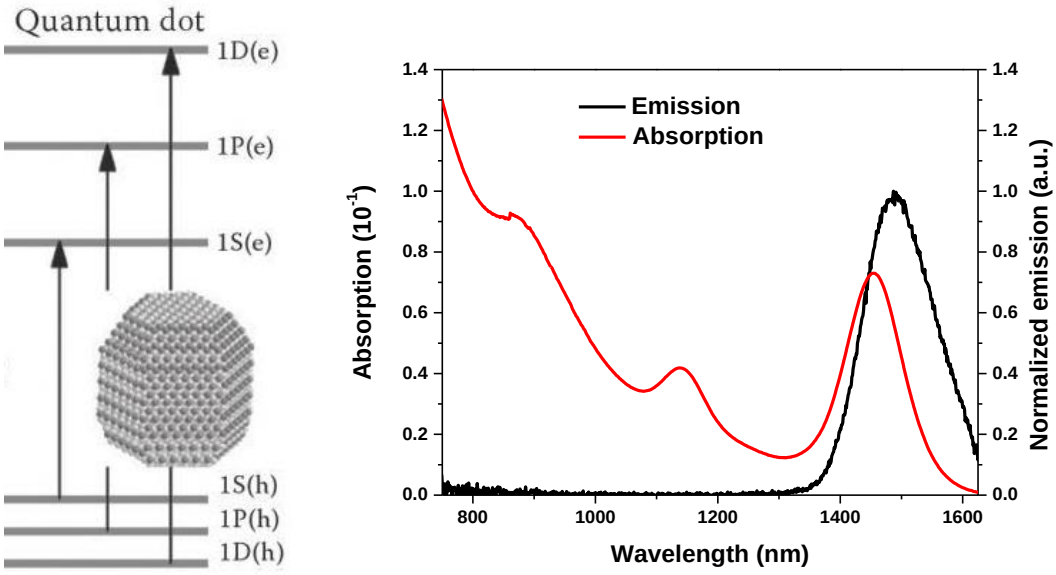

Figure 1.3. (left) Discrete energy levels of NIR QDs[10] (With permission from publisher) and (right) absorbance and emission of a batch of PbSe QDs synthesized by me. (details in Chapter 2)

Recombination describes the process where the excited electron in the conduction band goes back to the valence band and recombines with the hole. For QDs, excited electrons will go to the first (lowest) energy level in the conduction band via non-radiative decay, which then goes back to the highest energy level in the valence band to recombine with holes. The energy released during this electron-hole pair recombination results in the photoluminescence (PL). Recombination isn't always accompanied by PL, which will be discussed in Chapter 3. The wavelength difference between the emission and first absorption peaks is known as the Stokes shift.[19] The Stokes shift of QDs originates because the electrons in the valance band can absorb different amounts of energy and get promoted to various energy levels in the conduction band. However, within a very short period of time (1 – 10 ns), excited electrons rests to the lowest level in the conduction band via vibrational relaxation. Then, the recombination takes place and the emission is generated. In the end, the emission will always has less energy (thus larger wavelength) compared to the absorption. Work has shown that the energy of Stokes shift changes linearly with the energy of emission.[20, 21]

1.5 Synthesis methods of QDs

1.5.1 Colloidal Synthesis

Most of recent work on the synthesis of colloidal QDs uses organic solvents. This kind of synthesis usually requires precursors, organic surfactants and solvents.[22, 23] Originally, C. B. Murray, D. J. Noms, and M. G. Bawendi did innovative work making CdE (E = S, Se, Te) QDs.[24] The synthesis of CdSe QDs was emphasized in that article. Dimethyl cadmium [$(CH_3)_2Cd$], tri-n-octylphosphine selenide (TOPSe) were used and injected into

a pre-heated solution of coordinating solvent tri-n-octylphosphine oxide (TOPO). This work built the foundation of following colloidal synthesis in organic solvents. By using similar method, J. Nozik et al. made InP, GaP, and $GaInP_2$ QDs by heating appropriate organometallic precursors with stabilizers in high boiling solvents for several days.[25]

Synthesis of QDs we have discussed so far all uses organometallic precursors. There are certain problems associated with these routes. For example, A. P. Alivisatos et al. found that technical grade TOPO (90% Aldrich) provided better conditions for CdSe QDs growth compared to distilled TOPO, suggesting the impurities boosted the growth.[26] This was further investigated by W. E. Buhro and co-workers, who confirmed that different compounds known in the impurities would assist growth of CdSe quantum dots, quantum rod and quantum wire growth, respectively.[27] Also, the method invented by C. B. Murray et al. used a very high temperature (300 ℃), which was above the flash point of the solvent. If the reaction was not taken care of well enough, it might lead to an explosion. Moreover, $(CH_3)_2Cd$ is extremely toxic and air-sensitive, which requires extra caution. A few other non-organometallic precursors like CdO[28] and $Cd(OAc)_2$[29] were used to avoid these.

Apart from organic solutions, certain QDs can also be prepared in aqueous phase. The earliest published work was by L.E. Brus.[30] Although the quality wasn't good due to the large size dispersion and low yield, CdSe, ZnSe and ZnS QDs were successfully made. J. Nozik et al. performed aqueous synthesis of high quality CdTe QDs by using NaHTe as the precursor.[31] Highly luminescent CdTe QDs could also be synthesized with the help of microwave in aqueous solution.[32] Other aqueous synthesis of ZnS[33], ZnSe[34] and CdS[35] QDs have been reported as well.

1.5.2 Deposition synthesis

Deposition synthesized quantum dots are usually made using molecular beam epitaxy (MBE) or metallorganic vapor phase epitaxy (MOVPE). These require certain conditions so that QDs will nucleate spontaneously.[36] To understand this, we must consider what is known as Stranski–Krastanov growth.[37] When a material is grown on a substrate whose lattice doesn't match, the resulting strain produces strained islands on top of a two-dimensional wetting layer. The islands can be subsequently buried to form the quantum dot. Different QDs via deposition been realized, PbSe[36] for instance.

1.5.3 Synthesis in glass/polymer hosts

Instead of aqueous phase, successful attempts were made to embed QDs in glass and polymer hosts. One of the earliest synthesis in glass was performed by N. F. Borrelli and D. W. Smith in 1994.[38] They incorporated PbS QDs in an oxide glass host. Synthesis of the same QDs done also using this method were by D. Chakravorty and co-workers, in a multi-component oxide glass by passing H_2S gas over at temperatures varying from 773 to 943 K in the year 1997.[39] Similar work on PbS QDs was also reported by A. A. Lipovskii et al.,[40] who were the first to publish glass host synthesis on PbSe QDs.[41] The making of QDs in glass usually requires mixing and melting of glass components and the semiconductor material, followed by annealing and another thermal treatment to allow the semiconductor to crystallize.

Another widely used host for QDs synthesis is polymers. A great effort had been done on the synthesis of PbS QDs in polymer hosts over the years.[42-46] The system needs to incorporate the metal ion of interest (Pb^{2+}) while polymerization, then treat the polymer

with H_2S. There are other methods employed to build a polymer-QDs structure, which was well reviewed by G. J. Vancso et al.[47]

Although there are applications that requires QDs embedded in certain materials, synthesis of QDs in hosts is still not as versatile as colloidal synthesis due to low yield and lack of extraction method of QDs. Semiconductor material not only has poor solubility in melt glass (1.5% by weight[41] for example), but also forms a low quality product with a large size dispersion.

1.5.4 Bio-synthesis of QDs

Other than commonly used methods, several innovative bio-synthesis methods were invented in the past decade. Based on the proven work that genetically engineered viruses can recognize specific semiconductor surfaces through the method of selection by combinatorial phage display,[48] A. M. Belcher and co-workers created ZnS quantum dot bio-composite structures using genetically engineered M13 bacteriophage.[49] H. Masahiko et al. synthesized uniform 6 nm CdSe QDs, inside cavities of the cage-shaped protein, apoferritin.[50] More recently, size tunable CdTe QDs grown inside of yeast cells was reported in 2010.[51] Another work published in 2013 even took on step further by realizing CdTe QDs inside of living earthworms.[52]

1.6 Mechanism of colloidal growth of QDs

The formation of particles in solution usually involves two stages, nucleation and growth, which is described in detail by J. W. Mullin.[53] By considering the total free energy of a

particle (surface and bulk free energies), it was found that there exists a critical radius. Particle sizes above the critical radius will keep growing while those below will be re-dissolved. In a homogeneous classic nucleation, the rate at which nuclei form is essentially affected by supersaturation, temperature and the surface free energy. After the nuclei are formed, classical crystal growth can be used to describe the process free monomers attach to nuclei. This phase is controlled by two factors, the surface reaction and monomers' diffusion rate.[54]

Several famous mechanism was put forward to describe the kinetics of these two stages. Two of them are the La Mer model and Ostwald ripening.[23, 55] The La Mer mechanism consists three steps. In the first step, there is a sudden increase in the concentration of precursors, which leads to supersaturation, and the second step, temporary nucleation. During the second step, with a very short time (almost instantly), nuclei are formed. Finally, the concentration of precursors go below the nucleation threshold, nuclei will keep growing with no more nuclei generated.

In the case of Ostwald ripening, due to their high surface free energy,[55] smaller particles start to dissolve, while larger ones keeps growing, which lowers their surface free energy. A scheme illustrating the La Mer model and Oswald ripening is shown below in Figure 1.4. QDs colloidal synthesis are quenched before the Ostwald ripening stage.

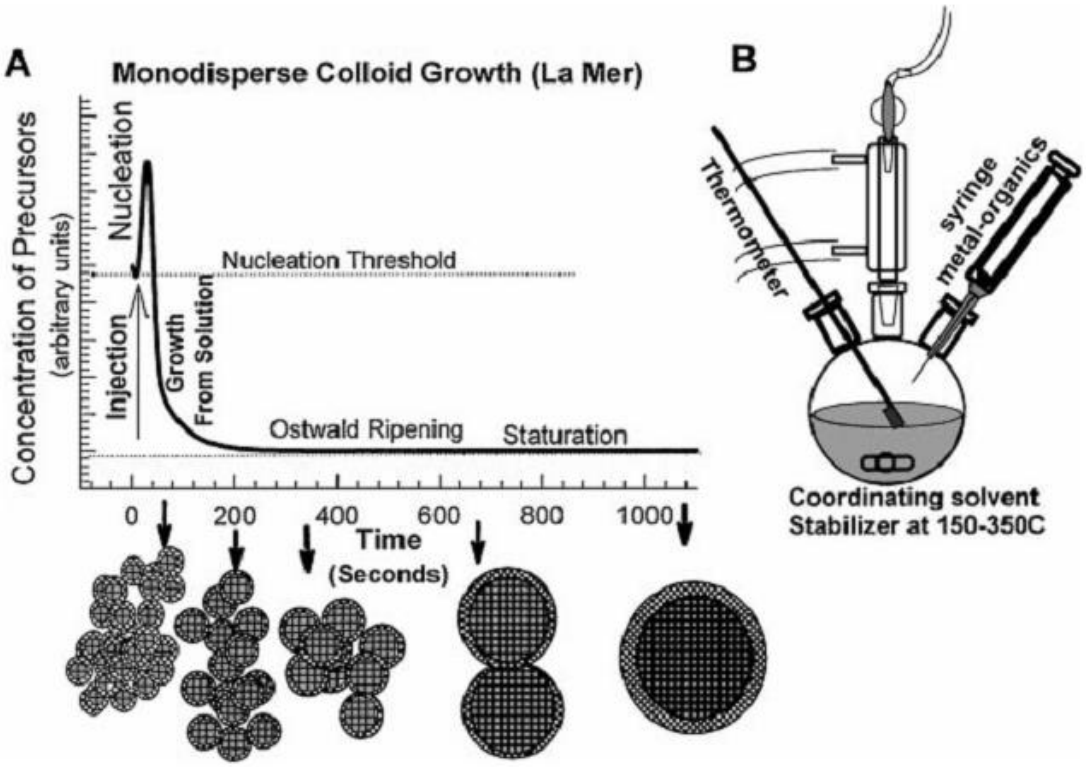

Figure 1.4. (A) LaMer model for stages of nucleation and Ostwald ripening of colloidal particles. (B) Hot-injection method for quantum dots synthesis. (With permission from publisher)[23]

K. Yu et al. utilized UV-vis spectrometry to study the growth of magic-sized CdSe QDs.[56] Magic-sized particles are those of a well-defined size such as $(CdSe)_{33}$ and $(CdSe)_{34}$.[57] Yu suggested that only nucleation was involved in the formation of magic-sized CdSe QDs. The same method was also used by A. L. Brazeau and N. D. Jones to study the synthesis of PbS QDs.[58] They showed that the actually mechanism was more complicated with the oriental attachment and Ostwald ripening weighing in. It was also proved that either of the two dominated at different temperature regimes. The SAXS (small angle X-ray scattering) is another method commonly used to characterize the growth mechanism of QDs. The growth of silica particles was looked into by A. R. Rennie and co-workers.[59] They believed that after the classical nucleation, coagulate was in charge of the particle growth. Coagulate happens when monomers bind to nuclei without any order, whereas oriental attachment forms crystalline structure.

Till now, efforts have been made to reveal the mechanism of QDs growth. People have confirmed different processes for different types of QDs, and it's very common that two or more mechanisms are seen in one synthesis. However, no literature has drawn a generalized conclusion on how nucleation was achieved. This is partially due to the fast nucleation in most QDs synthesis which makes it extremely hard to trace using normal lab equipment.

1.7 Near infrared QDs and Core-shell QDs

QDs have applications in telecommunication,[60] bio-imaging and diagnostic,[8, 61-64] solar cell,[65, 66] photovoltaic,[67, 68] and quantum computation.[69, 70] Among all these various applications, bio-imaging is probably the one attracting the most attention in recent years. One obstacle we are facing is the large amount water and hemoglobin in human body that absorbs light heavily as shown in Figure 1.5. The region where both water and hemoglobin absorb relatively low is known as the NIR window.[71] Fluorophores emitting in this region would be suitable for non-invasive in vivo imaging.

There are different types of NIR emitting QDs like PbS and PbSe,[72-76] HgTe,[77] InAs and InP,[78] Ag_2S[79] and etc. All of them can be potential candidates for bio-imaging material. However, before people move on to inject these fluorophores into human, they need to be stable and non-toxic. One common solution is to grow a core-shell structure. A layer of passivation shell can not only prevent the core material from oxidation, but it also blocks the toxic heavy metal compounds inside. A good example was shown by S. N. Bhatia et al.[80] CdSe QDs alone is prone to surface oxidation and toxic to cells. Whereas with the help of a ZnS capping layer, coated QDs showed long-term stability and no obvious deleterious effects.

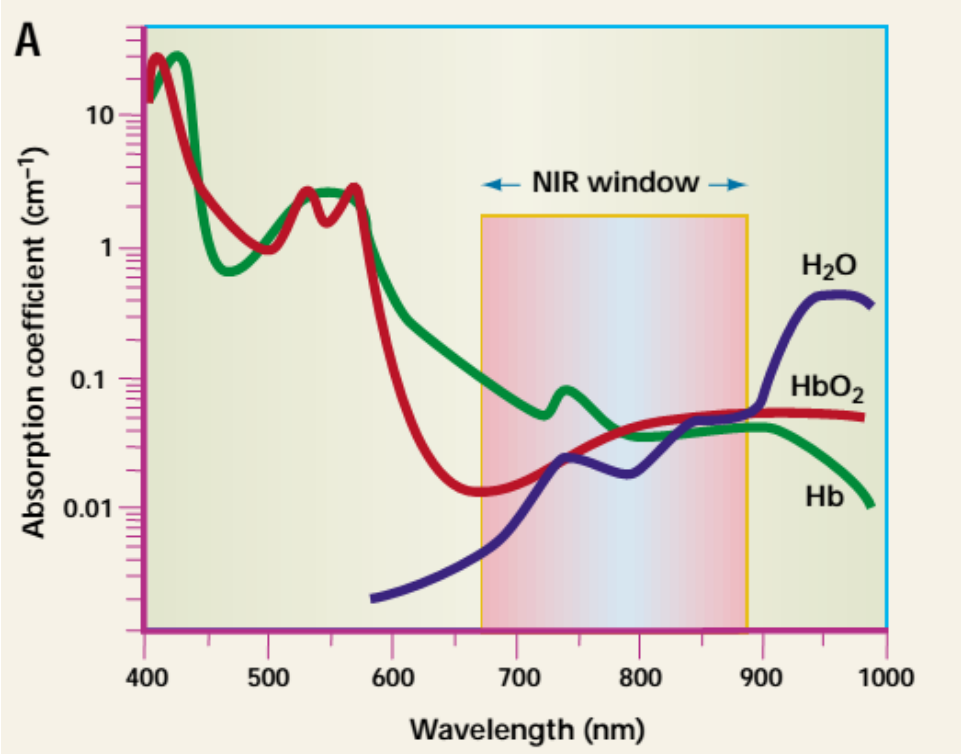

Figure 1.5. NIR window of human body. (With permission from publisher)[71]

There are essentially two types of core-shell QDs, type-I and type-II QDs.[81] In type-I QDs, the conduction band of the shell has a higher energy than that of the core, and the valence band has a lower energy than that of the core, so that both the electrons and the holes are confined in the core. In the case of type-II QDs, both the valence and conduction bands of the shell are higher (or lower) than that of the. As a result, when the electrons are confined in the core, the holes are in the shell, or vice versa.[82] A figure illustrating band layout of type-I and type-II QDs is shown below.

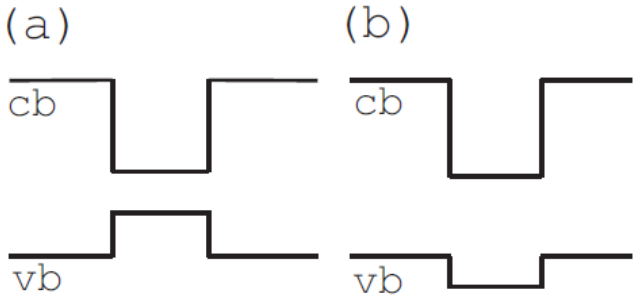

Figure 1.6. Band layout of (a) type-I and (b) type-II core-shell QDs. (With permission from publisher)[82]

In Figure 1.6, the y axis (not shown) means the electron energy of the band. Each horizontal line represents either the highest energy level in the valence band or the lowest in the conduction band for the respective material. The two horizontal lines in both (a) and (b) represents the conduction and valence band of the core, while the lines on both sides stand for those of the shell.

Chapter 2 Data and discussion of core-shell-shell QDs

2.1 Synthesis of PbSe and PbS colloidal quantum dots

For decades, a lot effort was put into the synthesis of PbSe QDs for, but not much was published before the 21st century. G. Hodes et al. were the very first to try chemical deposition to make PbSe nano-particles.[83] They successfully obtained PbSe crystalline thin films. However, those crystals were very large and not very well size-controlled. Using phosphate glass as the media, A. A. Lipovskii et al. synthesized PbSe QDs with diameters ranging from 2 to 15 nm.[41] In addition, they measured the UV-absorbance of these QDs, showing that bandgap of PbSe QDs decreased as size was enlarged, as expected. Although they had done preliminary measurements on PbSe QDs, much work was still needed to investigate the properties of PbSe QDs better. On one hand, PbSe QDs synthesized using this method were constrained in the glass; on the other hand, the chemical yield was low. Thus, the need for colloidal PbSe QDs emerged.

In 2001, C. B. Murray and co-workers became the first to synthesized colloidal PbSe QDs.[22] The reaction was done by injecting room-temperature lead oleate and trioctylphosphine selenide, into a rapidly stirred solution containing diphenylether at high temperature. The temperature of solution and growth time of QDs were tuned to obtain QDs with different sizes ranging from 3.5 to 15 nm in diameter. A size dispersion of about 10% was reported in the article. The oleic acid in this case acted as the coordinating ligand while diphenylether was used as the non-coordinating solvent. Following this method, several groups investigated the properties of PbSe QDs. T. D. Krauss et al. measured the absorbance of PbSe QDs of different diameter. The result matched what C. B. Murray had observed, and indicated a size variation of 5 to 10%.[84] The quantum yield of QDs synthesized by them was found to vary from 12 to 81%. The absorbance of PbSe QDs with different sizes is shown below.

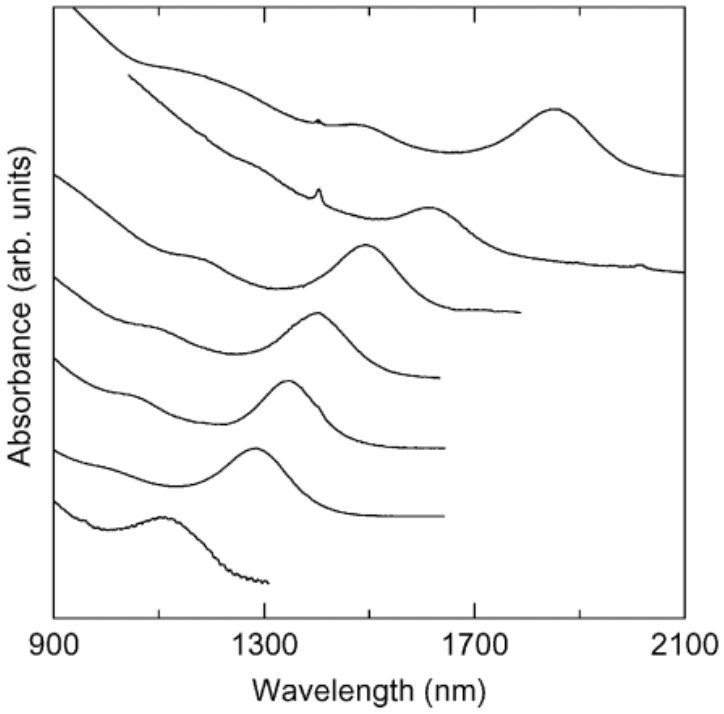

Figure 2.1. Linear absorption spectra of PbSe QDs ranging in size from 3 to 8 nm. (With permission from publisher)[84]

The same measurement was done by P. Guyot-Sionnest and co-workers.[85] They found that QY could be as high as 85%, agreeing well with what H. Du got.[84] Moreover, they observed that bandgap tuned strongly with the temperature. A similar hot-injection method using tributyl-phosphineselenide (TBP-Se) and lead 2-ethyl-hexanoate was reported by the Lifshitz group.[86] A modified synthesis using 1-octadecene as the non-coordinating solvent was published in 2004 by W. W. Yu et al.[87] 1-Octadecene is cheaper and more environmentally friendly compared to diphenylether. Additionally, it resulted in the growth of larger PbSe QDs, which had a narrower size dispersion (5 to 7%) compared to C. B. Murray's QDs and high quantum yield (85%).

Our group investigated the stability of PbSe QDs synthesized using the modified method.[88] It was found that PbSe QDs showed a blue shift in both absorption and emission spectra when stored in solvents. This blue shift could be accelerated upon light exposure.

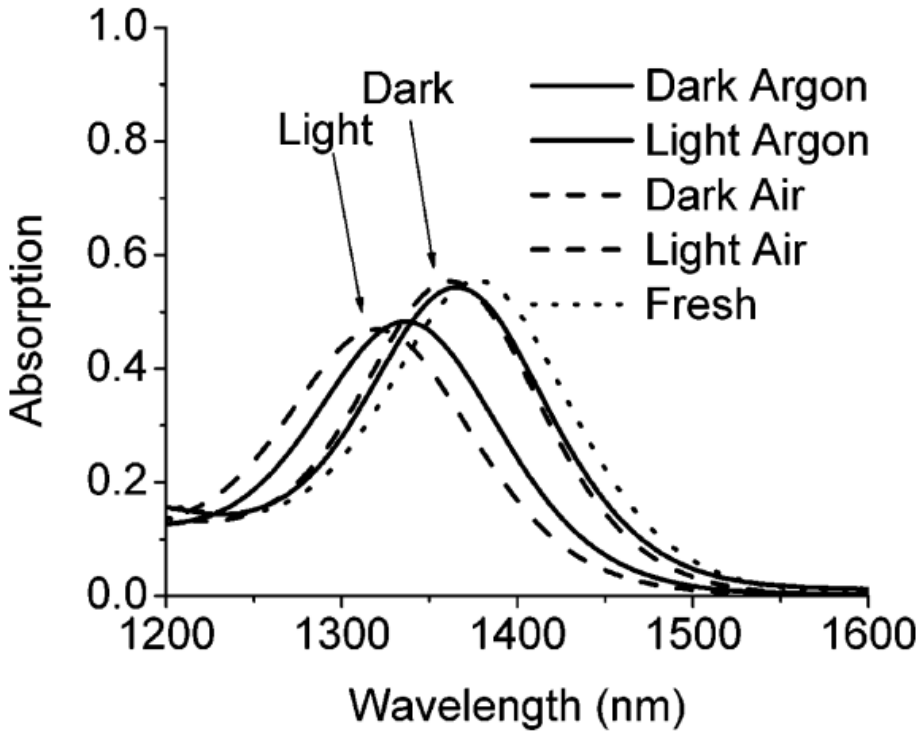

Figure 2.2. Absorption spectra of PbSe NCs stored for 42 days under different conditions. The NCs with the largest blue shift compared to the fresh sample were stored in room light; the other two were stored in the dark. The dashed spectra are of NCs stored under ambient conditions; the solid lines are of NCs stored under Ar. (With permission from publisher)[88]

It is shown in Figure 2.2 that when stored in either argon or air, the blue shift was more significant in the light-exposed batch compared to that was in darkness. This suggests that the oxidation of PbSe QDs is a photon-assisted process. The authors believed that light exposure can strip off the binding ligands on QDs' surface, making them more accessible for oxygen.

The preparation of PbSe QDs was done according to the method described in the experimental section. A typical batch of PbSe QDs under TEM and its size dispersion histogram are shown below.

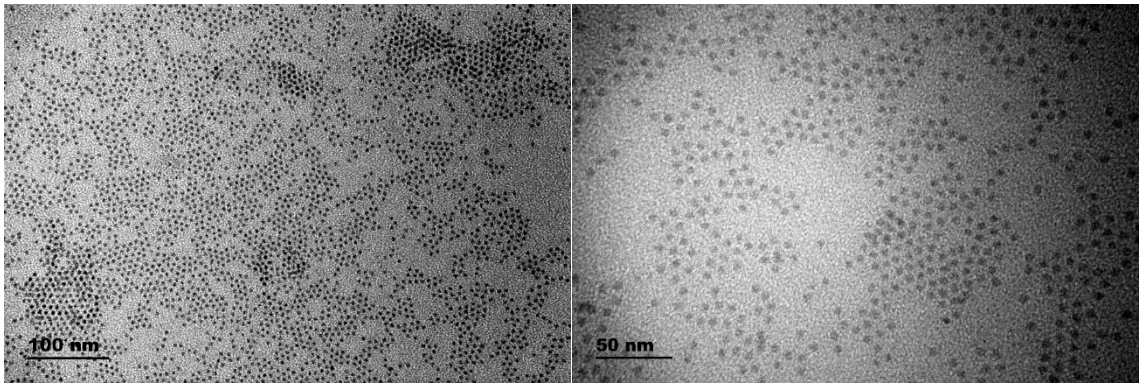

Figure 2.3. TEM images of PbSe QDs with different magnifications (left) 300,000 and (right) 600,000.

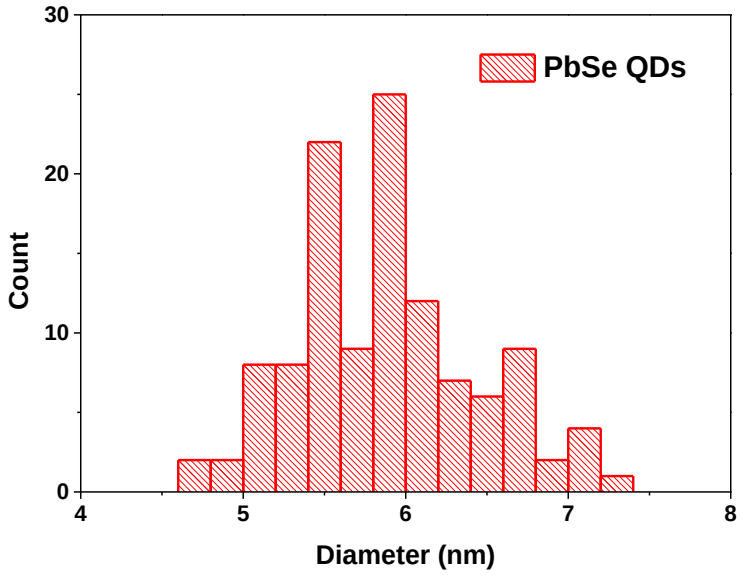

Figure 2.4. Histogram of PbSe QDs synthesized at 140 ℃ for 3 minutes.

This batch **(088/CJM/14)** was synthesized at 140 C° for 3 minutes. The size of it is determined to be 5.88 ± 0.56 nm, using imageJ as described in the experimental section. The size dispersion shows great mono-dispersity. The absorption and emission of it is as Figure 2.5. The quality of this batch is well, with well-defined emission and the first absorption peaks at 1355 and 1395 nm, respectively. The narrow FWHM (full width at half maximum) of the emission is about 80 meV. Also, higher order absorption peaks are

distinguished, also indicating good quality. The sharp spike at about 1380 nm in the emission curve is due to the correction file for water vapor.

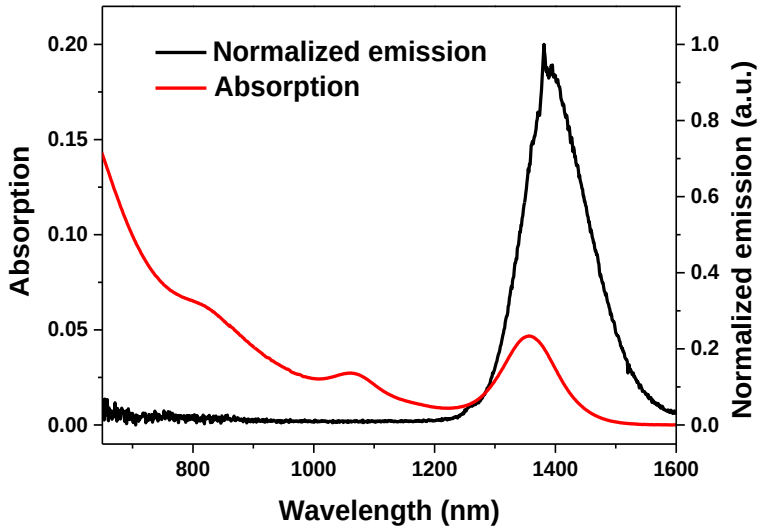

Figure 2.5. Absorption and normalized emission of PbSe QDs. Sample was dissolved in TCE with the 632 nm HeNe laser as the excitation source.

There were different approaches tried by many groups to synthesize PbS QDs. R. Kasowski et al. embedded PbS QDs in ethylene-15% methacrylic acid copolymer (E-MAA) and observed discrete absorption bands.[42] More polymer-embedded PbS QDs were made by several other groups.[43, 89, 90] N. F. Borrelli and D. W. Smith were the first to crystalize PbS in inorganic glass.[38] Similar to the work they did on PbSe QDs, A. A. Lipovskii et al. synthesized PbS QDs with diameters from 2.5 to 15 nm in phosphate glass.[40] Their UV-absorbance spectra indicated narrow size dispersion and different band transitions. There are other media like zeolite[91] and methods like chemical depositing on different substrates.[46, 92] The first colloidal synthesis was reported by L. E. Brus and co-workers.[93] A different route was put forward by O. I. Mitic[94] and followed by several other groups.[95]

Despite all this work, synthesis of high yield PbS QDs was only first reported in 2003, by M. A. Hines and G. D. scholes.[96] A narrow size-dispersion (10 to 15%) was achieved

via an organometallic synthetic route. Using bis(trimethylsilyl)sulfide [$(TMS)_2S$] as the sulfur source, QDs with absorption ranging from 800 nm to 1800 nm were prepared. The FWHM of the emission was determined to be about 100 meV, which resulted from a size dispersion of 10 to 15%. In addition, the quantum yield of these QRs was around 20%. However, the author observed size focusing after the product was isolated from the reaction mixture. In Figure 2.6 (a), the absorption peak of the original QDs shifted with time. The size dispersion of the QDs after 24 hours' storage [Figure 2.6 (c)] was much smaller compared to what it looked like in the beginning [Figure 2.6 (b)]. The authors believed that digestive ripening was the main reason for this phenomenon.

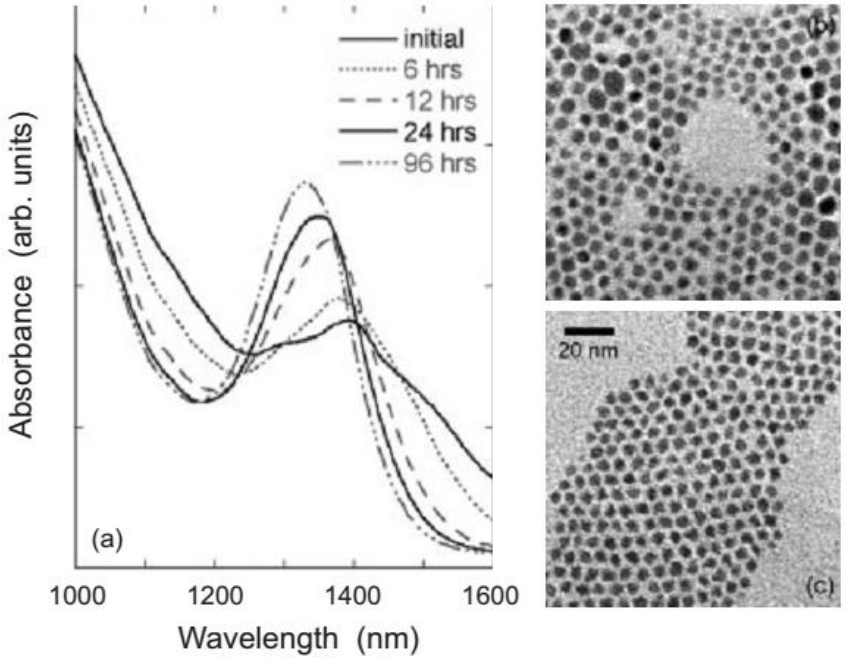

Figure 2.6. (a) Absorption of a batch of PbS QDs in toluene at different time intervals after synthesis. The evolution indicates a self-focusing of the size dispersion. (b) TEM image of original PbS QDs. (c) PbS QDs after 24 h. (With permission from publisher)[96]

Our group brought TOP into the synthesis of PbS QDs and changed the Pb:S ratio to get a better quality.[73] As a result, the final product had well mono-dispersity and quantum yield could be as high as 80% in good batches. In addition, the size focusing effect was not observed. The emission peaks of QDs synthesized shifted slightly after two weeks, which was due to photooxidation. Size-dependent absorption of PbS QDs synthesized by us is

shown in Figure 2.7. Another widely used colloidal preparation method of PbS QDs was developed by G. A. Ozin and his group.[97] Instead of PbO and ODE, they used $PbCl_2$ as the Pb source, and oleylamine as the solvent. Moreover, sulfur was dissolved in oleyamine and hot-injected, as the S source.

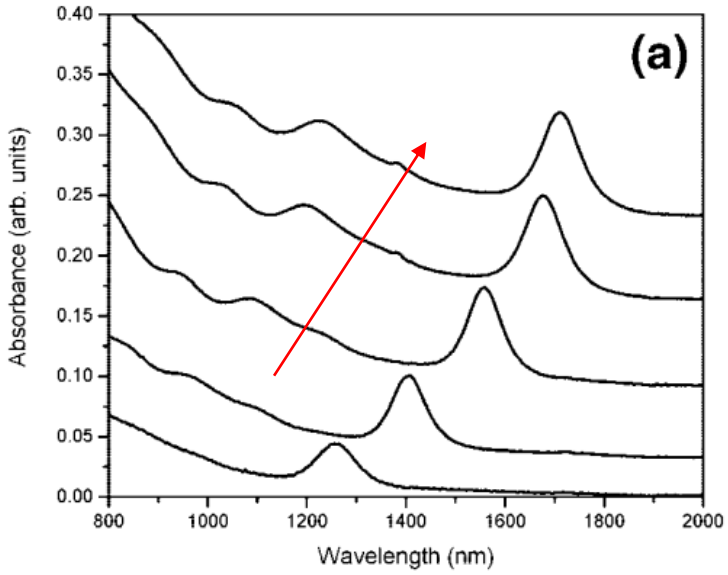

Figure 2.7. Absorption of PbS QDs with increasing sizes from left to right. (With permission from publisher)[73] The arrow indicates the size increase.

The synthesis of PbS QDs used the same method developed by us,[73] and the detail is presented in the experimental section. A typical batch of PbS QDs under TEM and its size dispersion histogram are shown below.

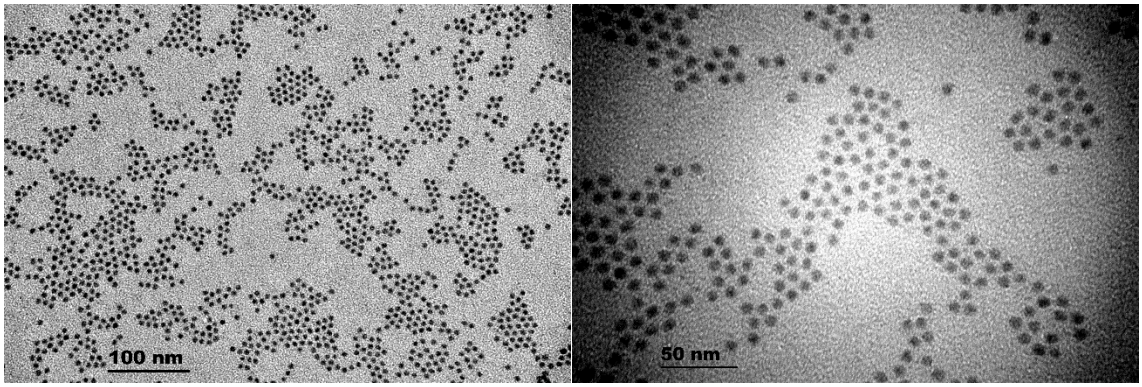

Figure 2.8. TEM images of PbS QDs with different magnifications (left) 300,000 (right) 600,000.

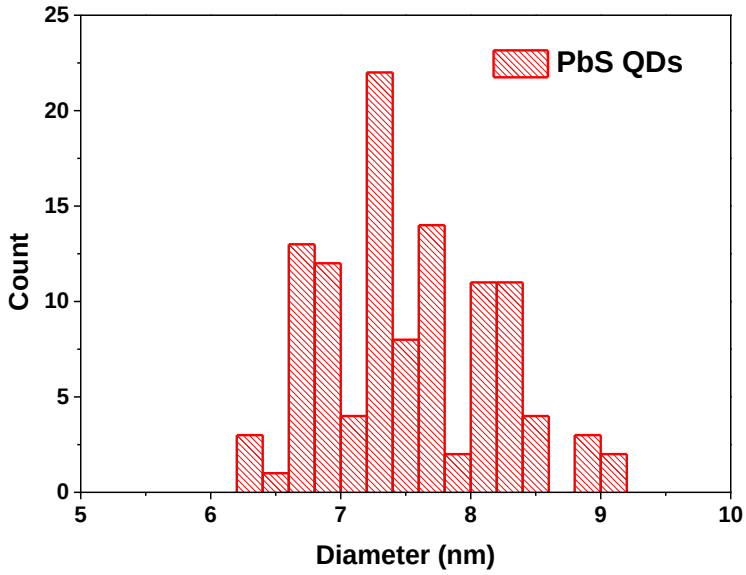

Figure 2.9. Histogram of PbS QDs synthesized at 120 ℃ for 4.5 minutes.

As shown in Figure 2.8, the PbS QDs **(117/CJM/14)** show very good mono-dispersity with an average size being 7.52 ± 0.65 nm. This batch was synthesized at 120 ℃ for 4.5 minutes. The absorption and emission of another batch (**096/CJM/14**) using the same temperature but 4 minutes is presented in Figure 2.10. This batch also show high quality with well-defined emission and first absorption peaks at 1520 and 1503 nm, respectively. The FWHM of the emission peak is about 60 meV, also suggesting a very narrow size dispersion.

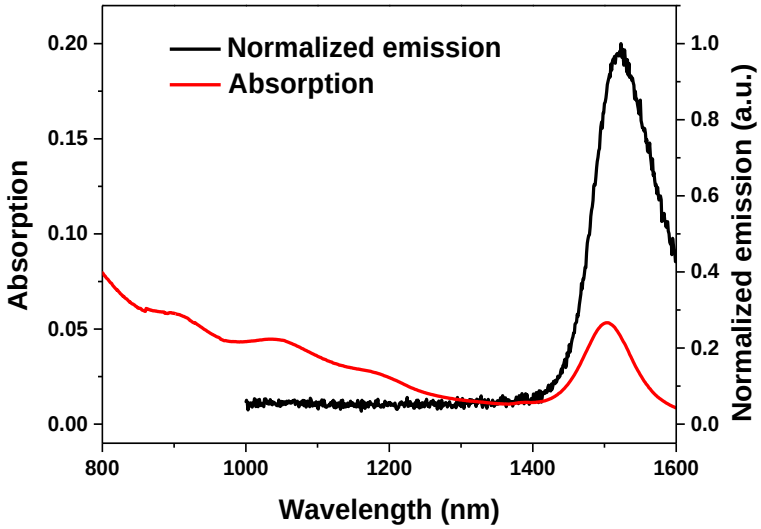

Figure 2.10. Absorption and normalized emission of PbS QDs. Sample was dissolved in TCE with the 632 nm HeNe laser as the excitation source.

2.2 Synthesis of PbSe-CdSe and PbS-CdS core-shell quantum dots

Lead-based QDs gradually experience oxidation once synthesized.[88] As a result, oxidation leads to size reduction of QDs, which opens up the energy gap. This is why lead-based QDs show blue shift after storage. In order to increase the stability of them, a second shell is normally used. There are two ways to get a core-shell structure: (i) to grow another layer outside, (ii) to use cation exchange to replace the outer layer of the the original core. Cation exchange on nanorsystals was first reported by A. P. Alivisatos and co-workers in 2004.[98] They showed that cation exchange on nanocrystals could be completely and reversibly in ambient environment, which is well illustrated by Figure 2.11. The CdSe QDs they made were completely cation exchanged, then fully recovered. This was supported by the XRD (X-ray diffraction), absorption and fluorescence measurements.

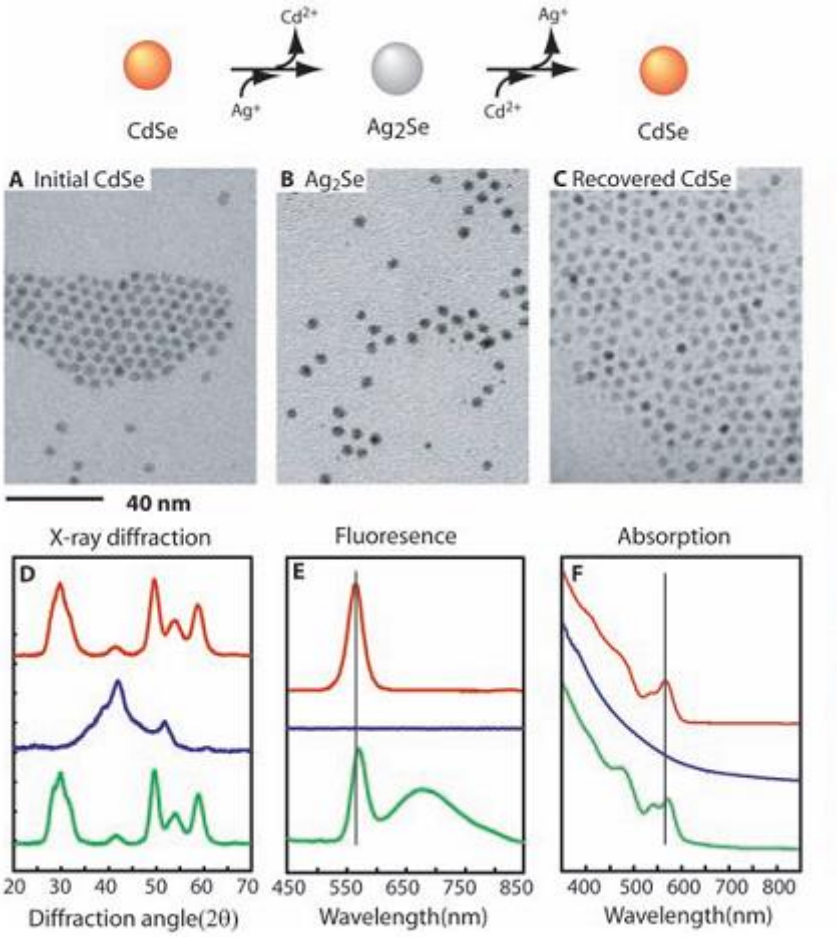

Figure 2.11. TEM images of (A) initial CdSe (diameter 4.2 nm), (B) Ag_2Se transformed from the forward cation exchange reaction, and (C) recovered CdSe nanocrystals from the reverse cation exchange reaction. (D to F) XRD patterns, fluorescence emission, and optical absorption spectra of initialCdSe (red), Ag_2Se (blue), and recovered CdSe (green) nanocrystals, respectively. (With permission from published)[98]

One of the most effective way is to grow a passivating CdSe shell, which was published by J. A. Hollingsworth and co-workers.[99] They obtained a PbSe-CdSe core-shell structure with Pb^{2+} partially exchanged by Cd^{2+}. The final product showed excellent stability against photo-oxidation compared to the original cores in ambient light exposure. A CdSe shell will keep electron-hole pairs confined in the PbSe core, as well as removing the surface defects, leading to a higher quantum yield. Moreover, this method is applicable to other lead-based QDs like PbS QDs. The author showed that PbS-CdS QDs that emit from 800 to 950 nm could be made successfully. Because this method is a cation exchange reaction,

the size of the original QDs won't change after the core-shell structure formation, but the size of the cores shrinks. Both PbSe-CdSe and PbS-CdS QDs are type-I QDs, and a smaller size opens up the energy gap of the core, leading to a blue shift. This is well illustrated by Figure 2.12.

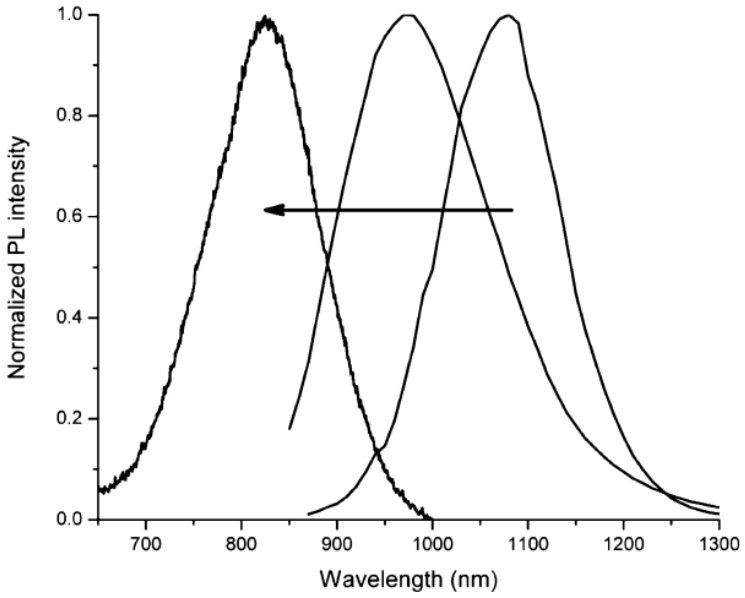

Figure 2.12. PL spectra of PbS and PbS/CdS NQDs. The arrow indicates progress of reaction during the CdS shell formation. (With permission from publisher)[99]

As we can see from the figure above, with longer reaction time, the Cd shell got thicker, and the core got smaller. Thus the blue shift became more obvious. Our group confirmed the core-shell structure formed using this method by the High-Angle Annular Dark Field imaging (HAADF) and energy-dependent X-ray Photoelectron Spectroscopy (XPS).[100] Images of the HAADF are generated by collecting elastically scattered electrons. The larger atomic number one element has, the higher electron density it will have. As a result, more incident electrons will be scattered and collected by the detector. Due to this, it is considered a good way for elemental analysis. Because Pb and Cd have atomic numbers of 82 and 48, respectively, they would present very different brightness in the HAADF images. As expected, a clear contrast (see Figure 2.13) between the brighter cores and darker shells evidently proves the core-shell structure.

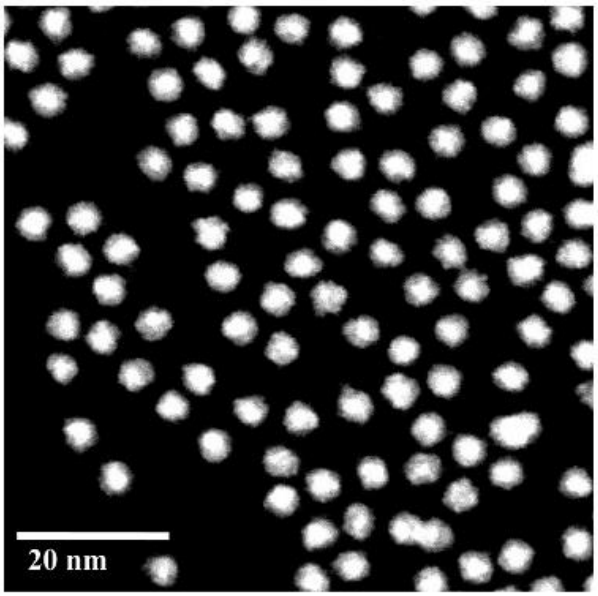

Figure 2.13. HAADF image of PbSe/CdSe core/shell QDs. Both core (bright) and shell (dark) contrast are visible in the image. (With permission from publisher)[100]

Synthesis of PbSe-CdSe and PbS-CdS QDs followed the same method, but with different temperature and concentrations of precursors. Detailed synthesis will be presented in the experimental section.

2.3 Synthesis of PbSe-CdSe-ZnS and PbS-CdS-ZnS core-shell-shell quantum dots

In the same article where the cation exchange was first used on lead-based QDs,[99] J. A. Hollingsworth et al. also successfully capped PbSe-CdSe core-shell QDs with ZnS shell. A second shell made of ZnS could potentially further enhance the optical property and stability of the original core-shell, although they didn't observe any increase in QY from core-shell to core-shell-shell in that article. Compared to Pb^{2+} and Cd^{2+}, ZnS will reduce the toxicity drastically by keeping those ions inside, making these QDs potential bio-imaging material.

We followed the same way that J. A. Hollingsworth et al. used to grow the second shell. Detailed synthesis is presented in the experimental section.

2.4 Data and discussion

2.4.1 TEM results

TEM images of both core-shell and core-shell-shell QDs were taken as described in the experimental part. All QDs look spherical and similar in size for the same sample. For each sample, one image at 300,000 and 600,000 magnification each are shown below. Size of each sample was calculated by taking the average and standard deviation of at least 100 isolated particles. Numbers are given by ImageJ software directly. The average diameter of PbSe-CdSe QDs is 4.93 $\pm$ 0.44 nm and the average diameter of PbSe-CdSe-ZnS QDs is 5.23 $\pm$ 0.53 nm. A 0.3 nm growth in size suggests that we have successfully grew a ZnS shell over CdSe. Similarly, the diameter of PbS-CdS QDs is 5.63 $\pm$ 0.56 nm, and the diameter of PbS-CdS-ZnS QDs is 6.30 $\pm$ 0.64 nm, also proves the existence of the second shell. The calculated standard deviation being about 10% of the average diameter indicates a narrow size dispersion.

Histograms of each core-shell and core-shell-shell QDs are shown below as well. It is easy to find the trend of size change by comparing histograms of core-shell QDs to that of core-shell-shell QDs.

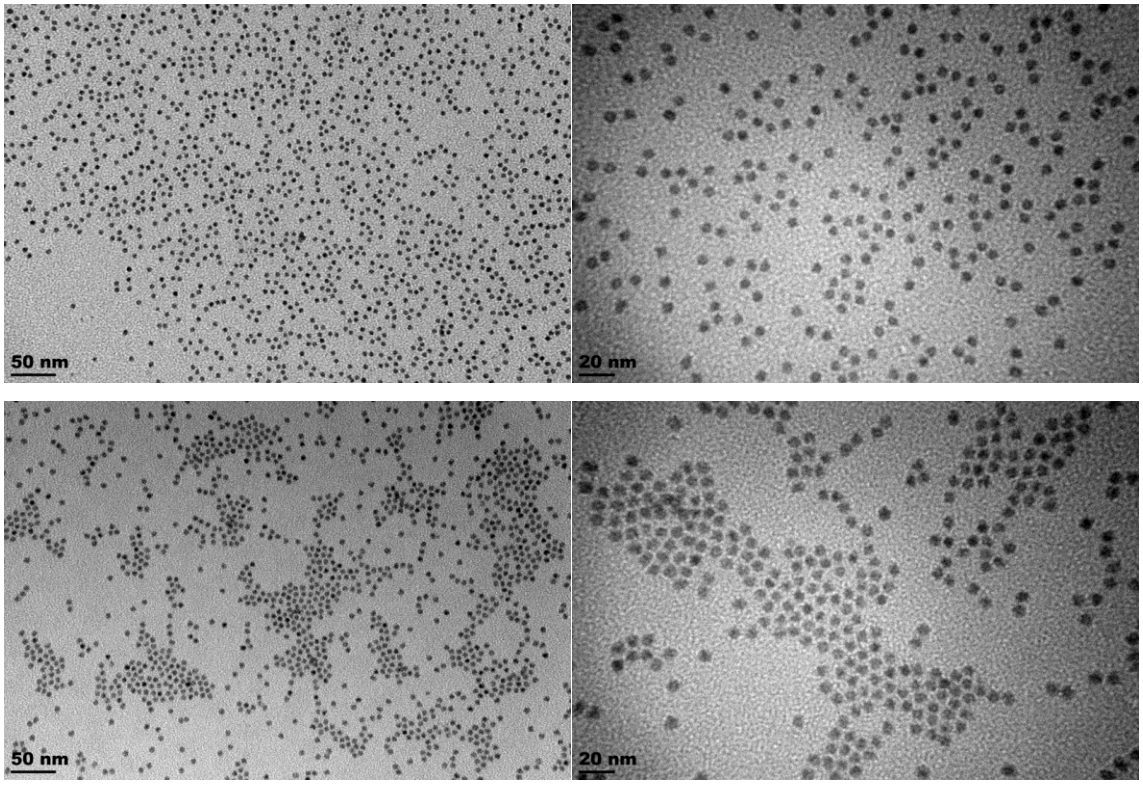

Figure 2.14. TEM of PbS/CdS (first row) and PbS/CdS/ZnS (second row) at 300,000 and 600,000 magnification, respectively.

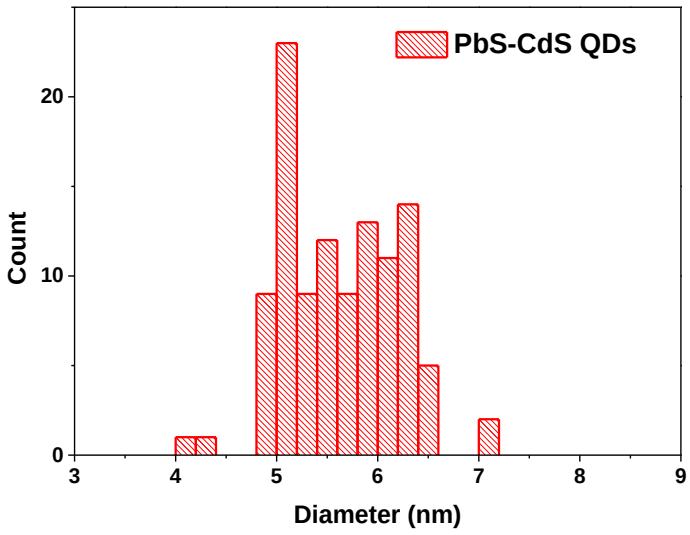

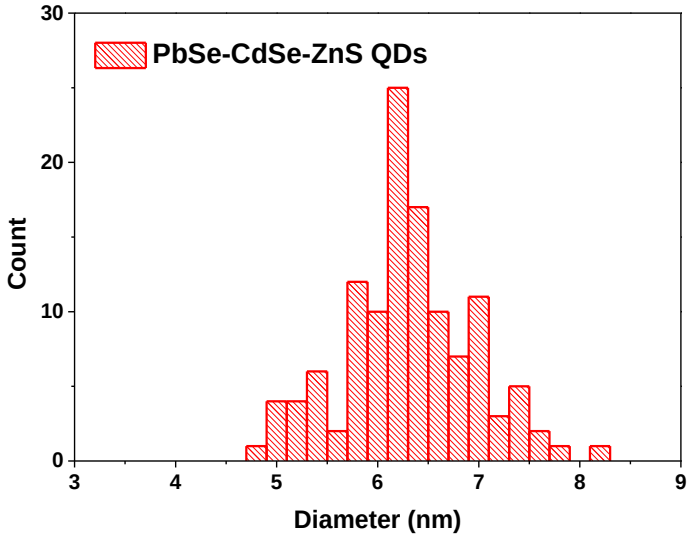

Figure 2.15. Histograms of PbS-CdS (top) and PbS-CdS-ZnS (bottom) QDs.

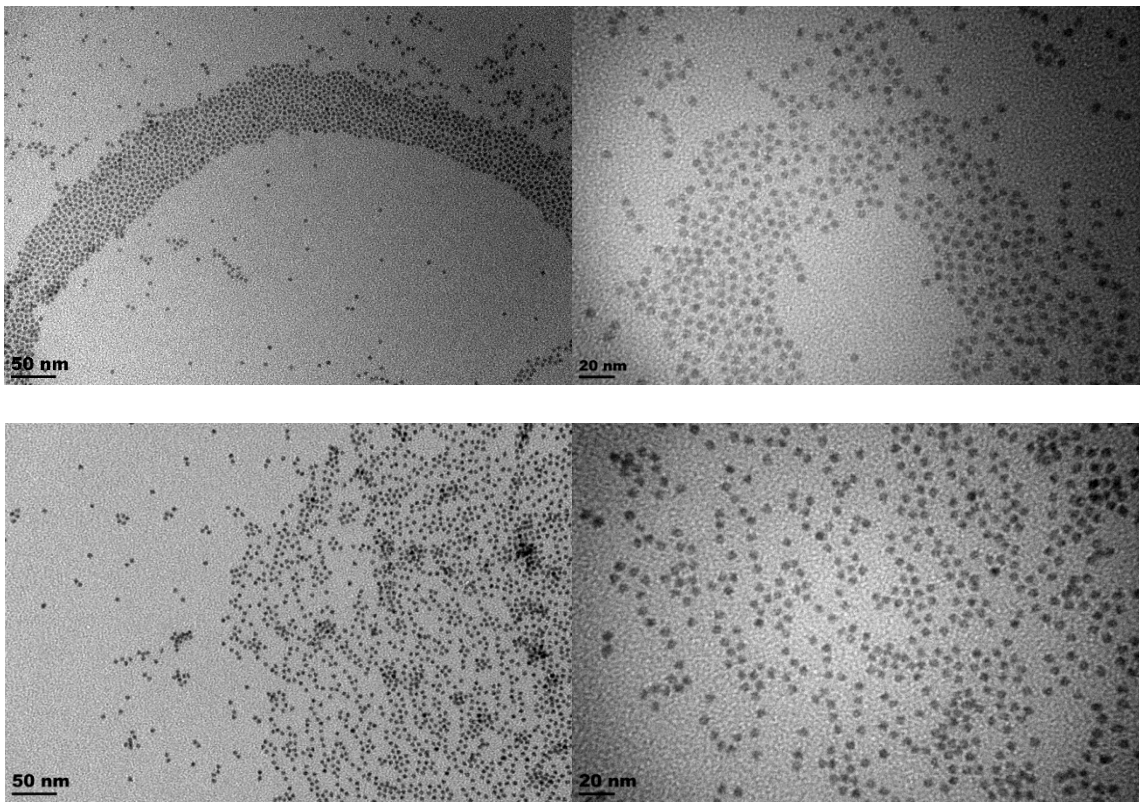

Figure 2.16. TEM of PbSe-CdSe (first row) and PbSe-CdSe-ZnS (second row) at 300,000 and 600,000 magnification, respectively.

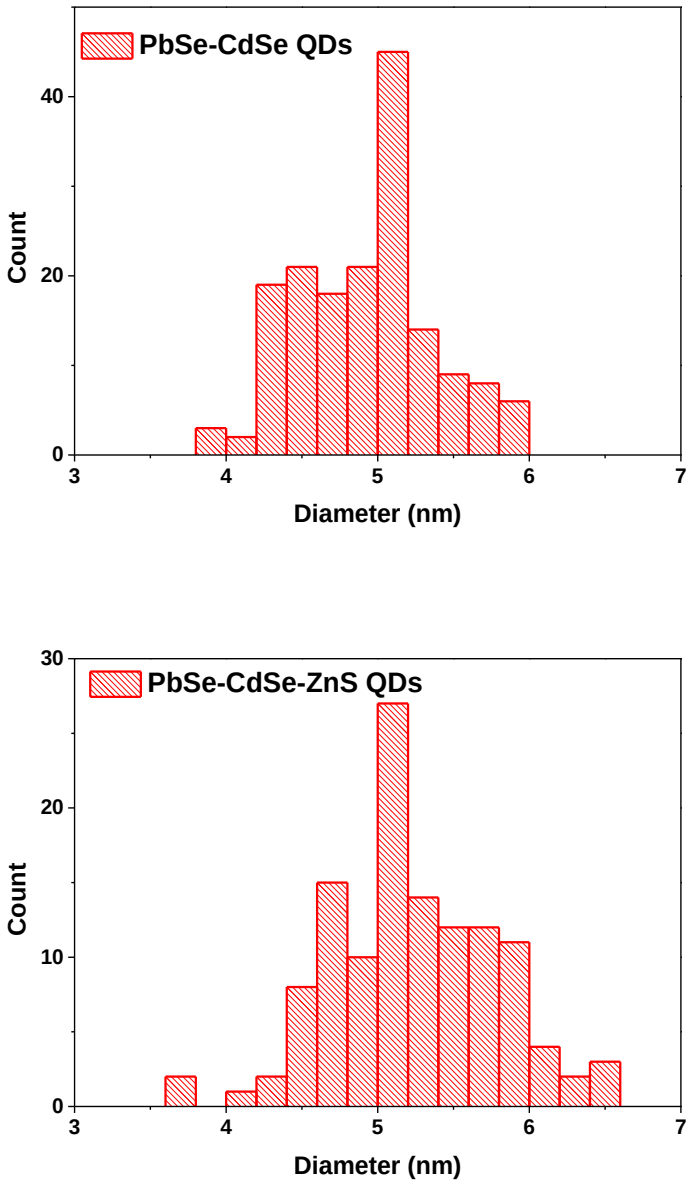

Figure 2.17. Histograms of PbSe-CdSe (top) and PbSe-CdSe-ZnS (bottom) QDs.

2.4.2 UV-absorption results

All UV-absorption measurements were done at room temperature. UV-spectra of core-shell and core-shell-shell QDs are shown below in Figure 2.18. The PbSe-CdSe and PbSe-

CdSe-ZnS QDs don't show very well-pronounced absorption peaks. This is also observed by J. A. Hollingsworth et al. in all their core-shell and core-shell-shell QDs.[99] The small curving up at about 1080 nm in the PbSe-CdSe QDs' absorption curve is from the first absorption peak.

Compared to the PbSe-CdSe QDs, the PbS-CdS QDs have a clear first exciton at 1350 nm. The peak is less obvious in the absorption curve of PbS-CdS-ZnS QDs, but it is still at the same position. CdSe and CdS have larger bulk bandgap of 1.74 eV and 2.42 eV compared to that of PbSe and PbS, which are 0.27 eV and 0.37 eV. Cubic bulk ZnS has an even larger band gap of 3.54 eV compared to CdS and CdSe.[101] The coating of ZnS wouldn't change the optical properties of the core-shell QDs inside. This explains why the absorption hardly change from core-shell to core-shell-shell QDs. This is supported by the same absorption peak location in PbS-CdS and PbS-CdS-ZnS QDs.The small dig or bulge in both figures at about 1380 nm are caused by the correction file for water vapour absorption. The other small dig at 860 nm is from the instrument itself, because the light source switches from a NIR light source to a visible one.

The core-shell solutions had concentrations of about 0.3 mg/ml, while those of core-shell-shell QDs were about 0.2 mg/ml. Consider the existence of one extra layer, each core-shell-shell QD is heavier than a core-shell QD. Combining the lower concentration and heavier weight of one particle, it makes sense that core-shell-shell QDs have less intense absorption curves as shown below.

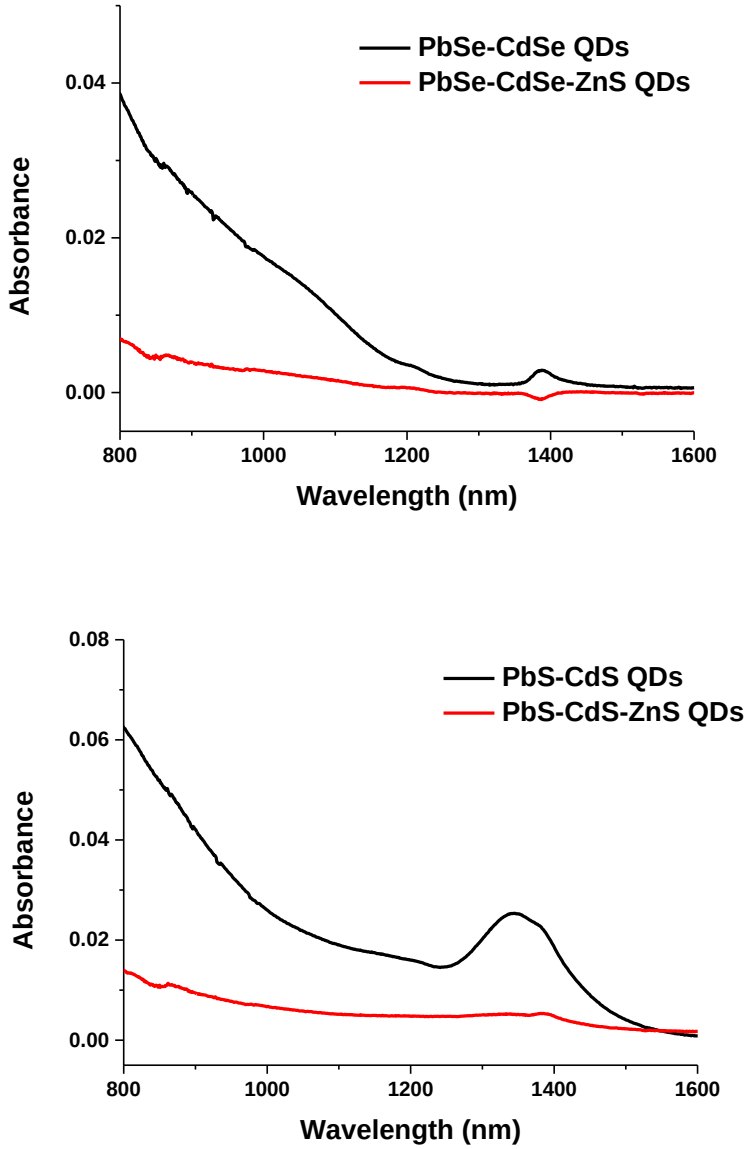

Figure 2.18. UV-absorption spectra of core-shell (top) and core-shell-shell (bottom) QDs. Sample was dissolved in TCE.

One possible explanation to the disappearance of absorption peaks from core to core-shell QDs is that, due to the larger surface to volume ratio of smaller cores over larger cores, they are likely to have a higher rate of cation exchange. As a result, the final cores in core-shell QDs have a larger size dispersion compared to that of before the cation exchange. When the dispersion is large enough, the first absorption peak in core-shell QDs will seem

to be missing. Another factor that contributed to it was the long cation exchange time, which was 19 hours. The longer the reaction lasts, the larger size dispersion of cores one will get. Thus the absorption will be even less distinguished. If the cation exchange was done for only 1 hour, the broadening of absorption peaks would be much less, just like what A. Keith et al. showed in Figure 2.19 from their paper.[72]

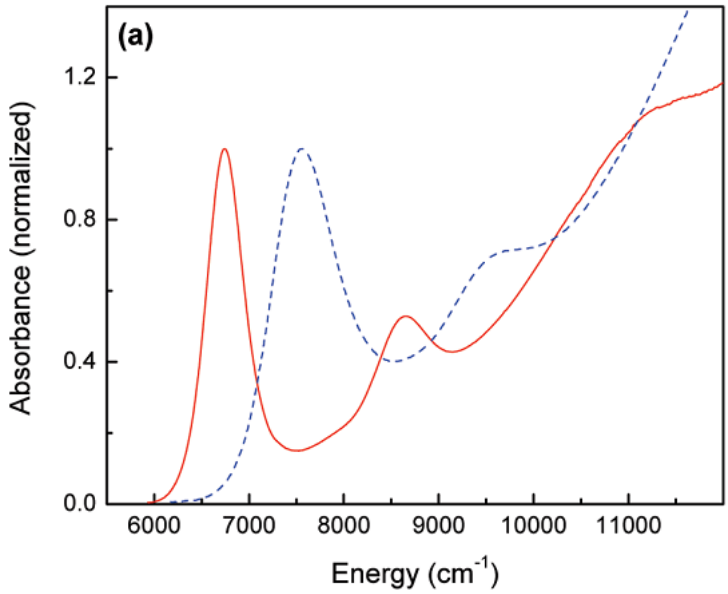

Figure 2.19. Absorption of PbSe (red) and PbSe-CdSe (dashed blue) QDs. (With permission from publisher)[72]

2.4.3 PL results

PL of core-shell and core-shell-shell QDs were taken using TCE (tetrachloroethylene) as the solvent. All PL spectra were measured from 650 to 1650 nm, which is the sensitive range of our detector. Seen in Figure 2.20, both core-shell and core-shell-shell QDs show very well defined emission peaks, indicating well mono-dispersed QDs, as supported by TEM size analysis. After coating with ZnS shell, both PbSe-CdSe and PbS-CdS QDs show a small red shift. This could be caused by loss of small core-shell particles during the ZnS shell growth. Smaller particles have a larger band gap as well as smaller emission

wavelength. The disappearance of them will red-shift the PL of the sample. Other than that, the shape and FWHM of PbSe-CdSe-ZnS hardly changed compared to the PbSe-CdSe QDs.

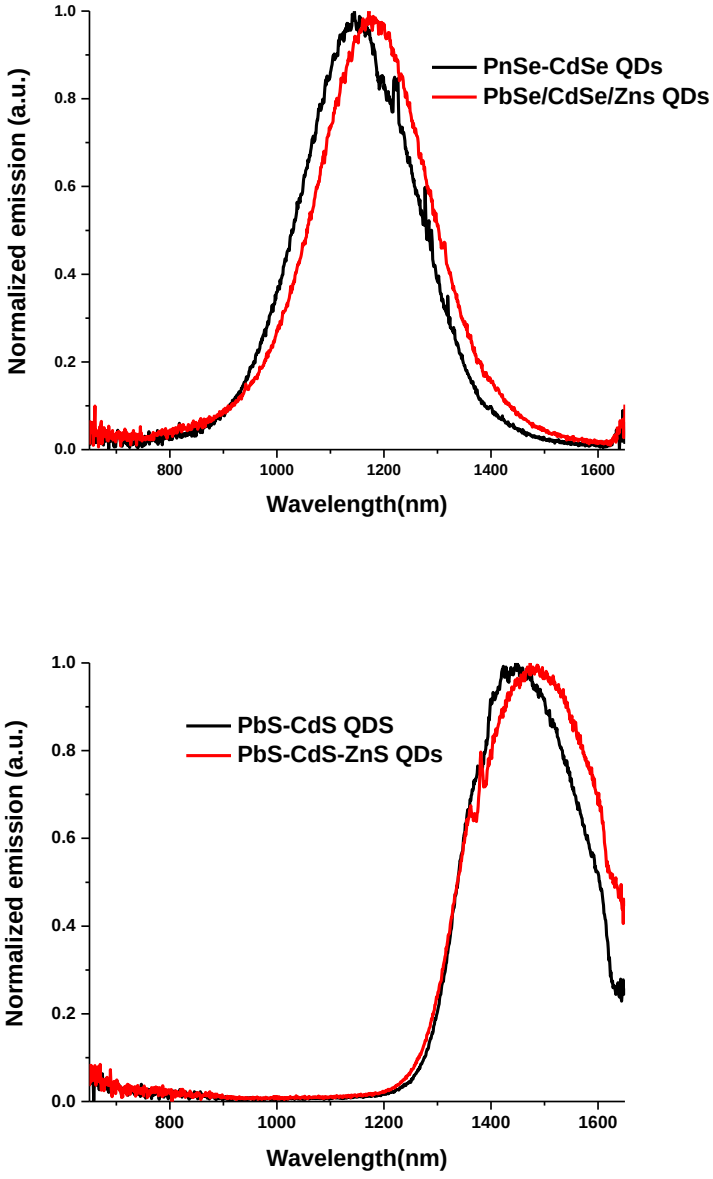

Figure 2.20. PL of core-shell and core-shell-shell QDs. Sample was dissolved in TCE with the 632 nm HeNe laser as the excitation source.

The FWHM of PbSe and PbS QDs are usually in the range of 50 to 100 meV depending on the quality of each batch. Core-shell and core-shell-shell QDs present much larger FWHM values (over 150 meV for PbS-CdS and PbS-CdS-ZnS QDs, and over 200 meV for PbSe-CdSe and PbSe-CdSe-ZnS QDs), which directly reflects a larger core size dispersion, compared to that of core QDs (less than 100 meV). This also supports the discussion on the absorption data above.

Interestingly, not all core-shell-shell QDs presented red shift compared to core-shell QDs. Two more PbSe-CdSe and PbSe-CdSe-ZnS QDs each were synthesized with different conditions, and their PL is shown in Figure 2.26. It can be seen that PbSe-CdSe-ZnS QDs in Figure 2.21 (top) had almost the same emission maximum at about 1100 nm, like its core-shell QDs precursor, instead of a red shift. Also, a slightly broader FWHM was achieved. Things got a little different on the other batch in Figure 2.21 (bottom). Rather than a red shift or the same maximum, a little blue shift was obtained. Similarly, a larger FWHM than that of its core-shell QDs precursor is presented.

If alloying happens between the PbSe-CdSe interface during the ZnS shell formation, the size of the PbSe cores would be reduced. This should give rise to the opening up of the energy gap, thus lead to emission with higher energy (smaller wavelength). The blue shift could be the result of this process.

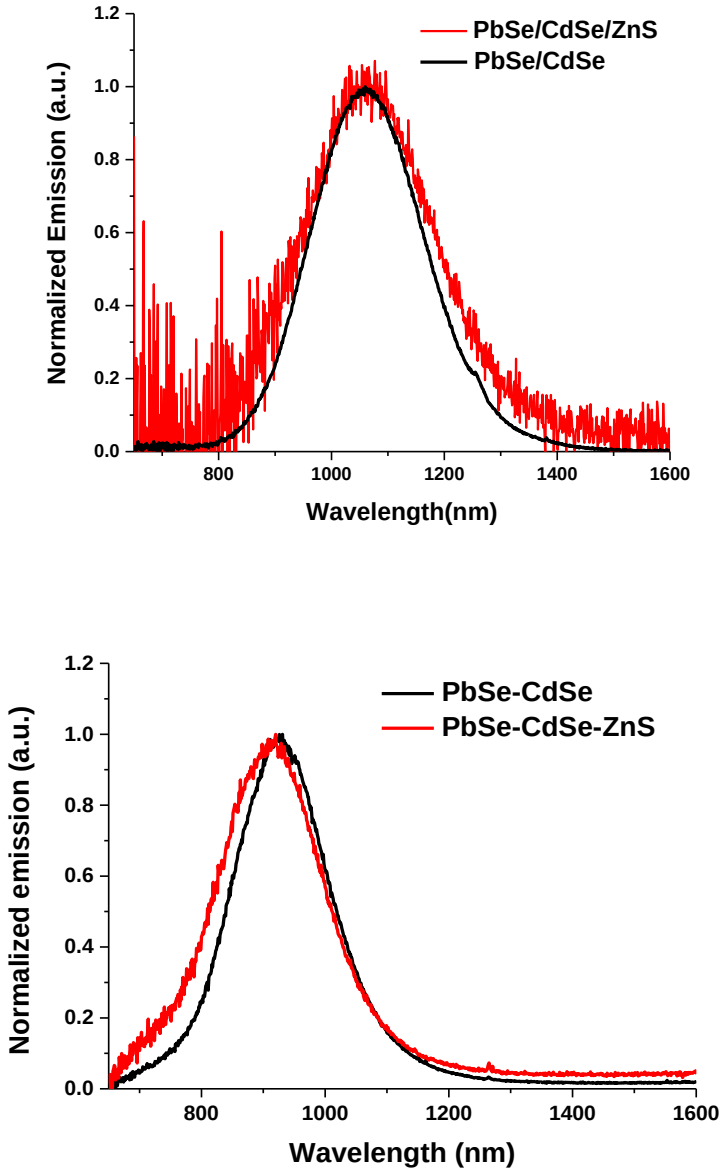

Figure 2.21. PL of **090/CJM/14** (top) and **122/CJM/14** (bottom) PbSe-CdSe-ZnS QDs and their core-shell QDs precursors. Sample was dissolved in TCE with the 632 nm HeNe laser as the excitation source.

The PL of another batch of PbS-CdS-ZnS QDs **(119/CJM/14)** was measured and compared to the PL of its original PbS-CdS QDs. No red shift but a slightly larger FWHM can be observed in Figure 2.22.

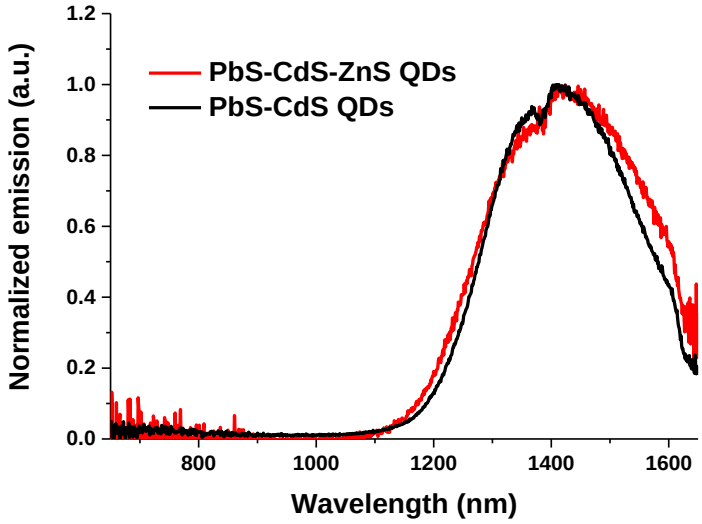

Figure 2.22. PL of **119/CJM/14** PbS-CdS-ZnS QDs and its core-shell QDs precursors. Sample was dissolved in TCE with the 632 nm HeNe laser as the excitation source.

The PL of core-shell-shell QDs are very much like their core-shell precursors in general, but always comes with a little larger FWHM. The emission maximum can be at the same position or slightly red or blue shifted. Possible reasons for the red and blue shifts are dissolution of smaller particles and alloying in the Pb-Cd interface during the reaction. Dissolution of smaller particles could reduce the FWHM in principle. If alloying happens, it will makes the cores of core-shell-shell QDs with all sizes smaller. At the end, this will broaden the size dispersion of the cores, leading to larger FWHM. The actual process may involve both them because there are batches whose emission maximum were not shifted. The scientific reasons for the shift is worthy of more research to confirm.

2.4.4 Long-time stability results

Core-shell and core-shell-shell QDs were kept in vials filled with air, away from light at room temperature. Emission of all samples were measured 10 and 20 months later and compared with emission measured on the day they were synthesized. All results are shown below in Figure 2.23 and Figure 2.24. PL of PbSe-CdSe and PbS-CdS QDs have no change over a long period. The curving up at after 1600 nm and below 800 nm in both figures is artifacts caused by the correction file of the detector. The peak is at the same position and FWHM has no change either. This proves that they have amazing stability against oxidation.

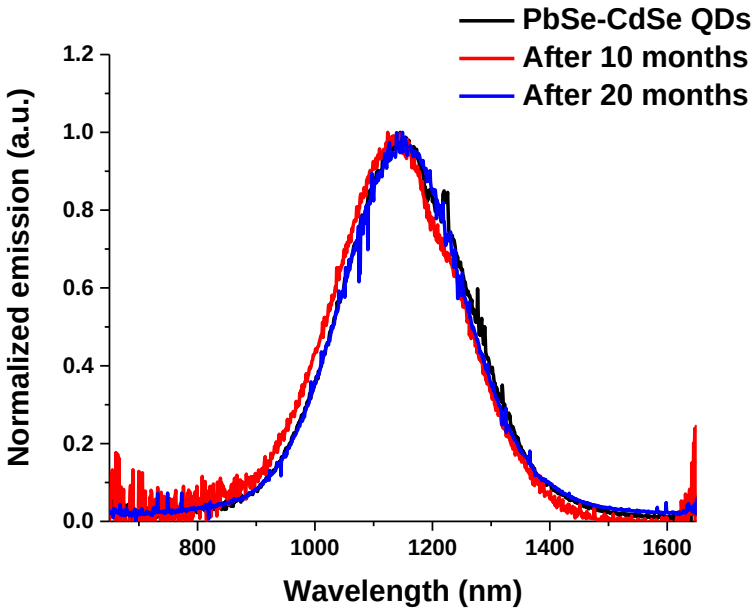

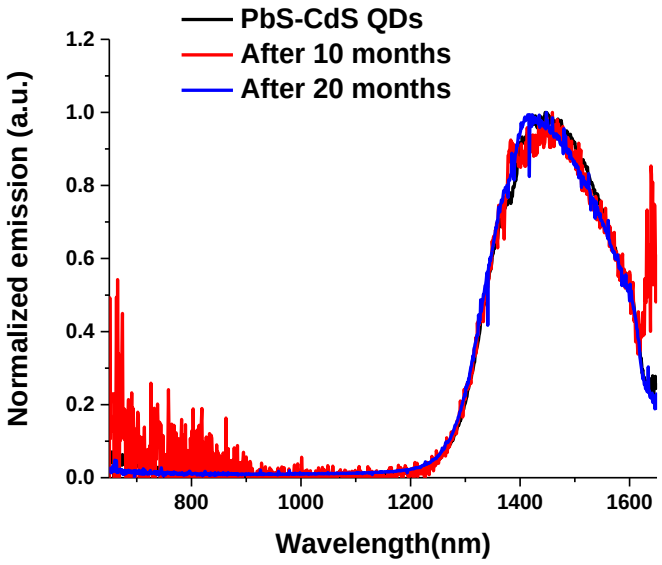

Figure 2.23. PL of PbSe-CdSe (top) and PbS-CdS (bottom) QDs measured at 0, 10 and 20 months after synthesis. Sample was dissolved in TCE with the 632 nm HeNe laser as the excitation source.

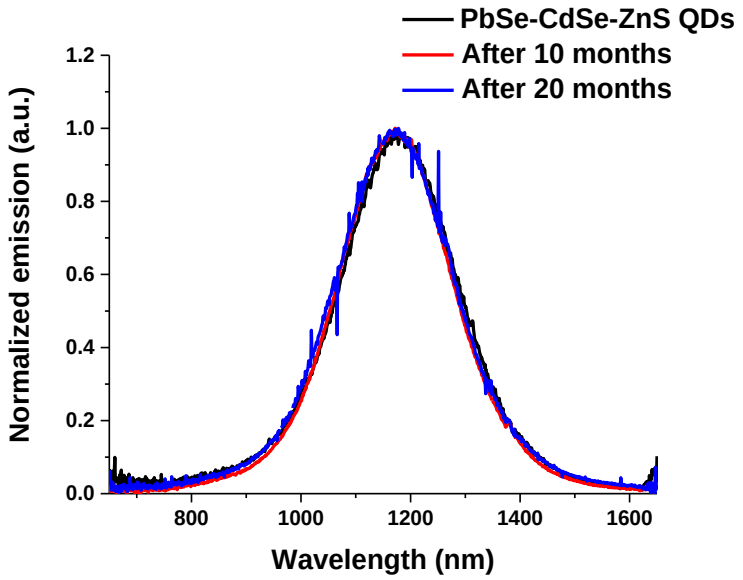

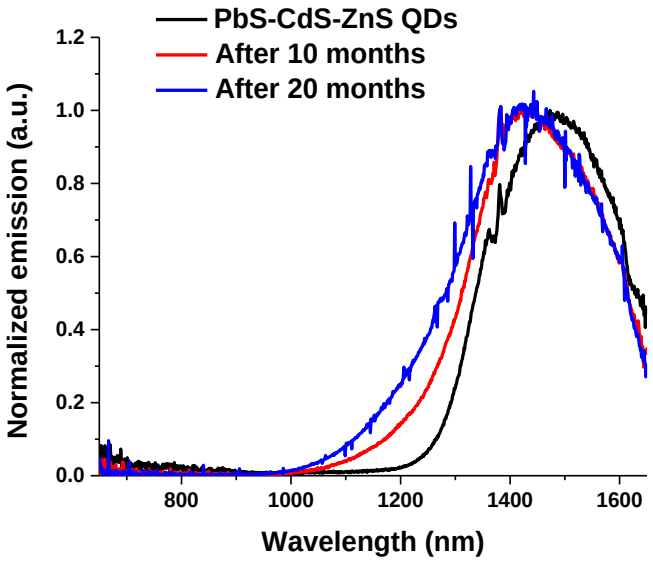

Figure 2.24. PL of PbSe-CdSe-ZnS (top) and PbS-CdS-ZnS (bottom) QDs measured at 0, 10 and 20 months after synthesis. Sample was dissolved in TCE with the 632 nm HeNe laser as the excitation source.

PbSe-CdSe-ZnS QDs also showed excellent stability. Nothing changed in the PL during the 20 months' storage. Meanwhile, PbS-CdS-ZnS QDs are less stable. After 10 months, a very obvious blue shift was observed. Ten more months later, the emission maximum didn't shift anymore, but the FWHM got larger. This finding suggests that PbS-CdS-ZnS QDs have weaker stability in air. Seen in Figure 2.23 (bottom), it seems that this batch has a tendency of shifting towards lower wavelength. The possible explanations includes slowly alloying at the PbS-CdS interface and dissolution of larger particles. Alloying will reduce the core size and red-shift the emission, which has been discussed before already. Loss of larger particles will make the average size of the cores small, which also shifts the emission towards lower wavelength.

In order to verify the weaker stability of PbS-CdS-ZnS QDs, PL of another batch **(119/CJM/14)** was measured 6 months after and compared with the emission measured on the day they were synthesized. The result is plotted in Figure 2.25. Contrasts to what has been mentioned above, this batch show very well stability with no notable change in PL at

all after half a year. So far, no conclusion can be drawn on why one batch of PbS-CdS-ZnS QDs has better stability than another. All core-shell and core-shell-shell QDs present good stability against oxidation, in general. More study needs to be done on PbS-CdS-ZnS QDs to identify what caused the small blue shift.

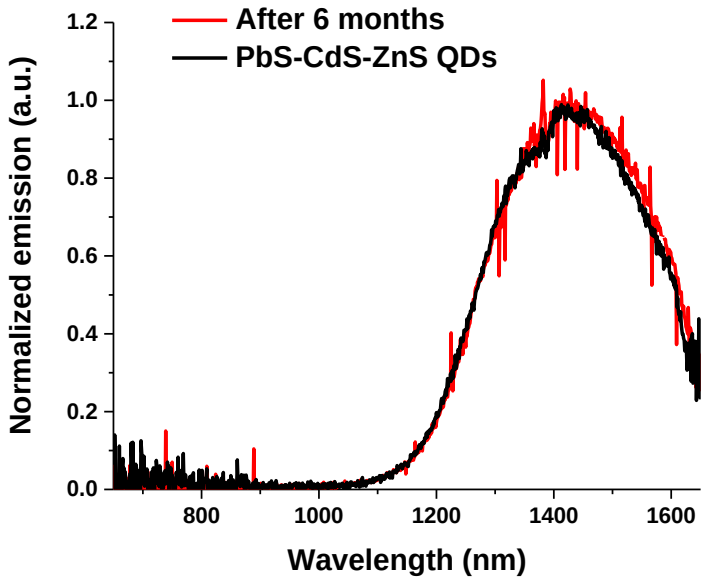

Figure 2.25. PL of core-shell and core-shell-shell QDs when newly made and 6 months later. Sample was dissolved in TCE with the 632 nm HeNe laser as the excitation source.

2.4.5 XPS measurement

The XPS (X-ray photoelectron spectroscopy) measurement is a proven technique for elemental analysis. In an XPS measurement, the sample is put in a vacuum chamber where the pressure is below 1×10^{-8} torr (the lower the better). The signal in this measurement is from collecting electrons, so one would expect less particles (air and dust) in the environment that could potentially collide with electrons. An XPS spectrum is obtained by irradiating an X-ray beam onto the sample and collecting ejected electrons from the sample. The sample being measured absorbs the energy from the beam and eject core

electrons, which are later picked up by a detector. The kinetic energy of an ejected electron can be calculated using the formula below:[102]

$$\mathrm{E}_k = h\nu - \mathrm{E}_b - \Phi$$

Where E_k and E_b are the kinetic and binding energies of thet alectron, respectively. $\hbar\nu$ is the energy of the incident X-ray, where h is the Plank's constant and ν is the frequency. Φ is the work function of the instrument.

Electrons from different orbitals of different atoms have different energies. In addition, these energies may vary depending on the state of the atom (might be cation or anion). By analyzing information of collected electrons and compare the energies to the X-ray data booklet,[102] one can identify the elemental composition and oxidation states of the elements. Moreover, due to the fact that the incident beam have a penetrating depth on the order of 1 to 10 nm,[103] XPS technique it is often used for surface studies. H. Borchert and co-workers synthesized two batches of CdTe QDs using different conditions and growth rates. With the help of XPS, they found that one had more Te atoms on the surface than the other, which could be the reason for the higher fluorescence efficiency.[104]

With higher energy, the irradiating beam will have the capability to penetrate deeper and endow ejected electrons more kinetic energy. A higher kinetic energy means a longer mean free path, which will allow electrons from deeper inside to escape and get detected. Taking advantage of this, people are able to depth profile a sample (especially nanocrystals) by looking into the change from the surface to a couple nanometers beneath using an energy-adjustable X-ray source. H. Borchert et al. performed energy-dependent XPS method to characterize core-shell QDs.[103] They successfully showed an increasing In/Zn ratio (Figure 2.26) as the energy of the X-ray was elevated on InP-ZnS core-shell QDs. This finding suggested that Zn was more on the outside of the particle, proving a core-shell structure.

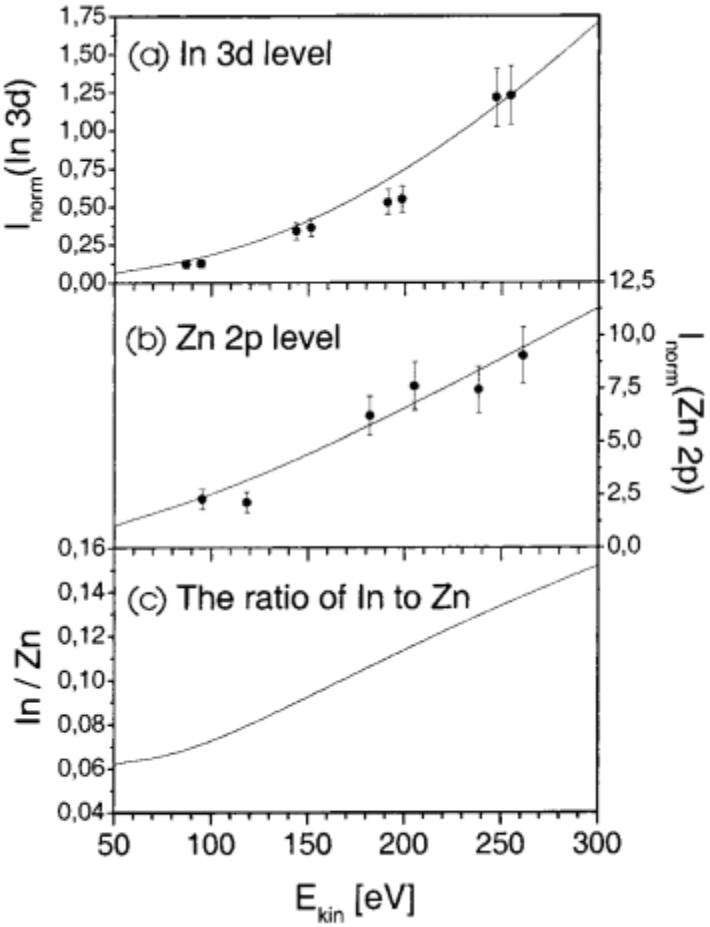

Figure 2.26. Normalized intensities of the In 3d (a) and Zn 2p (b) core levels as a function of photoelectron kinetic energy. Fitted curves are the results of the procedure described in the text. Dividing the numerical fit (a) by (b) yields the intensity ratio of the In 3d to Zn 2p core levels (c). (with permission from publisher)[103]

Inspired by that paper, our group successfully investigated the structure of PbSe-CdSe core-shell QDs using energy-dependent XPS.[100] All XPS measurements were carried out at the CLS (Canadian Light Source) where a continuous synchrotron radiation source was provided. Similar to what H. Borchert had observed, an increasing Pb/Cd ratio was presented as the beam energy was aggrandized. The PbSe-CdSe QDs were grown using the cation exchange method. Our initial interest was in the interface between PbSe and CdSe, which could be an alloy or a sharp interface. The final result supported a core-shell structure rather than a somewhat uniform interface.

Survey scans were done on core, core-shell and core-shell-shell QDs and shown in Figure 2.27. There are communal peaks like the Au 4f (used as reference), C 1s (from the carbon tape used, and/or the capping oleates on the surface of the QDs), O 1s (from residual air, and/or oleates), and Pb 4f peaks. The Cd 3d can be easily spotted by comparing the spectra of core-shell to core QDs. The Zn 2p peaks (the place where they turn up are pointed out with green arrows) could only be observed on PbSe-CdSe-ZnS and PbS-CdS-ZnS QDs by comparing spectra of core-shell-shell QDs to that of core-shell QDs. This suggests that the elemental composition on core, core-shell and core-shell-shell QDs are correct, just as expected. A typical Zn 2p signal from core-shell-shell QDs are shown in Figure 2.28.

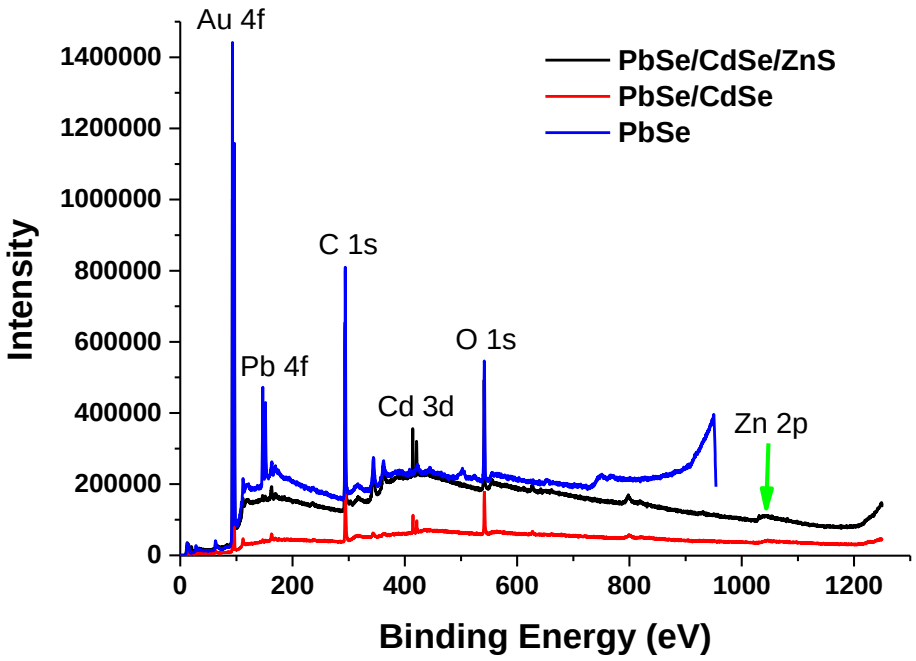

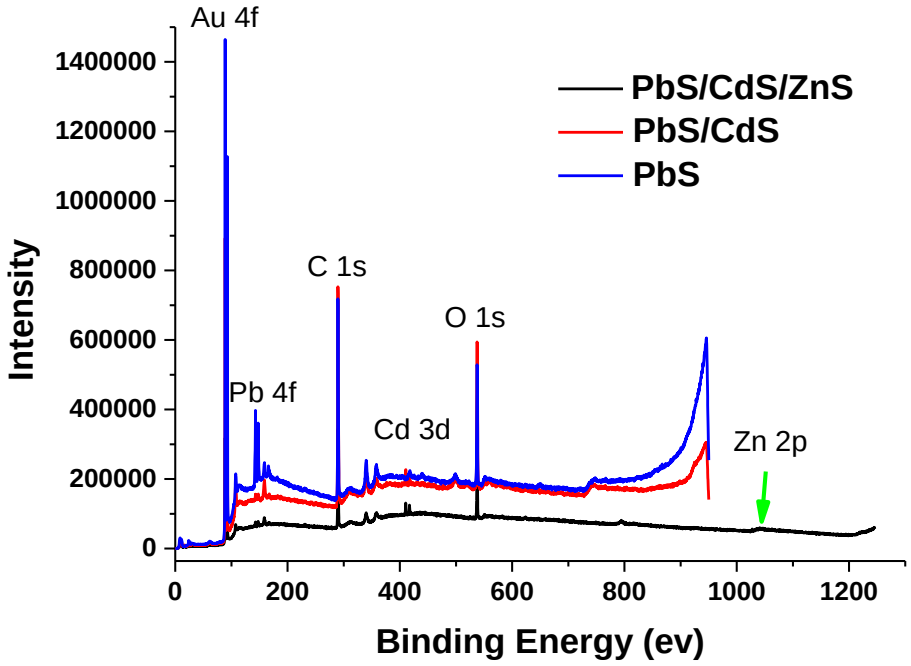

Figure 2.27. Survey scan results of core, core-shell and core-shell-shell QDs.

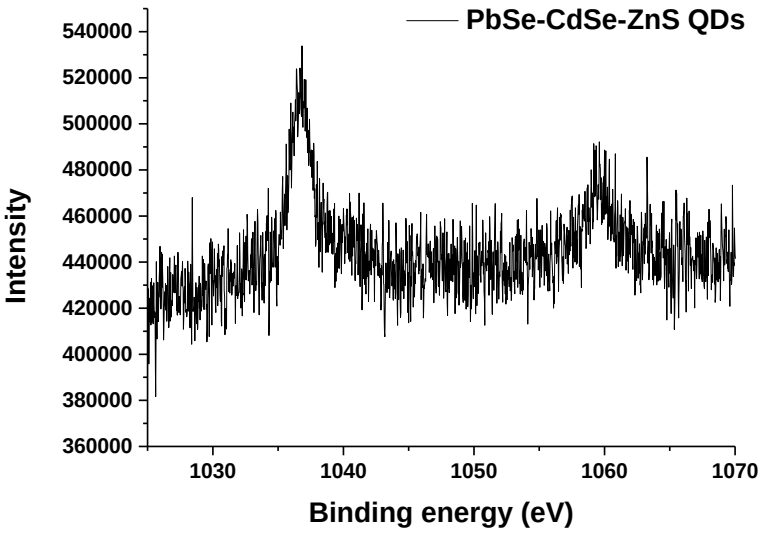

Figure 2.28. Typical Zn 2p signal seen on PbSe-CdSe-ZnS QDs.

Intensity of the Zn 2p peaks were much weaker compared to the Pb 4f and Cd 3d, because of a much smaller absorption cross section[105] and the very thin layer of ZnS. The TEM results (see previous discussion) showed that the ZnS layer widths are 0.15 and 0.34 nm in PbSe-CdSe-ZnS and PbS-CdS-ZnS QDs, respectively. This means that there's much less Zn compared to Pb and Cd.

The energy-dependent XPS measurement was done as stated in the experimental section. We successfully ran preliminary measurements on PbSe-CdSe-ZnS and PbS-CdS-ZnS QDs by measuring Zn 2p and Cd 3d peaks using 500, 400, 300, 200 and 100 eV kinetic energies, respectively. Kinetic energies were kept the same for both elements to make sure that ejected electrons from both would have the same mean free path, which guaranteed that they had equal chance of being picked up by the detector. Only 5 data points were collected because of our time limit at the CLS. The resulted curves were background-subtracted using polynomial fit in the Origin software. Three background polynomial fits were done on each peak, with 2, 3 and 4 polynomial order, respectively. After each fit, the background was subtracted and the peak intensity was integrated. Standard deviation of each peak originated from the three polynomial fits, and was propagated through the calculation. The integrated peak areas were corrected for the beam flux (recorded from the instrument during each measurement), ionization cross section,[105] and the number of scans. The ratio changes of Zn/Cd as kinetic energy increased for both QDs are given below in Figure 2.29.

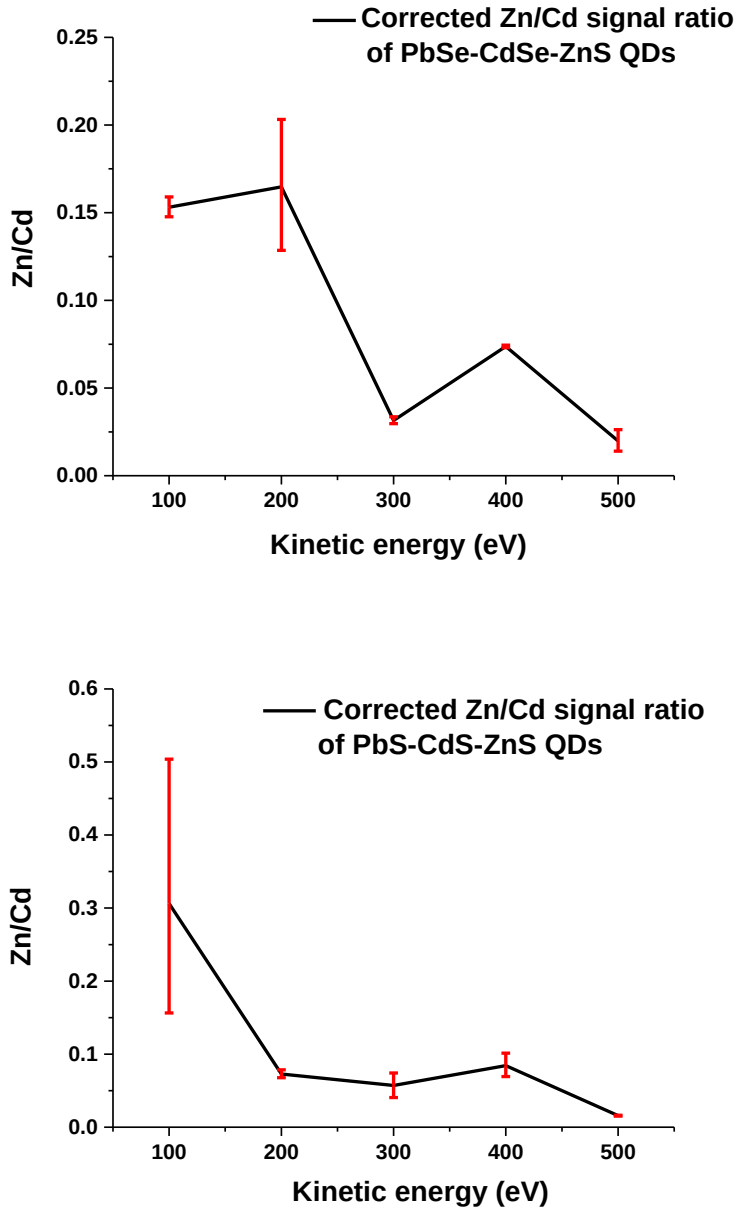

Figure 2.29. Zn/Cd ratio change of PbSe-CdSe-ZnS (top) and PbS-CdS-ZnS (bottom) QDs with increasing kinetic energy.

It can be seen that in PbSe-CdSe-ZnS QDs, there is a general trend of decreasing Zn/Cd as the kinetic energy increases from 100 to 500 eV. This suggests that Zn is richer on the outside compared to Cd, indicating a ZnS outer shell. The second point at 200 eV was slightly higher than the first, but it has a much larger error bar, which suggests that it could

well lie below the value of the first point. The third and fourth points seem to be misplaced since it will be more rational if the fourth has a lower value. More repetitive measurements should be done to verify the result. It could be an experimental error during the scan. The other possible reason is the wrongly estimation of the background, which is difficult and confusing at times. We don't know for sure what the real background is even if we use polynomial fits to describe it. If the estimation of background is not close enough to the real value, the peak intensity will be incorrect either, and the error will be scaled up.

A similar decreasing trend of Zn/Cd is also observed on PbS-CdS-ZnS QDs. The fourth point at 400 eV has slightly higher value compared to the third, but the bottom of its error bar is below the top of the error bar of the third point. The result shows that Zn is more on the outside of the particle over Cd. At 500 eV kinetic energy in both curves, there is very little amount of Zn signal compared to that of Cd, showing that almost no Zn can be found deep inside the surface.

Based on the trend of a decreasing Zn/Cd ratio alongside with an increasing kinetic energy, it is fair to draw the conclusion that there is ZnS layer outside of the PbSe-CdSe and PbS-CdS QDs. The core-shell-shell structure was successfully synthesized. More work can be done with the energy tunable XPS on our QDs. For example, a smaller step size like 50 eV and a larger energy range such as 50 to 600 eV (kinetic energy) can be used to describe the ratio change better, as well as confirming what we have observed so far, because there are a few points that don't follow the general trend. Moreover, the ratio change of Cd/Pb is an interesting topic to look into. If alloying happened when we made core-shell-shell QDs, the Pb-Cd interface would change from a sharp interface to a uniform or gradient layer made of PbSe and CdSe (or PbS and CdS). In this case, if the Cd/Pd ratio change would be obviously different from what A. Keith et al. had seen in the past.

2.5 Conclusions

I have successfully synthesized PbSe-CdSe-ZnS and PbS-CdS-ZnS QDs. The UV-absorption and emission of them were measured and compared to their core-shell precursors. Results prove that core-shell-shell QDs have similar optical properties to those of core-shell QDs, which is as expected. The variable relative position of emission maximum of core-shell-shell QDs compared to core-shell QDs yet needs to be investigated. Larger core size dispersion are found in core-shell and core-shell-shell QDs compared to the original cores, supported by the larger FWHM values from emission curves. In addition, the distinguished absorption features in cores are not seen on core-shell and core-shell-shell QDs.

TEM studies clearly reveal the size change from core-shell to core-shell-shell QDs. This suggests a ZnS shell on the outside of the original core-shell QDs. The long-time stability study shows that both core-shell and core-shell-shell QDs have excellent anti-photooxidation property, though one batch of PbS-CdS-ZnS QDs showed a trend shifting towards lower wavelength. The reason behind this needs more research to verify.

Preliminary XPS finding further supports the existence of ZnS shell by showing a decreasing Zn/Cd ratio as the kinetic energy increases. Together with the TEM data, we can confirm the core-shell-shell structure. More XPS measurements should be done in the future to study the influence of the second shell growth on the Pb-Cd interface. In addition, a repeating measurement on the Zn/Cd ratio change with smaller step size and larger range should be done.

Chapter 3 Introduction to quantum yield measurement

3.1 Definition of quantum yield

The Quantum yield (QY), is defined as the ratio of the number of photons emitted to the number absorbed, as shown by the formula below.[19] It is one of the most important characteristic of a photon-emitter, since it describes the efficiency of giving out photons in return.

$$\Phi_f = \frac{Number\ of\ photons\ emitted}{Number\ of\ photons\ absorbed}$$

3.2 Method of QY measurements

There are primarily two ways to measure the QY of a photon-emitter: a relative measurement using a standard fluorescent material with a known Φ_f value or an absolute measurement.[106]

3.2.1 Relative measurement

The relative measurement of QY using a reference material was discussed in detail by J. N. Demasa and G. A. Crosby in 1971.[107] An equation for calculating QY was given as shown below:

$$\Phi_{f,x} = \Phi_{f,s} \frac{f_s(\lambda_{ex,s}) n_x^2 \int_{\lambda_{em,s}} F_{P,s}(\lambda_{em,s})}{f_x(\lambda_{ex,x}) n_s^2 \int_{\lambda_{em,x}} F_{P,x}(\lambda_{em,x})}$$

Where subscribes x and s stand for the sample and standard reference. λ_{ex} and λ_{em} represent the excitation and emission wavelengths. F and f mean the fluorescence intensity and absorbance while n is the refractive index of the solvent if different solvents are used.

The standard procedure consists of several simple steps. Firstly, measure the absorption and emission spectra of the sample and determine a suitable reference standard. Secondly, decide on the parameters of measurements (temperature, excitation wavelength, etc.) and perform absorption and emission measurements on both sample and standard. Lastly, data processing and calculation. The processing (subtraction of background, correction for instrument response for instance) could vary depending on different circumstances.

For a material to be considered a reliable standard, its QY should have been well-tested and reported by different literature with similar values. In addition, the measurement should be carried out with extra care and specify all experimental conditions. These conditions include the temperature, wavelength used, solvent, pH, concentration, whether degasing was performed, and etc.[108] QYs from different literature on the same material using the same conditions should have similar (if not the same) values. Some of the most widely used standards are quinine bisulfate, fluorescein, and rhodamine 6G.[108]

Studies on standard materials started booming since the 1960s. One of the very first articles that systematically discussed QY of several organic fluorescent substances at 25 ℃ was published by W. H. Melhuis in 1961.[109] A value of 54.6% was reported on a 5×10^{-3} M quinine bisulfate in 1 N H_2SO_4 solution using 366 nm excitation wavelength. This value was considered accurate as confirmed by some other groups under identical conditions.[110, 111] Over the years, several other literature obtained values ranging from 50 to 60% using

different methods in 0.05 M H_2SO_4 solution.[112-114] QY of fluorescein was first reported by J. H. Brannon and D. Magde in 1977.[115] They used the thermal lensing method to measure the absolute QY of sodium fluorescein in 0.1 N aqueous NaOH solution at low concentrations (below 0.01 M). The calculated QY was 95 ±3%. The result was confirmed by people using both thermal lensing and integrating sphere methods.[116-118] All of them obtained QY in the range 91 to 93% with slight difference from one another, which is well within the normal range of experimental error. Rhodamine 6G has a shorter history of being a standard material. In 1996, M. Fischer and J. Georges utilized thermal lens spectrometry to determine QY of rhodamine 6G.[119] The QY obtained at low concentrations (10%) was found to be independent of concentration up to 2 x 10^{-4} M. This value was also supported by later work which examined QY of rhodamine 6G in various solvents.[117] There are other frequently used standards like benzene,[111] rhodamine 101,[120] 9,10-diphenylanthracene[110, 112] et al., which were summarized by D. F. Eaton[121] and IUPAC.[108]

3.2.2 Absolute measurement

In contrast to the relative measurement, an absolute measurement is without the involvement of a standard. Due to the fast development of commercial fluorimeter and integrating sphere, absolute measurement is becoming more and more handy and accurate.[122] Moreover, most of QY standard dyes emit in the visible range, very few emitting in the NIR range have been reported, especially those emitting at above 1000 nm with reliable QYs. One commonly used NIR emitting standard is IR-26, which has a very low QY of less than 0.1%.[123] It emits from 1000 to 1600 nm, with an emission maximum at about 1130 nm. In this case, to measure QY of NIR emitters, an absolute measurement will be a better option over a relative measurement.

3.2.2.1 Optical methods

An optical method normally utilizes an integrating sphere, a light source and a detector. An integrating sphere is a hollow spherical optical component, with the interior coated with a uniform layer of diffuse white reflective material [mostly barium sulfate ($BaSO_4$) or Polytetrafluoroethylene (PTFE)]. It has two or more small openings used as the entrance and exit of light. When the incident light hits on one point of on the interior, reflected light travels in all directions, which then goes through multiple scattering reflection. Ideally, light is conveyed equally to all points on the interior of a perfect integrating sphere.[124] A good example of utilizing an integrating sphere for an absolute QY measurement can be found in the article published by R. H. Friend and co-workers.[125]

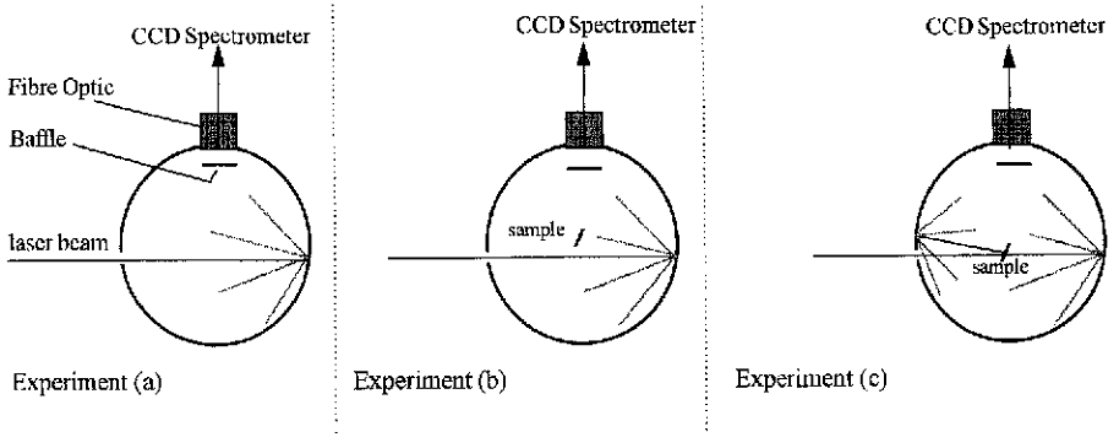

Figure 3.1. Diagram illustrating the three configurations of the sphere required for the efficiency measurement: a) the sphere is empty: b) the sample is in place and the laser beam is directed onto the sphere wall; c) the sample is in place and the laser beam is directed onto the sample. (With permission from publisher)[125]

As shown in Figure 3.1, one measurement usually takes three runs. In the first run, the intensity of incident light without sample absorption was taken. The second run measures the intensity of incident light after being partially absorbed by the sample. Finally, the

emission of the sample was recorded in the third run. Thus the QY can be calculated via the equation given by C. Würth:[126]

$$F = \int_{\lambda_{em}} \frac{I_x(\lambda_{em}) - I_b(\lambda_{em})}{s(\lambda_{em})} \lambda_{em}\, d\lambda_{em}$$

$$F_{abs} = \int_{\lambda_{ex}} \frac{I_x(\lambda_{ex}) - I_b(\lambda_{ex})}{s(\lambda_{ex})} \lambda_{ex}\, d\lambda_{ex}$$

$$\Phi_f = \frac{F}{F_{abs}}$$

Where F and F_{abs} are number of photons that emitted and absorbed respectively. I represents the intensity at a certain wavelength and s is the sensitivity of the detector at that wavelength.

3.2.2.2 Calorimetric methods

For a non-radiative sample, all absorbed light will be converted to heat, whereas in the case of a fluorescent sample, only some will become heat. Instead of counting the number of photons directly, QY can be measured through the efficiency with which the energy of absorbed photons is converted into heat. This is known as the calorimetric method.[106] There are mainly two methods used: the photoacoustic spectroscopy (PAS) and the thermal lensing, also called thermal blooming.

The PSA technique places a sample in a sealed cell with a microphone or acoustic transducer attached. When the sample is illuminated by a periodic excitation light, its temperature arises due to absorbed energy that is not emitted by the sample. A periodic pressure wave is then produced which is recorded by a detector. By working out the temperature increase, one can deduce how much of the light was absorbed but not emitted.

The thermal lensing requires a laser beam to pass through a liquid of the fluorescent molecules. Commonly, the laser beam has a nonlinear (radially symmetric) interaction with the propagation medium. It is known that the refractive index of a medium changes as temperature changes, the resulting temperature gradient caused by the laser generates a gradient in refractive index. As a result, the dispersion of the traveling beam is changed. This change can be picked up by a detector placed at a certain distance away. Accordingly, different heating rates lead to different thermal lenses and the development of the thermal lens until a thermal equilibrium where heat loss from the illuminated volume equals the heat diffusion rate into the surrounding can be traced on an oscilloscope or equivalent recorder.[106] Both the PSA and thermal lensing methods require a non-fluorescent material as a reference.

3.3 Errors in QY measurements

QY measurement is such a tricky measurement that every little change in either the surrounding or procedure can alter the result significantly.

A standard dye is required for relative measurements and suggested as a validation reference. It is important to check the purity of the dye and determine if further purification is needed.

Cuvettes used for QY measurement should be specially designed for fluorescent measurements. It is also important to make sure they are properly cleaned and dried before use. Additionally, any crack or scratch on the cuvette will cause unwanted scattering, so any cuvette with those should not be used.

Apart from basic protocols, some compounds may need special care when handled. Degasing is commonly seen as some dyes are sensitive to the presence of oxygen, which can quench the fluorescence. C. Würth et al. have reported oxygen-dependent QY of diphenylanthracene.[126]

If the sample is illuminated by a halogen lamp instead of a laser, the monodispersity of incident light is directly controlled by the slit width. Preferably, we would like it to be as narrow as possible. If it is too large, there will be a gradient in the wavelength of incident light, which will undoubtedly bring in inaccuracy.

The reabsorption of emitted light by the sample itself is another thing that we need to minimize. Normally, the concentration of the sample needs to be made as low as possible, while a strong enough emission spectrum can still be obtained.

To report reliable results, experimental conditions must be correctly recorded so that people can reproduce your measurement. Wavelength and temperature was frequently missing in literature when they reported a QY value.[127]

3.4 Radiative and non-radiative decay of QDs

The emission of QDs are the result of recombination of electron-hole pairs, as discussed in Chapter 2. However, not all excitons end up with emission. There are defects in QDs where charge carriers (electrons or holes) can be trapped.[128] If a trapped charge carrier is re-excited, the other carriers will lead to Auger effects that release energy through non-radiative decay.[129-131]

Chapter 4 Data and discussion for quantum yield measurement

4.1 Previous work on lead-based QDs

The QY is a common character to evaluate the quality of QDs. P. Guyot-Sionnest and co-workers measured the QY of PbSe QDs synthesized using the method developed by C. B. Murray et al.[85] An infrared dye IR-26 was used as a reference to define a QY value of 85%. M. A. Hines and G. D. Scholes reported a QY of 20% for the PbS QDs they made.[96] A standard dye IR 125 was used as the reference. As mentioned in previous chapters, G. A. Ozin et al. synthesized PbS QDs using $PbCl_2$ as the precursor.[97] With IR-26 as the reference, they found the QY was about 40%. Z. Hens and his group synthesized PbS QDs following this method and studied QY of PbS QDs with different sizes.[132] They found that QY dropped from 90% to 20% as size increased. Similar result was previously reported by A. Keith from our group in 2008.[73] For smaller PbS QDs (those emitting in the range of 1100 to 1300 nm), the QY could be as high as 80% (4 out of 10 batches) and otherwise between 40 to 60%. However, QY of larger QDs with emission from 1300 to 1600 nm were determined to be 25% to 40%. In 2010, M. C. Beard and et al. first identified a 0.05% QY value of the infrared dye IR-26, then used it as a reference to study the size dependence of PbS and PbSe QDs.[123] The result accords with others' finding that QY is dependent on the size.

4.2 Excitation-dependent QY

Excitation-dependent QY of CdSe QDs, which emits in the visible light range, was reported by A. P. Alivisatos and co-workers in 1994.[133] They showed that the QY of one batch dropped drastically when the excitation energy was elevated from 1.65 to 2.175 eV. The reason behind this was attributed to excited state trapping. A similar phenomenon was

observed by G. Rumbles et al. in 2001 on InP QDs.[134] By changing the excitation wavelength from 400 to 660 nm, with a 20 nm step size, an increasing QY was obtained. The authors believed that larger dots within the finite size dispersion that absorb preferentially on the low energy side of the absorption profile. Both of CdSe and InP QDs reported by these two groups emitted in the visible range. So far, no excitation-dependent QY of NIR emitting QDs has been reported.

4.3 QY study on PbSe QDs

Before the systematic QY measurements on our QDs, a measurement on a standard quinine bisulfate purchased from a manufactory was performed first. A number of 50% was obtained compared to literature-reported value of 54 to 56%. Considering an experimental error of 10 to 20% (which was found out later), this QY value lies well within an acceptable range, thus the measurement was considered reliable.

A set of PbSe QDs were synthesized adopting the same method used in the last chapter, which is described in detail in the experimental section. Four batches of PbSe QDs with different PL and absorption were chosen. This is to make sure that what we observe on any batch of QDs is not by accident. In addition, quality of different batches should be different due to conditions used and random errors. Their PL and size were controlled by the reaction temperature and time, which is shown in Table 4-1.

Table 4-1. Experiment condition used for PbSe QDs synthesis

Sample	Experimental number	Temperature (℃)	Time (minute)	Estimated size (nm)
A	**111/CJM/14**	120	2.5	3
B	**015/BG/14**	130	2	3.5
C	**091/CJM/14**	135	3	4
D	**014/BG/14**	145	3	5

PL of these QDs was measured and shown in Figure 4.1. All of them show very well defined Gaussian-shape emission peaks at different wavelengths. The sharp peak in emission spectrum of sample C is an artifact from the correction file for the water absorption at about 1380 nm. The Gaussian shape emission is a reflection of the fact that size variation of each batch follows the Gaussian dispersion.

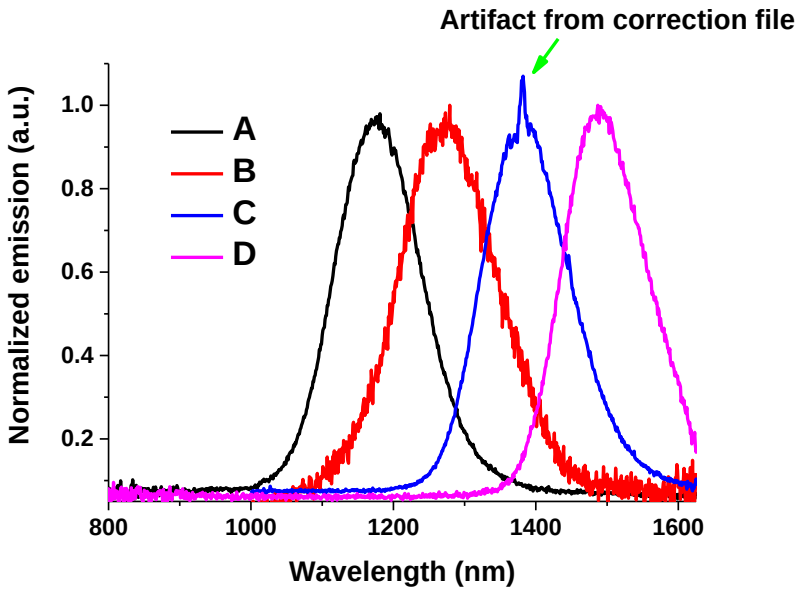

Figure 4.1. PL of four batches of PbSe QDs after normalization. Sample was dissolved in TCE with the 632 nm HeNe laser as the excitation source.

Absorbance of all four batches were also measured and shown in Figure 4.2.

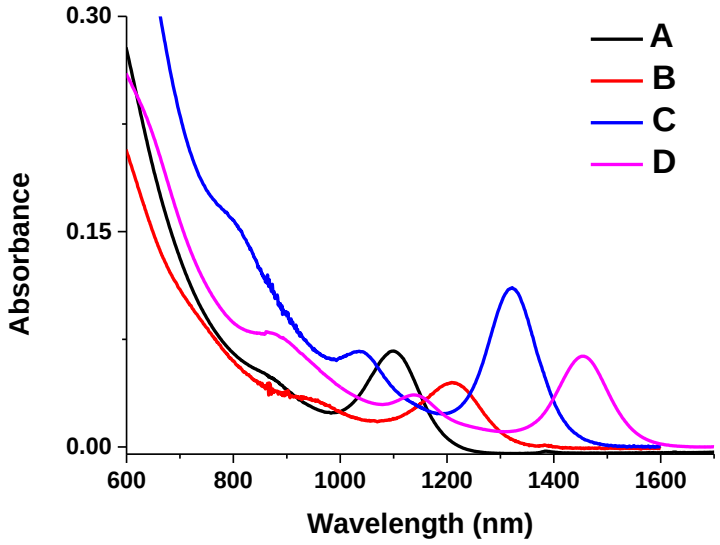

Figure 4.2. UV-absorption of four batches of PbSe QDs. Sample was dissolved in TCE.

The summary of emission and absorbance wavelengths of 4 batches of QDs are given below in Table 4-2.

Table 4-2. Absorbance and emission wavelengths of PbSe QDs

Sample	Absorbance (nm)	Emission (nm)
A	1098	1176
B	1217	1270
C	1334	1380
D	1455	1485

With a larger size, PbSe QDs will have a smaller bandgap, which results in a lower absorption wavelength. From sample A to sample D, there is a consistent increase in

absorption wavelength, as we also see in emission wavelength. Figure 4.2 shows both the absorbance and emission of sample D. For each batch of PbSe QDs, three excitation wavelengths were used to do QY measurement. Three arrows in Figure 4.3 indicate the wavelengths used in this case, which are 1268, 1123 and 842 nm, respectively. The energy differences of these wavelengths to the absorbance peak are 0.126, 0.252 and 0.620 eV, respectively. These numbers were decided when doing measurements on the first batch. In order to avoid overlapping of the incident signal (and higher order light induced by the monochromator we used) and emission of QDs on spectra, a few excitation wavelengths and their corresponding energies were decided. Thus the energy differences were calculated.

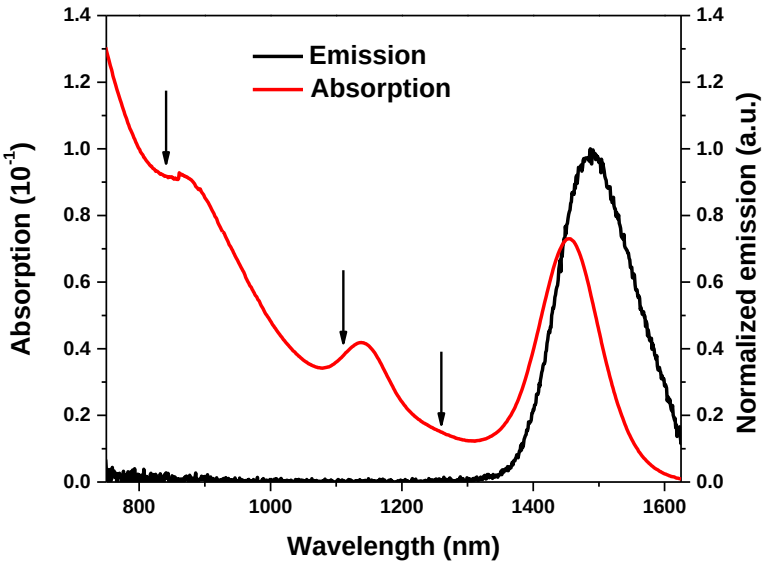

Figure 4.3. Absorbance and emission of sample D. Sample was dissolved in TCE with the 632 nm HeNe laser as the excitation source.

These values of energy differences were also used to determine excitation wavelengths used for QY measurements on other batches including core-shell and core-shell-shell QDs. All batches of QDs were excited using wavelengths with the same energies differences, so that excited electrons will have the same excessive energies above the energy gap. Potentially, all these electrons from different batches of QDs could go through the same

Auger processes if there is any. As a result, we will be able to compare data obtained from batch to batch.

A summary of excitation wavelengths used for PbSe QDs are shown below in Table 4-3.

Table 4-3. Experiment condition used for PbSe QDs synthesis

Sample	Wavelength at ΔE_1=0.126 eV	Wavelength at ΔE_2=0.252 eV	Wavelength at ΔE_3=0.620 eV
A	988 nm	898 nm	708 nm
B	1083 nm	976 nm	756 nm
C	1175 nm	1050 nm	800 nm
D	1268 nm	1123 nm	842 nm

4.3.1 Data processing

Three measurements on each batch of PbSe QDs were done with the three excitation wavelengths determined. The procedure of QY measurement is described in detail in the experimental section. The raw data obtained was processed using Origin 9.0.

The software that records signal plots spectra on wavelength scale. Because energy is not consistent on the wavelength scale, all spectra needed to be re-plotted on the wavenumber scale. The irradiating source we used is a 450 W xenon lamp, which emits light in a wide range (visible to near IR) once turned on. In the range it emits, light has consecutive energies, which is the reason why number of photons has to be counted on an energy scale. In Figure 4.4 (right), the integrated area of both curves was calculated. The differential between the two was the part of light absorbed by QDs.

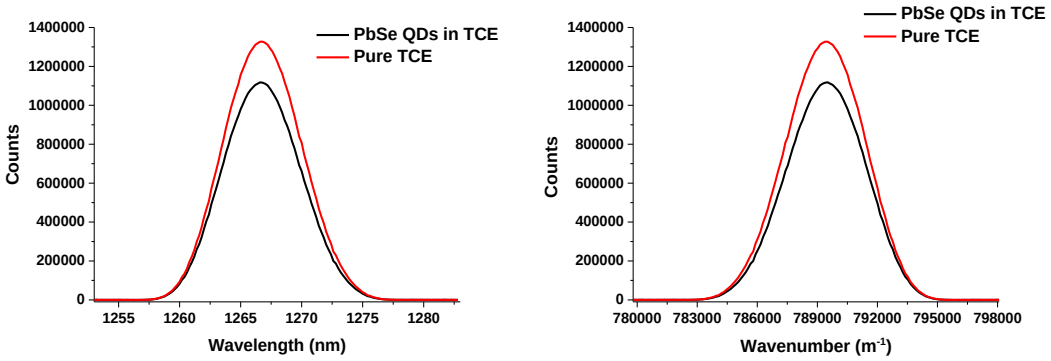

Figure 4.4. Incident light intensity with pure TCE and PbSe QDs in TCE on wavelength (left) and wavenumber (right) scale, excitation wavelength is 1268 nm.

In Figure 4.5 (left), the high noise level part over 1600 nm was caused by the correction file of the detector used. Before any further processing, this part was removed because it's not the real shape of emission. The curve was re-plotted in Figure 4.5 (right) with adjusted scale. A Gaussian fit was carried out using Origin to the rest of the data, still on the wavelength scale. Then, the Gaussian fit curve was re-plotted on the wavenumber scale and integrated. The integration result was the total amount of light emitted.

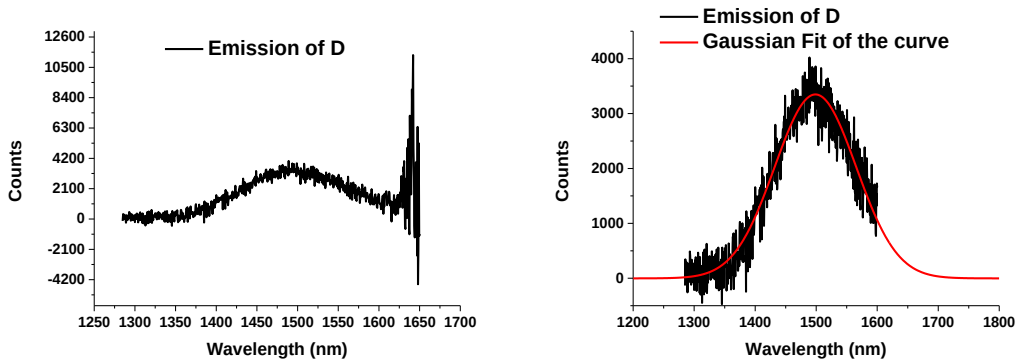

Figure 4.5. Emission of sample D without any processing (left), after removing high noise part, and Gaussian fit (right), excitation wavelength was 1268 nm.

There are cases where the emission was not as smooth as Figure 4.6. In Figure 4.6 (left), the emission of sample A was spiky with a few small sharp peaks. Also, the huge peak at

around 1420 nm was the second order light of excitation, cause by the monochromator. The small peaks were possible Raman shifted lines, and were not from the sample emission. When the sample shown in the Figure 4.4 was excited with another decided wavelength, those small peaks were no longer at present anymore.

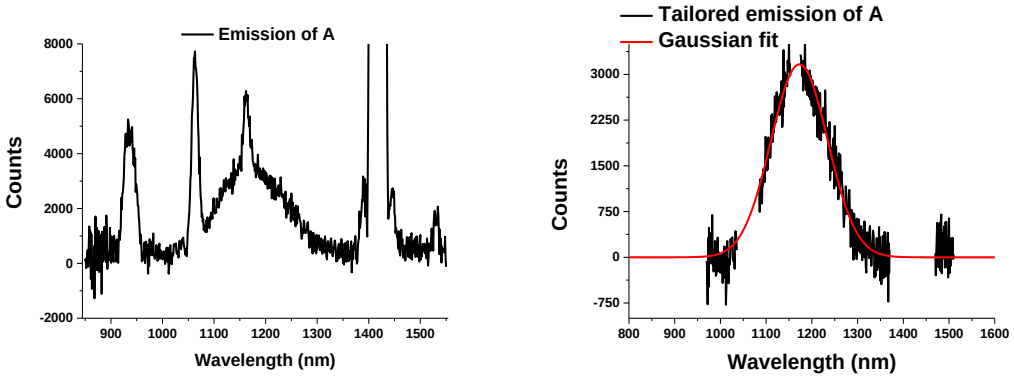

Figure 4.6. Emission of sample A without any processing (left), emission after removing spikes, and Gaussian fit (right), excitation wavelength was 708 nm.

After removing those peaks, the curve was re-plotted in Figure 4.6 (right) with adjusted scale. A Gaussian fit was carried out using Origin to the rest of the data. Then, the Gaussian fit curve was re-plotted using wavenumber as the x axis, and integrated. The integration result was the total amount of light emitted.

The QY was calculated using the equation given for absolute QY measurement in Chapter 3. Full results for all batches are given below:

Table 4-4. QY results of PbSe QDs

Sample	QY (%) at ΔE_1=0.126 eV	QY (%) at ΔE_2=0.252 eV	QY (%) at ΔE_3=0.620 eV
A	48	15	5
B	19	12	5
C	40	13	4
D	11	9	2

All the numbers shown above are calculated results after rounded to integers. The measurement was done trice on sample D at ΔE_2 to obtain the experimental error in this measurement. The three QYs turned out to be 11.0%, 9.6% and 7.5%, respectively. The average value was determined to be 9.37 ±1.76%. Thus one can expect a standard deviation in the range of 10 to 20% for all the values reported in this thesis.

Within every batch of PbSe QDs, the calculated QY keeps decreasing as the excitation wavelength increases. This is a common trend from batch to batch, suggesting that it is not caused by QDs size. Moreover, different batches of QDs can have a very varied QY values at the same ΔE. This is anticipated because QY can be greatly affected by the quality of QDs. As mentioned above, K. Abel from our group studies the QY of 10 batches of PbS QDs synthesized in the same way.[73] He found that for 4 out of 10 reactions, the quantum yield could be as high as 80% for the smaller NCs with emission peaks in the range of 1100 to 1300 nm. The other 6 batches were between 40 to 60 %. For larger QDs emitting between 1300 to 1600 nm, the quantum yield was found to be between 25 to 40%. What Keith observed was caused by quality variation of different batches.

4.4 QY study on PbS QDs

Three batches of PbS QDs were synthesized adopting the same method used in the last chapter, which is described in detail in the experimental section. Conditions used for each batch is shown in Table 4-5.

Table 4-5. Experiment condition used for PbS QDs synthesis

Sample	Experimental number	Temperature (℃)	Time (minute)	Estimated size (nm)
A	**130/CJM/15**	110	5	4.5
B	**127/CJM/15**	120	3	5
C	**117/CJM/14**	120	4.5	5.5

QY of sample A was measured within a couple of days since it was synthesized. However, measurements on sample B and C were carried out after 2 months post synthesis respectively. Although our particles were kept in vials that filled with argon gas, there was small amount of oxygen left inside. Over a period of months, the oxidation process was enough to produce a notable blue shift in emission. The emission shift of sample B with time is shown below in Figure 4.7.

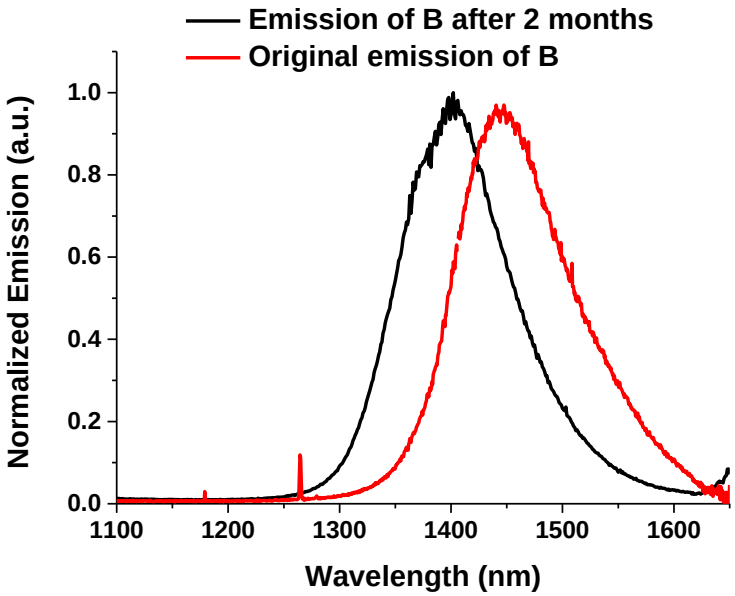

Figure 4.7. PL shift of sample B during a period of 2 months. Sample was dissolved in TCE with the 632 nm HeNe laser as the excitation source.

The emission of the three batches of PbS QDs were recorded right before QY measurements and shown below in Figure 4.8.

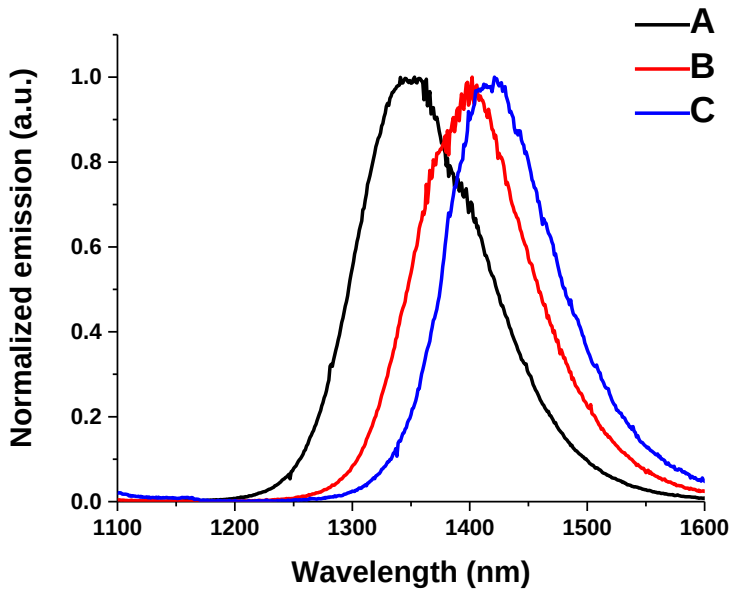

Figure 4.8. PL of PbS QDs before QY measurements. Sample was dissolved in TCE with the 632 nm HeNe laser as the excitation source.

The data treatment and calculation for PbS QDs were just like those of PbSe QDs. The final QY results are listed in Table 4-6.

Table 4-6. QY results of PbS QDs

Sample	QY (%) at ΔE_1=0.126 eV	QY (%) at ΔE_2=0.252 eV	QY (%) at ΔE_3=0.620 eV
A	51	35	4
B	52	22	4
C	21	10	2

The results of PbS QDs fit well with that of PbSe QDs. A similar decreasing QY is obtained as the excitation moves further away in energy differential. The quality of these PbS QDs are pretty good as the QY could be as high as 52%. At ΔE_3, the QY dropped to below 5%, which is also seen on PbSe QDs. Not much can be extrapolated from comparing the QY of one batch to another except that they all have the same trend.

4.5 QY study on PbSe-CdSe core-shell QDs

Three batches of PbSe-CdSe QDs were synthesized adopting the same method used in the last chapter, which is described in detail in the experimental section. Conditions used for each batch is shown in Table 4-7. The emission of these three batches are drawn in Figure 4.9.

Table 4-7. Experiment condition used for PbSe-CdSe QDs synthesis

Sample	Condition of PbSe core synthesis		Condition of cation exchange		Estimated core size (nm)
	Temperature (℃)	Time (minute)	Temperature (℃)	Time (hour)	
A	140	3	90	1	2.5
B	145	3	110	1	3
C	140	4	90	1	3.5

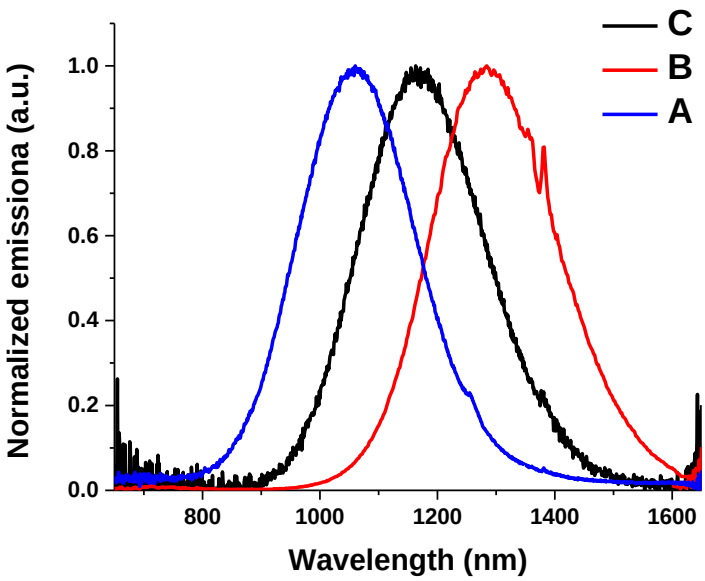

Figure 4.9. PL of PbSe-CdSe QDs before QY measurements. Sample was dissolved in TCE with the 632 nm HeNe laser as the excitation source.

The measurement of QY on core-shell QDs are totally the same as the cores. All data treatment and calculation were done using the same protocols. The results are listed in Table 4-8.

Table 4-8. QY results of PbSe-CdSe QDs

Sample	Experimental number	QY (%) at ΔE_1=0.126 eV	QY (%) at ΔE_2=0.252 eV	QY (%) at ΔE_3=0.620 eV
A	**089/CJM/14**	10	8	3
B	**092/CJM/14**	14	9	3
C	**039/CJM/13**	18	2	1

Interestingly, the highest reading of QY of PbSe-CdSe QDs are below 20%, which is much smaller than that of the cores. This is probably due to bad quality of the original cores used to synthesize these core-shell QDs. Also, the cation exchange broadened the size dispersion of the cores, which lowered their QYs. The QY values at ΔE_3 being below 5% accords with previous results well. Sample B here originated from sample D from PbSe QDs. Theoretically, the cation exchange can remove the surface defects of the core and constrain electron-hole pair inside. As a result, the exciton won't be trapped by the defects, making the QY higher. In this case, the PbSe core has QY values of 11%, 9% and 2%, while the PbSe-CdSe core-shell has values of 14%, 9% and 3%, respectively. A slight increase in QY proves the effect of enhancing emission efficiency by the shell.

4.6 QY study on PbS-CdS core-shell QDs

Two batches of PbS-CdS QDs were chosen to be used for systematic QY study. The conditions used during synthesis are presented below in Table 4-9. Their emission curves are plotted in Figure 4.10.

Table 4-9. Experiment condition used for PbS-CdS QDs synthesis

Sample	Condition of PbS core synthesis		Condition of cation exchange		Estimated core size (nm)
	Temperature (℃)	Time (minute)	Temperature (℃)	Time (hour)	
A	120	6	110	19	3
B	145	3	110	1	3.5

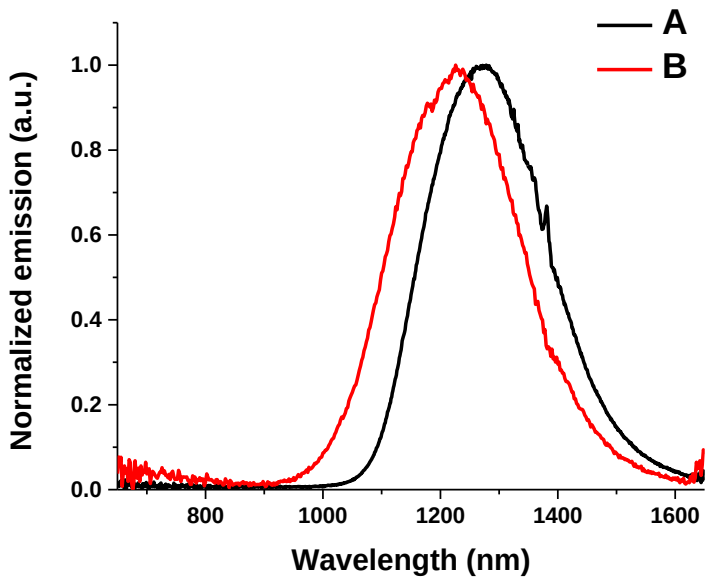

Figure 4.10. PL of PbS-CdS QDs before QY measurements. Sample was dissolved in TCE with the 632 nm HeNe laser as the excitation source.

The measurement of QY on PbS-CdS QDs are totally the same as the cores. All data treatment and calculation were done using the same protocols. The results are listed in Table 4-10.

Table 4-10. QY results of PbS-CdS QDs

Sample	Experimental number	QY (%) at ΔE_1=0.126 eV	QY (%) at ΔE_2=0.252 eV	QY (%) at ΔE_3=0.620 eV
A	**100/CJM/14**	38	11	2
B	**050/CJM/13**	13	6	2

The same trend can be seen on PbS-CdS QDs, just like other core-shell QDs and cores. It is convincing to draw the conclusion that we have observed excitation-dependent QY on PbSe, PbS, PbSe-CdSe and PbS-CdS QDs. The reason of this phenomenon could be non-radiative decays from higher excited states.[133] A. P. Alivisatos et al. believed that when electrons are excited to the third and higher levels in the conduction band, they would have higher chance of going through other non-radiative decay pathways that the first two levels can't have. This caused the QY decrease they observed on CdSe QDs.[133] In our case, with higher excitation energy, promoted electrons would jump into higher energy levels, ending up with more non-radiative processes, which lowers the QY.

The other effect that may have an impact on the QY is the Auger effect. When the electron-hole recombination happens, the energy released can not only be emitted as a photon, but also used to eject an electron (or electrons), which is known as the Auger effect.[130] The Auger effect is essentially the process where excited electrons in the conduction band get ejected by absorbing energy from those returning to the valence band. V. I. Klimov and co-workers have shown size-dependent Auger effect of CdSe QDs.[130] When the excitation energy increases and exceeds twice the energy of the energy gap of a quantum dot, the effect of multiple exciton generation (MEG) can happen.[135] It describes the process when one photon gets absorbed, two or more excitons are generated. Compared to lower excitation energy, a higher energy boosts the MEG effect, creating more excitons.

More excited electrons in the conduction band are likely to increase the possibility of Auger effect, leading to a lower fluorescent efficiency.

Errors in this measurements come from different sources. Preferably, the wavelength of the excitation light should be quite mono-dispersed. Lasers are definitely a better choice over a xenon lamp in this case. In addition, the monochromator we used may have slightly different efficiency of selecting light at a certain wavelength, which leads to intrinsic experimental errors that we cannot estimate. Also, not all measurements were done on the same day. As a result, the experimental and random errors from one measurement to another are not the same, though they should not be remarkably different. Also, the size dispersion of QDs will have an impact on the outcome because a batch with poor size-dispersion will contain quite varied band structures, and they can have different Auger rates as shown by V. I. Klimov et al.[130] Moreover, as discussed above, an experimental error of 10 to 20% (relative error) is considered high in common sense. The QY values listed can qualitatively reveal the trend, but they may not be quantitatively accurate enough. This numbers could have been over estimated since it was determined through three runs on one batch only. More repetitive runs on different batches should be done to re-evaluate the error.

QY measurements were not successfully conducted on core-shell-shell QDs. Our detector was not stable enough in the past months, giving a lot of sharp artifacts and unstable backgrounds. Also, none of the batches tested showed a very strong PL intensity exiting the integrating sphere. One of the reasons is the low chemical yield of core-shell-shell QDs. Most of the product were not properly precipitated as the supernatant was still coloured when discarded. Lack of fluorophores in the solution will lead to a low intensity, which cannot be properly processed with softwares. Also, the relative high noise level of our detector will have a larger influence on spectra with low intensities compared to those with high readings. The other possible reason could be that the ZnS shell reduced the QY of original core-shell QDs when being coated. This is less likely compared to the first conjecture, because this layer hardly changed the either PL or UV-absorption of core-shell QDs.

Although the QY values of core-shell-shell QDs could not be measured directly, they can be estimated by comparing to those of core-shell QDs. When both core-shell and core-shell-shell QDs where re-dissolved in TCE for PL measurements (using the same slits widths, light source and filters), with approximately the same concentration by weight, the PL intensities of the core-shell-shell QDs were about one third of the core-shell QDs. Considering core-shell-shell QDs are heavier than core-shell QDs, the same concentration by weight means there are slightly less core-shell-shell QDs in solution. By estimation, the QY of core-shell-shell QDs will not exceed half of those of core-shell QDs. This agrees with J. A. Hollingsworth's result.[99] The numbers she reported were 90% for PbSe-CdSe QDs and 48% for PbSe-CdSe-ZnS QDs. The authors stated that at early shell growth stages, the QY was substantially diminished, but when growth continued, PL efficiency appreciably recovered until an apparent "ideal" shell thickness, after which it started to decline again. They were not sure whether refinement of the shell synthesis could remove this effect.

4.7 Conclusions

A decreasing QY with an increasing excitation energy is observed on both core and core-shell QDs. I believe that this excitation-dependent QY is not a coincident. It could be the result of non-radiative decays from higher excited states or increased Auger effect as discussed above.

In general, the QY of PbSe or PbS could be as high as 53% when excited close to the first absorption peak, showing good quality. People have reported values as high as 85% (see previous discussion) for lead-based QDs, but they were either exciting at the first absorption peak or without saying how they measured. Both core and core-shell QDs have no higher than 5% QYs when excited at the furthest ΔE.

Although the QY measurements on core-shell-shell QDs were not successfully done, they are believed to have no more than half the fluorescent efficiency of their core-shell precursors. Refinements on the ZnS shell growth may be able to improve the QY in the future.

Based on this work, more measurements can be done to further support our findings, on lead-based core, core-shell and especially core-shell-shell QDs. The reasons for not seeing an increased QY from core-shell to core-shell-shell QDs worth more focus. Repetitive measurements should be done to define the error scale better.

Moreover, this systematic QY study can be conducted on other QDs emitting in the NIR range, and visible light range as well, to find out if this characteristic is unique or communal. A more delicately designed system (including a new integrating sphere) and more sensitive detectors can be used to obtain results that are more accurate.

Chapter 5 Summary and outlook

Lead-based core, core-shell and core-shell-shell QDs were successfully synthesized. Different techniques including transmission electron microscopy, photoluminescence (PL) measurement, UV-absorption and X-ray photoelectron spectroscopy (XPS) were used to characterize them. The particles we made have very good quality as supported by small FWHM values (less than 100 meV for core QDs) from PL spectra and narrow size dispersions calculated from TEM images. The position of the PL maximum of core-shell-shell QDs can be adjusted by controlling the reaction conditions of core-shell QDs synthesis. It is shown that the core-shell-shell structure was established by TEM images and energy-dependent XPS measurements. This is the first time that the ZnS shell is proved by energy-dependent XPS technique. Also, we showed that these core-shell-shell QDs have very good stability against oxidation for as long as 20 months.

So far, a few questions yet need to be answered, which will require more research in the future. The relative position of PL maximum of core-shell-shell QDs to that of core-shell QDs is not fixed based on my results. The reasons behind this might be a combination of multiple effects, such as dissolution of smaller particles and alloying on the Pb-Cd interface. Moreover, one batch of PbS-CdS-ZnS QDs seemed to be less stable compared to all other core-shell-shell QDs, which are all quite oxidation prove. In addition, more XPS measurements can be a good way to resolve the actual structure of these QDs better, and verify our conclusions.

Following this work, some bio-studies could be done. For example, the toxicity of these core-shell-shell QDs can be tested because the ZnS layer should be able to retain the poisonous compounds inside from contact. If they can show good biocompatibility, they will be good candidates for bio-labelling and imaging.

In Chapter 4, the excitation-dependent QY were tested and it is shown that lead-based core and core-shell QDs have a lower PL efficiency at higher excitation energy. The QY could drop from almost 50% to less than 10% for core QDs. This is the first time this phenomenon is observed on QDs emitting in the NIR range. It is a pity that we weren't able to collect the data we were hoping for on core-shell-shell QDs. It could be that the low chemical yield affected the signal intensity or the QY dropped drastically during the stage when ZnS shell formed, which certainly worth more focus in the future.

More core-shell-shell QDs should be synthesized using the method described in this thesis and have their QY measured with different excitation wavelengths. In addition, the excitation-dependent property should be re-examined on lead-based core and core-shell QDs to confirm our findings.

After this phenomenon is fully confirmed, the cause of it should be studies thoroughly. It will be interesting to try the same measurements on other NIR emitting QDs to find out whether this property is unique on lead-based QDs or communal.

Experimental work

Chemicals

The following chemicals were bought from Sigma Aldrich: Lead(II) oxide (powder, >99.9%, catalog# 211907), selenium (powder, >99.5%, catalog# 209651), cadmium acetate hydrate (>99.99%, catalog# 229490), hexamethyldisilathiane [$(TMS)_2S$] (synthesis grade, catalog# 283134), octadecene (ODE) (technical grade, 90%, catalog# 0806), oleic acid (OA) (technical grade, 90%, catalog# 364525), trioctylphosphine (TOP) (technical grade, 90%, catalog# 117854), diethylzinc solution (1.0 M in hexane, catalog# 296112), hexane (mixture of isomers, ACS reagent, >98.5%, catalog# 178918) and tetrachloroethylene (TCE) (ACS reagent grade, >99%, catalog# 443786. Chloroform (spectroscopic grade, >99.8%, catalog# UN1888) was obtained from VWR. Lead acetate trihydrate (ACS reagent, >99.0%, catalog# 4360-1) was from Caledon Labs. Methanol (HPLC grade, catalog# MX0475) was purchased from EMD. Ethanol (anhydrous, catalog# P016EAAN) was received from Commercial Alcohols. All chemicals were used as received.

Cuvette

All cuvettes used were fluorimeter screw cap cells with closed caps, purchased from Starnar cells. The catalog number for them is 3-Q-10-GL14-C. They were made from 4 spectrosil far UV quartz windows, allowing the usable range to be 170 – 2500 nm. The interior size of each cuvette is 10×10 mm^2, and the volume is 3.5 ml.

Gold foil

The gold foil (99.99% trace metal basis) used for XPS measurements was from Sigma Aldrich. Thickness of the foil is 0.1 mm, and the catalog number is 265810.

TEM grid and tweezer

TEM grids used were from Electron Microscopy Sciences. The catalog number is FCF300-CU-50. Tweezers used for TEM grids preparation were bought from Electron Microscopy Sciences, with a catalog# 0304-N2-PO.

Instruments and measurements

UV-Vis absorption measurements

A Perkin Elmer Lambda 1050 spectrometer was used to measure absorption for all samples. In the beginning, a scan was performed by the instrument with no cuvette inside for instrument internal calibration. For the data collection of the sample, two quartz cuvettes were inserted, one of which was filled with pure TCE as reference. The other cuvette was prepared by adding 5 – 7 drops of QDs sample, which was pre-dispersed in pure TCE, and diluted to full volume with more TCE. The final concentration was about

0.3 mg/ml. Transmitted light from both cuvette was collected, thus absorption was calculated accordingly.

Photoluminescence (PL) measurements

PL measurements were done using an Edinburgh Instrument FLS 920 fluorescence system. The sample was put in a cuvette and placed in the sample holder, where the excitation beam can pass through. The cuvette was prepared by adding 5 – 7 drops of QDs sample, which was pre-dispersed in pure TCE, and diluted to full volume with more TCE. The final concentration was around 0.3 mg/ml. A 450 W xenon lamp, which has a continuous emission spectrum from 200 to 900 nm and a monochromator to select a certain wavelength was used as the excitation source. Light from the xenon lamp was collimated by an aperture, resulting in a 3×10 mm^2 spot on the cuvette. Apart from the xenon lamp, a 5.0 mW HeNe laser (fixed emission at 633 nm) was also be used to excite the sample on occasions. While beam from the HeNe laser is highly focused, a few crystals was used to bend the beam and guide it into our fluorimeter to give a 3 mm diameter spot on the cavette. With both entrance and exit slits opened to 0.55 mm, a resolution of 1 nm can be obtained. A R5509 NIR-PMT detector (effective detection range: 650-1650 nm, made by Hamamatsu) was used to collect signal emitted by sample. A 645 nm longpass filter was placed between the cuvette and the detector to block scattered incident light. All measurements were run using 1 nm step size, 0.1 s dwell time. Spectra were subtracted for background noise level, followed by correction with the correction file for the specific detector.

Transmission electron microscopy (TEM)

TEM images of all sample were taken by a JEOL JEM-1400 microscope. 1 – 2 drops of TCE-dispersed samples was added to 2 ml of hexane prior to drop-casted on copper grids. Concentration of samples was made to so low that it's almost colourless. This was to avoid overlapping of several layers of sample. Each grid was held by a tweezer on the edge, then one drop of sample was put on it. The grid was allowed to dry in air for about 2 minutes to evaporate all the solvent. When observing using TEM, different magnifications were used to obtain general and detailed view of QDs. For size analysis, all pictures were taken under 600,000 magnification, which is the best resolution we can get while maintaining a clear view of each particle. Size analysis was done by counting the diameter of at least 100 particles. Diameter was measured by hand using the software ImageJ 1.48. The mean value and standard deviation were given by the software after counting.

X-ray photoluminescence spectroscopy (XPS) measurements

XPS measurements were carried out using the Spherical Grating Monochromator (SGM) 11ID-1 beamline at Canadian Light Source, locating in Saskatoon. The gold foil was cut into small pieces (about $5 \times 5\ mm^2$) prior to sample preparation. All samples were dispersed in hexane and drop-casted onto the gold pieces. Concentration of samples were made to be about 0.2 mg/ml. To avoid potential charging issue (electrons accumulating on the surface of sample instead of being conducted away), 3 drops of sample was deposited on each piece. All gold pieces were allowed to dry well in air before put into the measuring chamber, where a rotary pump degased to produce the needed vacuum. Apart from sample-covered pieces, a clean piece of gold was also used as a reference. Gold pieces were attached to a copper sample holder by carbon tape. Once the pressure inside the chamber reached the required value (less than 1×10^{-8} torr), a test run on that piece of clean gold was done first. A visible light that hit the same spot as the electron beam was used to make sure the beam was hitting right on the gold. After adjusting the angle and position of the sample holder to

maximize the gold signal, a survey scan from 50 – 1010 eV was performed to make sure the instrument was correctly set up, with step size and dwell time set to be 100 or 250 meV and 67 ms respectively. Then, surveys scans on samples were performed to identify peaks from different elements with the same conditions. For survey scans, a full range from 50 to 1300 eV was selected. To observe specific peaks better, high-resolution scans were done, with a much smaller step size (25 meV) and more iterations (3 to 20 depending on the S/N ratio). For well pronounced peaks, 3 iterations was good enough, while 20 might be needed until we can get distinguished zinc peaks by eyes. Energy-dependent XPS measurements were then conducted by changing the energy from 500 eV to 100 eV higher than the characteristic peak we were interested in.

Quantum yield measurements

Quantum yield measurements were done by using the Edinburgh Instrument FLS 920 fluorescence system. The 450 W xenon lamp was chosen to excite samples with desired wavelengths, which was selected by the monochromator, and the NIR-PMT detector was used to collect emission signal. A 15-cm-diameter integrating sphere, inside of which was coated with barium sulfate ($BaSO_4$), was used for these measurements. The $BaSO_4$ coating is designed to reflect light with high efficiency (over 99%).[136] The sphere comes with four small holes. An entrance hole allows incident light to come in and hit the sample while two exit holes allow photons to be counted by the either a NIR or visible detector (NIR actually used for all OY measurements). The fourth hole, which locates on the top of the sphere, is where we put the sample holder in. The sample holder is located in the center of the sphere with a $BaSO_4$ coated baffle on one side, stopping direct scattered light hitting the detector. The sample solution used was the same as the one used for PL measurement with pure TCE as the solvent. To reduce the self-absorbing of emitted light, only 3 – 4 drops of sample was added to the cuvette, which was filled up with TCE later. Another cuvette was loaded with pure TCE as reference. When incident light hit the sample (QDs), a small part of it was absorbed while the majority transmitted or got scattered and was diffused by the

$BaSO_4$ coating. Then a part of the diffused light was absorbed again by the sample. Every time the sample absorbed, it emitted afterwards. That emitted light was diffused by the coating as well. This process kept repeating until eventually unabsorbed incident light and emitted light came out from the exit hole.

To calculate the QY of one sample, three scans were needed. Firstly, with the cuvette holding pure TCE inside the sphere, a scan on the region of incident light was done. After that, another scan with exactly same condition but using the cuvette with the sample was done. The step size and dwell time were 0.2 nm and 0.5 s respectively, and three repeats were performed. The third run scanned the region of the emission, but used a 1.0 nm step size (Because the minimum slit width I used was 0.55 mm, which mean the best resolution was 1 nm. In this case, a step size smaller than 1.0 nm wouldn't affect the counts) and 5 – 10 scans. Before any data calculation, all resulted spectra were corrected by subtracting background noise, followed by applying the correction file for the PMT detector, which was used in all three scans.

Synthesis of core, core-shell and core-shell-shell QDs

1. TOP-Se was made in a glovebox filled with pure nitrogen gas. In a 100 ml round bottom flask, 1.58 g of selenium powder and 50 ml of TOP were mixed, resulting in a 0.4 M TOP-Se solution. A complete disappearance of the black colour of selenium power was the sign of a complete dissolving. The freshly prepared solution was kept inside the glovebox under stirring and used or discarded within a month.

2. PbSe quantum dots were synthesized using a well-established hot-injection method[22]. In a 150 ml three-neck flask, 0.4458 g of lead (II) oxide was mixed up

with 1.3 ml of oleic acid and 30 ml of octadecene. While the flask was being degased by a Welch direct-drive rotary vane vacuum pump, the solution was heated up to 130 ℃ for 2 hours using an oil bath, with the temperature sensor in the oil. After 2 hours, temperature was brought up to 150 ℃, then and the flask was bubbled through with argon gas. With vigorous stirring, 5 ml of 0.4 M TOP-Se was injected. 7 minutes later, the reaction was quenched by quickly removing the flask from heating and pouring the solution into 120 ml of ice-cold ethanol, which was also under stirring in a 1000 ml beaker. One minute later, the solution was poured into four 50 ml centrifuge tubes, which was then filled up with more ethanol. Every tube contained an equal amount of solution before they were filled up and vortexed for 10 s. Centrifugation was done at 1717 g-force for 5 minutes. After that, centrifuge tubes were emptied of the supernatant and filled up with pure ethanol and vortexed again. This ethanol-vortex-centrifugation-empty step was repeated 4 times including the first one before tubes were dried by argon stream in the end. 3 tubes of QDs were dispersed in 10 ml of chloroform for further use, while the last tube of QDs were dispersed in 10 ml TCE and degased by argon stream for storage in darkness at room temperature.

3. PbS quantum dots were synthesized in a similar way[73] as PbSe QDs. In a 150 ml three neck flask, 0.57 g of lead acetate, 1.95 ml of oleic acid and 30ml of octadecene were mixed up. After degasing the flask with the rotary pump for 3 minutes, argon gas was used to bubble through the flask, followed by the injection of 3 ml of TOP. Again, the flask was degased using the rotary pump and heated up to 120 ℃ for 2 hours in an oil bath, with the temperature sensor in the oil. Then, the flask was bubbled through with argon gas, and 27 μl of $(TMS)_2S$ was injected very fast with vigorous stirring. The reaction was quenched after 8 minutes by quickly removing the flask from heating and pouring the solution into 120 ml of ice-cold ethanol, which was also under stirring in a 1000 ml beaker. One minute later, the solution was poured into four 50 ml centrifuge tubes. Each tube contained an equal amount of solution before they were filled up with more ethanol and vortexed for 10 s. Centrifugation was done at 1717 g-force for 5 minutes. After that, centrifuge tubes

were emptied of the supernatant and filled up with pure ethanol and vortexed again. This ethanol-vortex-centrifugation-empty step was repeated 4 times including the first one before tubes were dried by argon stream in the end. 3 tubes of QDs were dispersed in 10 ml of chloroform for further use, while the last tube of QDs were dispersed in 10 ml TCE and degased by argon stream for storage in darkness at room temperature.

4. PbSe-CdSe QDs were synthesized by a cation exchange, which was first reported by J. A. Hollingsworth and co-workers[99] and implemented by our group[72 100]. In a 150 ml flask, 25.6 ml of octadecene, 20.4 ml of oleic acid and 2.0 g of cadmium acetate hydrate were mixed up. The flask was degased by the rotary pump and heated up to 120 ℃ in oil bath, with the temperature sensor in the oil. Meanwhile, PbSe QDs previously dispersed in chloroform were dried by argon stream and re-dispersed in 3 ml of octadecene. After 2 hours, the flask was bubbled through with argon gas, and the temperature was lowered to 100 ℃. PbSe QDs were then injected. The flask was removed from heating and cooled down naturally after 19 hours. Then, 50 ml of methanol was added into the flask with vigorous stirring. The solution was poured into four 50 ml centrifuge tubes, with each tube having approximately the same amount. Tubes were then filled up with more methanol and vortexed for 10 s. Centrifugation was done at 1717 g-force for 5 minutes. After that, centrifuge tubes were emptied of the supernatant and filled up with pure methanol and vortexed again, followed by centrifugation. Instead of methanol, this solvent-vortex-centrifugation-empty step was repeated twice more with ethanol before tubes were dried by argon stream in the end. 3 tubes of QDs were dispersed in 10 ml of chloroform for further use, while the last tube of QDs were dispersed in 10 ml TCE and degased by argon stream for storage in darkness at room temperature.

5. PbS-CdS QDs were also synthesized by the same cation exchange[99]. In a 150 ml flask, 25.6 ml of octadecene, 20.4 ml of oleic acid and 2.0 g of cadmium acetate

hydrate were mixed up. The flask was degased by the rotary pump and heated up to 120 ℃ in oil bath, with the temperature sensor in the oil. Meanwhile, PbS QDs previously dispersed in chloroform were dried by argon stream and re-dispersed in 3 ml of octadecene. After 2 hours, the flask was bubbled through with argon gas, and the temperature was lowered to 100 ℃. PbS QDs were then injected. The flask was removed from heating and cooled down naturally after 19 hours. Then, 50 ml of methanol was added into the flask with vigorous stirring. The solution was poured into four 50 ml centrifuge tubes, with each tube having approximately the same amount. Tubes were then filled up with more methanol and vortexed for 10 s. Centrifugation was done at 1717 g-force for 5 minutes. After that, centrifuge tubes were emptied of the supernatant and filled up with pure methanol and vortexed again, followed by centrifugation. Instead of methanol, this solvent-vortex-centrifugation-empty step was repeated twice more with ethanol before tubes were dried by argon stream in the end. 3 tubes of QDs were dispersed in 10 ml of chloroform for further use, while the last tube of QDs were dispersed in 10 ml TCE and degased by argon stream for storage in darkness at room temperature.

6. The synthesis of PbSe-CdSe-ZnS core-shell-shell QDs follows the method developed by J. A. Hollingsworth and co-workers[99]. PbSe-CdSe QDs that were dispersed in chloroform were dried by argon stream and re-dispersed in 3 ml of octadecene. In a 150 ml 3-neck flask, 16ml of octadecene, 5ml of oleic acid and 1ml of TOP were added. The mixture was heated to 140 ℃ in oil bath for half an hour with the temperature sensor in the oil, while being degased by the rotary pump. After bubbling through the flask with argon gas, the core-shell QDs were injected. In the glovebox, a small vial containing 20 μl of diethylzinc, 1.5ml of TOP and 15 μl of $(TMS)_2S$ was prepared. Immediately after this solution was made, it was added into the flask dropwise (2 drops per second). The reaction was quenched after 20 minutes by cooling the whole flask down in ice-cold water bath, followed by adding 50 ml of ethanol into the flask with vigorous stirring. The solution was poured into four 50 ml centrifuge tubes. Each tube contained an equal amount of solution before they were filled up with more ethanol and vortexed for 10 s.

Centrifugation was done at 1717 g-force for 5 minutes. After that, centrifuge tubes were emptied of the supernatant and filled up with pure ethanol and vortexed again. This ethanol-vortex-centrifugation-empty step was repeated thrice including the first one before tubes were dried by argon stream in the end. 3 tubes of QDs were dispersed in 10 ml of TCE and degased for storage in darkness at room temperature, while the last tube of QDs were dispersed in 10 ml hexane for XPS measurements.

7. The synthesis of PbS-CdS-ZnS QDs used the same method[99]. PbSe-CdSe QDs that were dispersed in chloroform were dried by argon stream and re-dispersed in 3 ml of octadecene. In a 150 ml 3-neck flask, 16ml of octadecene, 5ml of oleic acid and 1ml of TOP were added. The mixture was heated to 140 ℃ in oil bath for half an hour with the temperature sensor in the oil, while being degased by the rotary pump. After bubbling through the flask with argon gas, the core-shell QDs were injected. In the glovebox, a small vial containing 20 μl of diethylzinc, 1.5ml of TOP and 15 μl of $(TMS)_2S$ was prepared. Immediately after this solution was made, it was added into the flask dropwise (2 drops per second). The reaction was quenched after 20 minutes by cooling the whole flask down in ice-cold water bath, followed by adding 50 ml of ethanol into the flask with vigorous stirring. The solution was poured into four 50 ml centrifuge tubes. Each tube contained an equal amount of solution before they were filled up with more ethanol and vortexed for 10 s. Centrifugation was done at 1717 g-force for 5 minutes. After that, centrifuge tubes were emptied of the supernatant and filled up with pure ethanol and vortexed again. This ethanol-vortex-centrifugation-empty step was repeated thrice including the first one before tubes were dried by argon stream in the end. 3 tubes of QDs were dispersed in 10 ml of TCE and degased for storage in darkness at room temperature, while the last tube of QDs were dispersed in 10 ml hexane for XPS measurements.

References

1. Reed, M. A.; Randall, J. N.; Aggarwal, R. J.; Matyi, R. J.; Moore, T. M.; Wetsel, A. E. *Physical Review Letters* **1988,** 60, (6), 535-537.
2. Ekimov, A. I.; Efros, A. L.; Onushchenko, A. A. *Solid State Communications* **1985,** 56, (11), 921-924.
3. Rossetti, R.; Hull, R.; Gibson, J. M.; Brus, L. E. *The Journal of Chemical Physics* **1985,** 82, (1), 552-559.
4. Levine, I. N., *Physical chemistry*. McGraw-Hill: 2008.
5. Bawendi, M. G.; Steigerwald, M. L.; Brus, L. E. *Annual Review of Physical Chemistry* **1990,** 41, (1), 477-496.
6. Gaponenko, S. V., *Optical properties of semiconductor nanocrystals*. Cambridge university press: 1998; Vol. 23.
7. Ma, Q.; Su, X. *Analyst* **2010,** 135, (8), 1867-1877.
8. Michalet, X.; Pinaud, F. F.; Bentolila, L. A.; Tsay, J. M.; Doose, S.; Li, J. J.; Sundaresan, G.; Wu, A. M.; Gambhir, S. S.; Weiss, S. *Science* **2005,** 307, (5709), 538-544.
9. Kittel, C.; McEuen, P.; McEuen, P., *Introduction to solid state physics*. Wiley New York: 1976; Vol. 8.
10. Klimov, V. I., *Nanocrystal quantum dots*. CRC Press: 2010.
11. Haug, H.; Koch, S. W., *Quantum theory of the optical and electronic properties of semiconductors*. World Scientific: 1990; Vol. 5.
12. Wise, F. W. *Accounts of Chemical Research* **2000,** 33, (11), 773-780.
13. Harrison, P., *Quantum wells, wires and dots: theoretical and computational physics of semiconductor nanostructures*. John Wiley & Sons: 2005.
14. Alivisatos, A. P. *Science* **1996,** 271, (5251), 933-937.
15. Pokutnii, S. I. *Semiconductors* **2010,** 44, (4), 488-493.
16. Engel, T., *Quantum chemistry and spectroscopy*. Pearson Education India: 2006.
17. Kang, I.; Wise, F. W. *Journal of the Optical Society of America B* **1997,** 14, (7), 1632-1646.
18. Trinh, M. T.; Houtepen, A. J.; Schins, J. M.; Piris, J.; Siebbeles, L. D. A. *Nano Letters* **2008,** 8, (7), 2112-2117.

19. Lakowicz, J. R., *Principles of fluorescence spectroscopy*. Springer Science & Business Media: 2007.

20. Yang, F.; Wilkinson, M.; Austin, E. J.; O'Donnell, K. P. *Physical Review Letters* **1993,** 70, (3), 323-326.

21. Martin, R. W.; Middleton, P. G.; O'Donnell, K. P.; Van der Stricht, W. *Applied Physics Letters* **1999,** 74, (2), 263-265.

22. Murray, C. B.; Sun, S.; Gaschler, W.; Doyle, H.; Betley, T. A.; Kagan, C. R. *IBM Journal of Research and Development* **2001,** 45, (1), 47-56.

23. Murray, C. B.; Kagan, C. R.; Bawendi, M. G. *Annual Review of Materials Science* **2000,** 30, (1), 545-610.

24. Murray, C. B.; Norris, D. J.; Bawendi, M. G. *Journal of the American Chemical Society* **1993,** 115, (19), 8706-8715.

25. Micic, O. I.; Sprague, J. R.; Curtis, C. J.; Jones, K. M.; Machol, J. L.; Nozik, A. J.; Giessen, H.; Fluegel, B.; Mohs, G.; Peyghambarian, N. *The Journal of Physical Chemistry* **1995,** 99, (19), 7754-7759.

26. Peng, X.; Manna, L.; Yang, W.; Wickham, J.; Scher, E.; Kadavanich, A.; Alivisatos, A. P. *Nature* **2000,** 404, (6773), 59-61.

27. Wang, F.; Tang, R.; Buhro, W. E. *Nano Letters* **2008,** 8, (10), 3521-3524.

28. Peng, Z. A.; Peng, X. *Journal of the American Chemical Society* **2001,** 123, (1), 183-184.

29. Qu, L.; Peng, Z. A.; Peng, X. *Nano Letters* **2001,** 1, (6), 333-337.

30. Chestnoy, N.; Hull, R.; Brus, L. E. *The Journal of Chemical Physics* **1986,** 85, (4), 2237-2242.

31. Rajh, T.; Micic, O. I.; Nozik, A. J. *The Journal of Physical Chemistry* **1993,** 97, (46), 11999-12003.

32. Qian, H.; Qiu, X.; Li, L.; Ren, J. *The Journal of Physical Chemistry B* **2006,** 110, (18), 9034-9040.

33. Hui, L.; Wan, Y. S.; Wei-Heng, S. *Nanotechnology* **2007,** 18, (20), 205604.

34. Wang, C.; Gao, X.; Ma, Q.; Su, X. *Journal of Materials Chemistry* **2009,** 19, (38), 7016-7022.

35. Li, H.; Shih, W. Y.; Shih, W.-H. *Industrial & Engineering Chemistry Research* **2007,** 46, (7), 2013-2019.

36. Skolnick, M.; Mowbray, D. *Annual Review of Materials Research* **2004,** 34, 181-218.

37. Daudin, B.; Widmann, F.; Feuillet, G.; Samson, Y.; Arlery, M.; Rouvière, J. L. *Physical Review B* **1997,** 56, (12), R7069-R7072.

38. Borrelli, N. F.; Smith, D. W. *Journal of Non-Crystalline Solids* **1994,** 180, (1), 25-31.

39. Mukherjee, M.; Datta, A.; Chakravorty, D. *Journal of Materials Research* **1997,** 12, (10), 2507-2510.

40. Lipovskii, A. A.; Kolobkova, E. V.; Olkhovets, A.; Petrikov, V. D.; Wise, F. *Physica E: Low-dimensional Systems and Nanostructures* **1999,** 5, (3), 157-160.

41. Lipovskii, A.; Kolobkova, E.; Petrikov, V.; Kang, I.; Olkhovets, A.; Krauss, T.; Thomas, M.; Silcox, J.; Wise, F.; Shen, Q.; Kycia, S. *Applied Physics Letters* **1997,** 71, (23), 3406-3408.

42. Wang, Y.; Suna, A.; Mahler, W.; Kasowski, R. *The Journal of Chemical Physics* **1987,** 87, (12), 7315-7322.

43. Sankaran, V.; Cummins, C. C.; Schrock, R. R.; Cohen, R. E.; Silbey, R. J. *Journal of the American Chemical Society* **1990,** 112, (19), 6858-6859.

44. Kane, R. S.; Cohen, R. E.; Silbey, R. *Chemistry of Materials* **1996,** 8, (8), 1919-1924.

45. Lifshitz, E.; Sirota, M.; Porteanu, H. *Journal of Crystal Growth* **1999,** 196, (1), 126-134.

46. Meldrum, F. C.; Flath, J.; Knoll, W. *Thin Solid Films* **1999,** 348, (1–2), 188-195.

47. Tomczak, N.; Jańczewski, D.; Han, M.; Vancso, G. J. *Progress in Polymer Science* **2009,** 34, (5), 393-430.

48. Whaley, S. R.; English, D. S.; Hu, E. L.; Barbara, P. F.; Belcher, A. M. *Nature* **2000,** 405, (6787), 665-668.

49. Lee, S.-W.; Mao, C.; Flynn, C. E.; Belcher, A. M. *Science* **2002,** 296, (5569), 892-895.

50. Yamashita, I.; Hayashi, J.; Hara, M. *Chemistry Letters* **2004,** 33, (9), 1158-1159.

51. Bao, H.; Hao, N.; Yang, Y.; Zhao, D. *Nano Research* **2010,** 3, (7), 481-489.

52. Sturzenbaum, S. R.; HocknerM; PanneerselvamA; LevittJ; Bouillard, J. S.; TaniguchiS; Dailey, L. A.; Khanbeigi, R. A.; Rosca, E. V.; ThanouM; SuhlingK; Zayats, A. V.; GreenM. *Nature Nanotechnology* **2013,** 8, (1), 57-60.

53. Mullin, J. W., *Crystallization*. Butterworth-Heinemann: 2001.

54. Thanh, N. T. K.; Maclean, N.; Mahiddine, S. *Chemical reviews* **2014,** 114, (15), 7610-7630.

55. LaMer, V. K.; Dinegar, R. H. *Journal of the American Chemical Society* **1950,** 72, (11), 4847-4854.

56. Yu, K.; Hu, M. Z.; Wang, R.; Piolet, M. L.; Frotey, M.; Zaman, M. B.; Wu, X.; Leek, D. M.; Tao, Y.; Wilkinson, D.; Li, C. *The Journal of Physical Chemistry C* **2010,** 114, (8), 3329-3339.

57. Kasuya, A.; Sivamohan, R.; Barnakov, Y. A.; Dmitruk, I. M.; Nirasawa, T.; Romanyuk, V. R.; Kumar, V.; Mamykin, S. V.; Tohji, K.; Jeyadevan, B.; Shinoda, K.; Kudo, T.; Terasaki, O.; Liu, Z.; Belosludov, R. V.; Sundararajan, V.; Kawazoe, Y. *Nature Materials* **2004,** 3, (2), 99-102.

58. Brazeau, A. L.; Jones, N. D. *The Journal of Physical Chemistry C* **2009,** 113, (47), 20246-20251.

59. Pontoni, D.; Narayanan, T.; Rennie, A. R. *Langmuir* **2002,** 18, (1), 56-59.

60. Sugawara, M.; Hatori, N.; Ishida, M.; Ebe, H.; Arakawa, Y.; Akiyama, T.; Otsubo, K.; Yamamoto, T.; Nakata, Y. *Journal of Physics D: Applied Physics* **2005,** 38, (13), 2126.

61. Kairdolf, B. A.; Smith, A. M.; Stokes, T. H.; Wang, M. D.; Young, A. N.; Nie, S. *Annual Review of Analytical Chemistry* **2013,** 6, (1), 143-162.

62. Kobayashi, H.; Ogawa, M.; Alford, R.; Choyke, P. L.; Urano, Y. *Chemical reviews* **2009,** 110, (5), 2620-2640.

63. Smith, A. M.; Duan, H.; Mohs, A. M.; Nie, S. *Advanced Drug Delivery Reviews* **2008,** 60, (11), 1226-1240.

64. Jamieson, T.; Bakhshi, R.; Petrova, D.; Pocock, R.; Imani, M.; Seifalian, A. M. *Biomaterials* **2007,** 28, (31), 4717-4732.

65. Nozik, A. J. *Physica E: Low-dimensional Systems and Nanostructures* **2002,** 14, (1–2), 115-120.

66. Semonin, O. E.; Luther, J. M.; Choi, S.; Chen, H.-Y.; Gao, J.; Nozik, A. J.; Beard, M. C. *Science* **2011,** 334, (6062), 1530-1533.

67. Leschkies, K. S.; Divakar, R.; Basu, J.; Enache-Pommer, E.; Boercker, J. E.; Carter, C. B.; Kortshagen, U. R.; Norris, D. J.; Aydil, E. S. *Nano Letters* **2007,** 7, (6), 1793-1798.

68. Guo, C. X.; Yang, H. B.; Sheng, Z. M.; Lu, Z. S.; Song, Q. L.; Li, C. M. *Angewandte Chemie International Edition* **2010,** 49, (17), 3014-3017.

69. Loss, D.; DiVincenzo, D. P. *Physical Review A* **1998,** 57, (1), 120-126.

70. Awschalom, D. D.; Loss, D.; Samarth, N., *Semiconductor spintronics and quantum computation*. Springer Science & Business Media: 2002.

71. Weissleder, R. *Nat Biotech* **2001,** 19, (4), 316-317.

72. Abel, K. A.; Qiao, H.; Young, J. F.; van Veggel, F. C. J. M. *The Journal of Physical Chemistry Letters* **2010,** 1, (15), 2334-2338.

73. Abel, K. A.; Shan, J.; Boyer, J.-C.; Harris, F.; van Veggel, F. C. J. M. *Chemistry of Materials* **2008,** 20, (12), 3794-3796.

74. Pichaandi, J.; Abel, K. A.; Johnson, N. J. J.; van Veggel, F. C. J. M. *Chemistry of Materials* **2013,** 25, (10), 2035-2044.

75. Quintero-Torres, R.; Foell, C. A.; Pichaandi, J.; van Veggel, F. C. J. M.; Young, J. F. *Applied Physics Letters* **2012,** 101, (12), 121904.

76. Qiao, H.; Abel, K. A.; van Veggel, F. C. J. M.; Young, J. F. *Physical Review B* **2010,** 82, (16).

77. Rogach, A.; Harrison, M.; Kershaw, S.; Kornowski, A.; Burt, M.; Eychmüller, A.; Weller, H. *physica status solidi (b)* **2001,** 224, (1), 153-158.

78. Micic, O. I.; Curtis, C. J.; Jones, K. M.; Sprague, J. R.; Nozik, A. J. *The Journal of Physical Chemistry* **1994,** 98, (19), 4966-4969.

79. Du, Y.; Xu, B.; Fu, T.; Cai, M.; Li, F.; Zhang, Y.; Wang, Q. *Journal of the American Chemical Society* **2010,** 132, (5), 1470-1471.

80. Derfus, A. M.; Chan, W. C. W.; Bhatia, S. N. *Nano Letters* **2004,** 4, (1), 11-18.

81. Pichaandi, J.; van Veggel, F. C. J. M. *Coordination Chemistry Reviews* **2014,** 263-264, 138-150.

82. Tytus, M.; Krasnyj, J.; Jacak, W.; Chuchmała, A.; Donderowicz, W.; Jacak, L. In *Differences between photoluminescence spectra of type-I and type-II quantum dots*, Journal of Physics: Conference Series, 2008; IOP Publishing: p 012011.

83. Gorer, S.; Albu-Yaron, A.; Hodes, G. *The Journal of Physical Chemistry* **1995,** 99, (44), 16442-16448.

84. Du, H.; Chen, C.; Krishnan, R.; Krauss, T. D.; Harbold, J. M.; Wise, F. W.; Thomas, M. G.; Silcox, J. *Nano Letters* **2002,** 2, (11), 1321-1324.

85. Wehrenberg, B. L.; Wang, C.; Guyot-Sionnest, P. *The Journal of Physical Chemistry B* **2002,** 106, (41), 10634-10640.

86. Sashchiuk, A.; Langof, L.; Chaim, R.; Lifshitz, E. *Journal of Crystal Growth* **2002,** 240, (3–4), 431-438.

87. Yu, W. W.; Falkner, J. C.; Shih, B. S.; Colvin, V. L. *Chemistry of Materials* **2004,** 16, (17), 3318-3322.

88. Stouwdam, J. W.; Shan, J.; van Veggel, F. C. J. M.; Pattantyus-Abraham, A. G.; Young, J. F.; Raudsepp, M. *The Journal of Physical Chemistry C* **2006,** 111, (3), 1086-1092.

89. Gao, M.; Yang, Y.; Yang, B.; Shen, J.; Ai, X. *Journal of the Chemical Society, Faraday Transactions* **1995,** 91, (22), 4121-4125.

90. Yang, J.; Fendler, J. H. *The Journal of Physical Chemistry* **1995,** 99, (15), 5505-5511.

91. Chen, W.; Wang, Z.; Lin, Z.; Qian, J.; Lin, L. *Applied Physics Letters* **1996,** 68, (14), 1990-1992.

92. Guglielmi, M.; Martucci, A.; Menegazzo, E.; Righini, G. C.; Pelli, S.; Fick, J.; Vitrant, G. *Journal of Sol-Gel Science and Technology* **1997,** 8, (1-3), 1017-1021.

93. Rossetti, R.; Hull, R.; Gibson, J. M.; Brus, L. E. *The Journal of Chemical Physics* **1985,** 83, (3), 1406-1410.

94. Nenadovic, M. T.; Comor, M. I.; Vasic, V.; Micic, O. I. *The Journal of Physical Chemistry* **1990,** 94, (16), 6390-6396.

95. Machol, J. L.; Wise, F. W.; Patel, R.; Tanner, D. B. *Physica A: Statistical Mechanics and its Applications* **1994,** 207, (1–3), 427-434.

96. Hines, M. A.; Scholes, G. D. *Advanced Materials* **2003,** 15, (21), 1844-1849.

97. Cademartiri, L.; Bertolotti, J.; Sapienza, R.; Wiersma, D. S.; von Freymann, G.; Ozin, G. A. *The Journal of Physical Chemistry B* **2006,** 110, (2), 671-673.

98. Son, D. H.; Hughes, S. M.; Yin, Y.; Paul Alivisatos, A. *Science* **2004,** 306, (5698), 1009-1012.

99. Pietryga, J. M.; Werder, D. J.; Williams, D. J.; Casson, J. L.; Schaller, R. D.; Klimov, V. I.; Hollingsworth, J. A. *Journal of the American Chemical Society* **2008,** 130, (14), 4879-4885.

100. Abel, K. A.; FitzGerald, P. A.; Wang, T.-Y.; Regier, T. Z.; Raudsepp, M.; Ringer, S. P.; Warr, G. G.; van Veggel, F. C. J. M. *The Journal of Physical Chemistry C* **2012,** 116, (6), 3968-3978.

101. Streetman, B. G.; Banerjee, S., *Solid state electronic devices*. Prentice Hall Upper Saddle River, NJ: 2000; Vol. 4.

102. Williams, G. P. *X-RAY DATA BOOKLET* **2001**. U.S. Government Printing Office: 2001.

103. Borchert, H.; Haubold, S.; Haase, M.; Weller, H.; McGinley, C.; Riedler, M.; Möller, T. *Nano Letters* **2002,** 2, (2), 151-154.

104. Borchert, H.; Talapin, D. V.; Gaponik, N.; McGinley, C.; Adam, S.; Lobo, A.; Möller, T.; Weller, H. *The Journal of Physical Chemistry B* **2003,** 107, (36), 9662-9668.

105. Yeh, J.; Lindau, I. *Atomic data and nuclear data tables* **1985,** 32, (1), 1-155.

106. Rurack, K., Fluorescence Quantum Yields: Methods of Determination and Standards. In *Standardization and Quality Assurance in Fluorescence Measurements I*, Resch-Genger, U., Ed. Springer Berlin Heidelberg: 2008; Vol. 5, pp 101-145.

107. Crosby, G. A.; Demas, J. N. *The Journal of Physical Chemistry* **1971,** 75, (8), 991-1024.

108. Brouwer, A. M. *Pure and Applied Chemistry* **2011,** 83, (12), 2213-2228.

109. Melhuish, W. *The Journal of Physical Chemistry* **1961,** 65, (2), 229-235.

110. Meech, S. R.; Phillips, D. *Journal of photochemistry* **1983,** 23, (2), 193-217.

111. Dawson, W. R.; Windsor, M. W. *The Journal of Physical Chemistry* **1968,** 72, (9), 3251-3260.

112. Suzuki, K.; Kobayashi, A.; Kaneko, S.; Takehira, K.; Yoshihara, T.; Ishida, H.; Shiina, Y.; Oishi, S.; Tobita, S. *Physical Chemistry Chemical Physics* **2009,** 11, (42), 9850-9860.

113. Velapoldi, R. A.; Tønnesen, H. H. *Journal of Fluorescence* **2004,** 14, (4), 465-472.

114. Adams, M.; Highfield, J.; Kirkbright, G. *Analytical Chemistry* **1977,** 49, (12), 1850-1852.

115. Brannon, J. H.; Magde, D. *The Journal of Physical Chemistry* **1978,** 82, (6), 705-709.

116. Porres, L.; Holland, A.; Pålsson, L.-O.; Monkman, A. P.; Kemp, C.; Beeby, A. *Journal of Fluorescence* **2006,** 16, (2), 267-273.

117. Magde, D.; Wong, R.; Seybold, P. G. *Photochemistry and Photobiology* **2002,** 75, (4), 327-334.

118. Shen, J.; Lowe, R. D.; Snook, R. D. *Chemical physics* **1992,** 165, (2), 385-396.

119. Fischer, M.; Georges, J. *Chemical Physics Letters* **1996,** 260, (1), 115-118.

120. Karstens, T.; Kobs, K. *The Journal of Physical Chemistry* **1980,** 84, (14), 1871-1872.

121. Eaton, D. F. *Pure and Applied Chemistry* **1988,** 60, (7), 1107-1114.

122. Würth, C.; Grabolle, M.; Pauli, J.; Spieles, M.; Resch-Genger, U. *Analytical Chemistry* **2011,** 83, (9), 3431-3439.

123. Semonin, O. E.; Johnson, J. C.; Luther, J. M.; Midgett, A. G.; Nozik, A. J.; Beard, M. C. *The Journal of Physical Chemistry Letters* **2010,** 1, (16), 2445-2450.

124. Jacquez, J. A.; Kuppenheim, H. F. *Journal of the Optical Society of America* **1955,** 45, (6), 460-466.

125. de Mello, J. C.; Wittmann, H. F.; Friend, R. H. *Advanced Materials* **1997,** 9, (3), 230-232.

126. Würth, C.; Grabolle, M.; Pauli, J.; Spieles, M.; Resch-Genger, U. *Nat. Protocols* **2013,** 8, (8), 1535-1550.

127. Grabolle, M.; Spieles, M.; Lesnyak, V.; Gaponik, N.; Eychmüller, A.; Resch-Genger, U. *Analytical Chemistry* **2009,** 81, (15), 6285-6294.

128. Babentsov, V.; Sizov, F. *Opto-Electronics Review* **2008,** 16, (3), 208-225.

129. Wang, L.-W.; Califano, M.; Zunger, A.; Franceschetti, A. *Physical Review Letters* **2003,** 91, (5), 056404.

130. Klimov, V. I.; Mikhailovsky, A. A.; McBranch, D. W.; Leatherdale, C. A.; Bawendi, M. G. *Science* **2000,** 287, (5455), 1011-1013.

131. Bockelmann, U.; Egeler, T. *Physical Review B* **1992,** 46, (23), 15574-15577.

132. Moreels, I.; Justo, Y.; De Geyter, B.; Haustraete, K.; Martins, J. C.; Hens, Z. *ACS Nano* **2011,** 5, (3), 2004-2012.

133. Hoheisel, W.; Colvin, V. L.; Johnson, C. S.; Alivisatos, A. P. *The Journal of Chemical Physics* **1994,** 101, (10), 8455-8460.

134. Rumbles, G.; Selmarten, D. C.; Ellingson, R. J.; Blackburn, J. L.; Yu, P.; Smith, B. B.; Mićić, O. I.; Nozik, A. J. *Journal of Photochemistry and Photobiology A: Chemistry* **2001,** 142, (2–3), 187-195.

135. Ellingson, R. J.; Beard, M. C.; Johnson, J. C.; Yu, P.; Micic, O. I.; Nozik, A. J.; Shabaev, A.; Efros, A. L. *Nano letters* **2005,** 5, (5), 865-871.

136. Carr, K. *Labsphere Technical Guide* **1997**. Labsphere Company: 1997.

Appendix I

List of sample numbers of batches used in this thesis

PbSe QDs in Figure 1.3	091/CJM/14
PbSe QDs in Figure 2.3	063/CJM/13
PbSe QDs in Figure 2.4 and Figure 2.5	088/CJM/14
PbS QDs in Figure 2.8	064/CJM/13
PbS QDs in Figure 2.9	117/CJM/14
PbS-CdS QDs in Figure 2.14	066/CJM/13
PbS-CdS-ZnS QDs in Figure 2.14	068/CJM/13
PbSe-CdSe QDs in Figure 2.16	065/CJM/13
PbSe-CdSe-ZnS QDs in Figure 2.16	067/CJM/13
PbSe-CdSe QDs in Figure 2.21 (top)	089/CJM/14
PbSe-CdSe-ZnS QDs in Figure 2.21 (top)	090/CJM/14
PbSe-CdSe QDs in Figure 2.21 (bottom)	121/CJM/14
PbSe-CdSe-ZnS QDs in Figure 2.21 (bottom)	122/CJM/14
PbSe QDs (sample A) in QY measurements	111/CJM/14
PbSe QDs (sample B) in QY measurements	015/BG/14
PbSe QDs (sample C) in QY measurements	091/CJM/14
PbSe QDs (sample D) in QY measurements	014/BG/14
PbS QDs (sample A) in QY measurements	130/CJM/15
PbS QDs (sample B) in QY measurements	127/CJM/15
PbS QDs (sample C) in QY measurements	117/CJM/14
PbSe-CdSe QDs (sample A) in QY measurements	089/CJM/14
PbSe-CdSe QDs (sample B) in QY measurements	092/CJM/14
PbSe-CdSe QDs (sample C) in QY measurements	039/CJM/13
PbS-CdS QDs (sample A) in QY measurements	100/CJM/14
PbS-CdS QDs (sample B) in QY measurements	050/CJM/13